

**R-08-98**

**Bedrock transport properties  
Data evaluation and  
retardation model**

**Site descriptive modelling  
SDM-Site Forsmark**

Johan Byegård, Eva Selnert, Geosigma AB

Eva-Lena Tullborg, Terralogica AB

December 2008

**Svensk Kärnbränslehantering AB**

Swedish Nuclear Fuel  
and Waste Management Co

Box 250, SE-101 24 Stockholm  
Phone +46 8 459 84 00



# **Bedrock transport properties Data evaluation and retardation model**

## **Site descriptive modelling SDM-Site Forsmark**

Johan Byegård, Eva Selnert, Geosigma AB

Eva-Lena Tullborg, Terralogica AB

December 2008

*Keywords:* Retardation model, Transport properties, Forsmark, Fracture mineralogy, Diffusivity, Porosity, Sorption.

This report concerns a study which was conducted for SKB. The conclusions and viewpoints presented in the report are those of the authors and do not necessarily coincide with those of the client.

A pdf version of this document can be downloaded from [www.skb.se](http://www.skb.se).

# Abstract

A descriptive model for the rock retardation properties of the Forsmark site has been developed. The model is based on the available data from the geology, hydrogeology, and hydrogeochemistry including fracture mineral studies and has integrated data from these areas with laboratory data from the porosity, diffusion and sorption experiments performed using site specific geological material. The outcome is described in tables in which the retardation properties of different geological structures (i.e. rock types, fracture types and deformation zone units) are summarized.

The geological description of the site shows that the granite to granodiorite, metamorphic, medium-grained, rock type (SKB code 101057) dominates the target volume of the site, 74% of the RFM029 rock domain. Besides that, there are a large number of rock types present in low quantities (referred to as minor rock types). A classification of fracture types is presented (8 different fracture types) and the statistics of their distribution among the open fractures are presented. Important geological features of the deformation zones are identified (4 different deformation zone units) and as an example a descriptive model of the zone ZFMA2 using the present concept is given.

Basically three water types are present in the Forsmark area (as identified by the hydrogeochemical investigations); these are fresh, brackish marine and brackish to saline non-marine groundwaters. In the laboratory experiments four different water types have been used; fresh water, two types of brackish-saline water (one of marine groundwater type and the other of a non-marine groundwater type). In addition, brine groundwater has been identified as a possible extreme and was therefore included in the laboratory experiments. The selection of different groundwater types is of large importance for the batch sorption experiment, where the composition is likely to influence the sorption; both from a surface/aqueous complexation perspective and also due to cation exchange competition.

Concerning the porosity properties of the different rock types, the major rock type (101057) shows porosity in the range of 0.2%, however with a considerable variation. It is indicated that samples taken from deformation zones generally has higher porosity. The different minor non-altered rock types studied show, with some variations, a porosity in the same range as for 101057. The only exception to this general trend is some of the samples from different deformation zones in which porosities in the range of 3–13% have been measured. However, the presence of these highly porous deformation zone units are associated to minor part of the deformation zones (e.g. less than 20% in the ZFMA2 zone).

Studies of the diffusive properties of the Forsmark rock types have yielded formation factors (i.e. how much lower the diffusivity in the rock type is compared to the diffusivity in pure water) mainly in the range of  $(1-3) \cdot 10^{-4}$ . An expected dependence of the formation factor on the porosity is well verified; showing e.g. formation factors in the range of  $1 \cdot 10^{-2}$  for the highly porous vuggy rock (as a result of quartz dissolution) with porosity in the range of 13%. Laboratory values for the formation factor have been found to be approximately 8 times higher than the corresponding measurements performed in situ which indicates that stress release and drilling may have caused sample disturbances and thus an overestimation of the diffusivities determined in laboratory experiments.

A large series of batch sorption experiments has been performed in order to describe the radionuclide sorption interaction in the different geologic materials and in the different water compositions. A large series of experiments have been performed using Cs, Sr and a trivalent lanthanide/actinide (Eu or Am) as tracer; for a few materials the tracers Ra, Ni, Np and U have also been added. For the major rock type 101057 in combination with saline Forsmark groundwater, the  $K_d$  values for Cs, Sr and Eu/Am are reported to  $4 \cdot 10^{-3}$ ,  $2 \cdot 10^{-4}$  and  $6 \cdot 10^{-1}$  m<sup>3</sup>/kg, respectively. A general trend is that the material adjacent to the different fractures (altered wall rock) gives higher  $K_d$  compared to non-altered rock and that tracers presumed to adsorb with a cation exchange mechanism (i.e. Cs, Sr and Ra) are more strongly adsorbed with decreasing ionic strength of the groundwater.

The outcome of the report is the retardation model tables in which the different retardation properties of the different geological compartments (rock types, fracture types and deformation zone units) are summarized.

# Sammanfattning

En beskrivande modell för bergets retardationsegenskaper har tagits fram baserat på data från SKB:s platsundersökning i Forsmark. Modellen baseras på tillgängliga data från geologi-, hydrogeologisk samt hydrogeokemi-programmen; dessa data har tillsammans med sprickmineralstudier integrerats med resultaten från laboratoriestudier av porositet, diffusivitet och sorptionsexperiment genomförda med platsspecifikt geologiskt material. Resultatet av denna process presenteras sedan i tabeller i vilka retardationsegenskaperna för de olika geologiska strukturerna (dvs bergarter, spricktyper och deformationszonsenheter) sammanfattas.

Den geologiska beskrivningen av Forsmarksplatsen visar att metamorfisk medelkornig granit till granodiorit, (SKB bergartskod 101057) dominerar den tänkta förvarsvolymen, 74 % av bergdomän RFM029. Förutom denna finns också ett stort antal bergarter i lägre kvantiteter. En klassificering av spricktyper har utförts (8 olika spricktyper) och statistik presenteras för fördelningen av dessa bland de öppna sprickorna. Viktiga vanligt förekommande geologiska strukturer inom deformationszonerna har identifierats (4 olika deformationszonsenheter) och en exemplifiering av retardationsmodellkonceptet applicerat på den deterministiskt identifierade deformationszonen ZFMA2 presenteras i rapporten.

Tre grundvattentyper har, baserat på de hydrogeokemiska undersökningarna, identifierats för Forsmarks platsundersökningsområde; dessa är sött, bräckt marint samt bräckt till salint icke-marint grundvatten. I laboratorieprogrammet för bestämning av retardationsparametrar har dessa tre använts och dessutom har det kompletterats med en brine-liknande vattentyp som har identifierats som en möjlig extrem variant av grundvatten som skulle kunna påverka i framtida scenarier. Val av grundvattentyper är av stor betydelse för sorptionsstudier, såväl rörande komplexbildning i vätskefas, ytkomplexering som katjonbyteskonkurrens.

Vad beträffar porositetsegenskaperna hos de olika bergarterna visar den dominerande bergarten (101057) en porositet på 0.2 %, dock med en avsevärd variation. Bergprover tagna från deformationszoner förefaller ha något högre porositet. De övriga icke-omvandlade bergarterna visar, med något undantag, porositetsvärden i samma härad som bergart 101057. Det enda påtagliga undantaget är enstaka prover från deformationszoner där porositeter i intervallet 3–13 % har mätts upp. Det är dock konstaterat att sådana högporösa deformationszonsenheter generellt utgör en liten del av deformationszonerna; t ex mindre än 20 % för ZFMA2-zonen.

Laboratoriestudier av diffusivitetsegenskaper med genomdiffusionsförsök för Forsmarksbergarter har givit formationsfaktorer (dvs hur mycket lägre diffusivitet bergarten har jämfört med diffusivitet i rent vatten) huvudsakligen i intervallet  $(1-3) \cdot 10^{-4}$ . Ett förväntat beroende av formationsfaktorn på porositeten verifieras av resultaten; för den p.g.a. kvartsupplösning högporösa vuggy rock med en porositet på cirka 13 % erhålls en formationsfaktor på  $1 \cdot 10^{-2}$ . Laboratoriebestämda formationsfaktorer har visat sig ligga ungefär en faktor 8 högre än motsvarande värden bestämde in situ genom mätning av elektrisk resistivitet. Detta skulle kunna tyda på att tryckavlastning och utborrninng har skapat störningar i det provtagna bergmaterialet och därför ger en överskattning av formationsfaktorer bestämde i laboratorieexperiment.

Ett stort antal batchsorptionsexperiment har genomförts för att beskriva radionuklidsorption för olika typer av platsspecifika geologiska material kombinerat med de olika vattensammansättningarna. Ett omfattande antal bergmaterial har undersökts med en cocktail bestående av Cs, Sr samt en trivalent lantanid/aktinid (Eu eller Am); för ett fåtal material bedömda såsom särskilt viktiga har även Ra, Ni, Np och U använts. För Cs, Sr och Eu/Am rapporteras  $K_d$ -värden till respektive  $4 \cdot 10^{-3}$ ,  $2 \cdot 10^{-4}$  samt  $6 \cdot 10^{-1} \text{ m}^3/\text{kg}$  för den dominerande bergarten 101057 i kombination med salint grundvatten. En generell trend är att bergmaterial närmast intill sprickor (olika former av omvandlat berg) ger högre  $K_d$ -värden jämfört med icke omvandlat berg. Det kan också tydligt ses att spårämnen som förväntas adsorbera genom katjonbytesmekanism (dvs Cs, Sr och Ra) adsorberar starkare med lägre jonstyrka i grundvattnet.

Rapportens olika delar sammanfattas slutligen i retardationsmodell-tabeller i vilka de olika retardationsegenskaperna för de geologiska strukturerna (dvs bergarter, spricktyper och deformationszonsenheter) anges.

# Contents

<b>1</b>	<b>Introduction</b>	7
1.1	Background	7
1.2	Conceptual model with potential alternatives	7
1.2.1	Basic conceptual model	7
1.2.2	The process of the development of the retardation model	9
1.3	Outline of this report	9
<b>2</b>	<b>Description of input data</b>	11
2.1	Data from geology, hydrogeology and hydrogeochemistry programme	11
2.1.1	Rock types and rock domains	11
2.1.2	Deformation zones (DZ)	15
2.1.3	Rock alteration	17
2.1.4	Fractures	17
2.1.5	Fracture domains (FFM)	19
2.1.6	Hydrogeology	21
2.1.7	Hydrogeochemistry	22
2.2	Data processing for the retardation model	23
2.2.1	Fracture groups	23
2.2.2	Transmissive fractures	27
2.2.3	Deformation zones	29
2.2.4	Hydrogeochemistry	34
2.3	Data from the laboratory programme	35
<b>3</b>	<b>Analyses and evaluation of Transport data</b>	37
3.1	General model	37
3.1.1	Uncertainty in data and statistical representation	37
3.2	Porosity	38
3.2.1	Methods	38
3.2.2	Statistical representation of the porosity measurements	42
3.3	Diffusion	43
3.3.1	Methods and parameters	43
3.3.2	Through-diffusion studies	43
3.3.3	Electrical resistivity	45
3.4	Sorption	47
3.4.1	BET surface area measurements	47
3.4.2	Cation exchange capacity (CEC)	51
3.4.3	Batch sorption data	54
3.5	Confirmation studies	63
3.5.1	Adsorption studies using intact drill cores	63
3.5.2	Electromigration sorption studies	63
<b>4</b>	<b>Development of retardation model</b>	65
4.1	Methodology	65
4.1.1	Selection and presentation of retardation data	65
4.1.2	Rock types	66
4.1.3	Fracture types and deformation zones units	66
4.2	Retardation model	67
4.2.1	Rock types	67
4.2.2	Fracture types	68
4.2.3	Deformation zones units	70
4.3	Application of the retardation model	71
<b>5</b>	<b>References</b>	73

# 1 Introduction

## 1.1 Background

The Swedish Nuclear Fuel and Waste Management Company (SKB) has conducted site investigations at two different locations, the Forsmark and Laxemar-Simpevarp areas, with the objective of siting a geological repository for spent nuclear fuel. The results from the investigations at the sites are used as a basic input to the site descriptive modelling.

A Site Descriptive Model (SDM) is an integrated description of the site and its regional setting, covering the current state of the geosphere and the biosphere as well as ongoing natural processes of importance for long-term safety. The SDM shall summarise the current state of knowledge of the site, and provide parameters and models to be used in further analyses within safety assessment, repository engineering and environmental impact assessment.

The process of site descriptive modelling of transport properties is described by /Berglund and Selroos 2004/. Essentially, the description consists of three parts.

- Description of rock mass and fractures/deformation zones, including relevant processes and conditions affecting radionuclide transport; the description should express the understanding of the site and includes therefore the subdivision into rock/fracture domains.
- Retardation model: Identification and description of “typical” rock materials and fractures/deformation zones, including parameterization.
- Transport properties model: Parameterization of the three-dimensional geological model and assessment of understanding, confidence and uncertainty.

The present report is produced as a part of the SDM-Site modelling of the Forsmark area. The methods used within the transport programme produce primary data on the retardation parameters, i.e. the porosity,  $\theta_m$ , the effective diffusivity,  $D_e$ , and the linear equilibrium sorption coefficient,  $K_d$ . The data for the Forsmark site-specific laboratory transport parameters are presented in /Selnert et al. 2008/. In the present report, these retardation parameters are evaluated, interpreted and presented in the form of a retardation model, all according to the strategy for laboratory measurements, data evaluation and development of retardation models described by /Widestrand et al. 2003/.

## 1.2 Conceptual model with potential alternatives

### 1.2.1 Basic conceptual model

The conceptual model underlying the site descriptive transport modelling is based on a description of solute transport in discretely fractured rock. Specifically, the fractured medium is viewed as consisting of mobile zones, i.e. fractures and deformation zones where groundwater flow and advective transport take place, and immobile zones in rock mass, fractures and deformation zones where solutes can be retained, i.e. be removed, temporarily or permanently, from the mobile water /Berglund and Selroos 2004/. In the safety assessment framework that provides the basis for identification of retardation parameters in the site descriptive models, retardation is assumed to be caused by diffusion and linear equilibrium sorption. These processes are reversible and are here referred to as retardation processes.

The conceptualization outlined above implies that radionuclide transport takes place along flow paths consisting of connected “sub paths” in fractures and deformation zones of different sizes. In this model, advection is the dominant process for moving the radionuclides in the transport direction, whereas the main role of diffusion is to remove the solutes from the mobile zone and transport them within the immobile zones, cf. Figure 1-1.

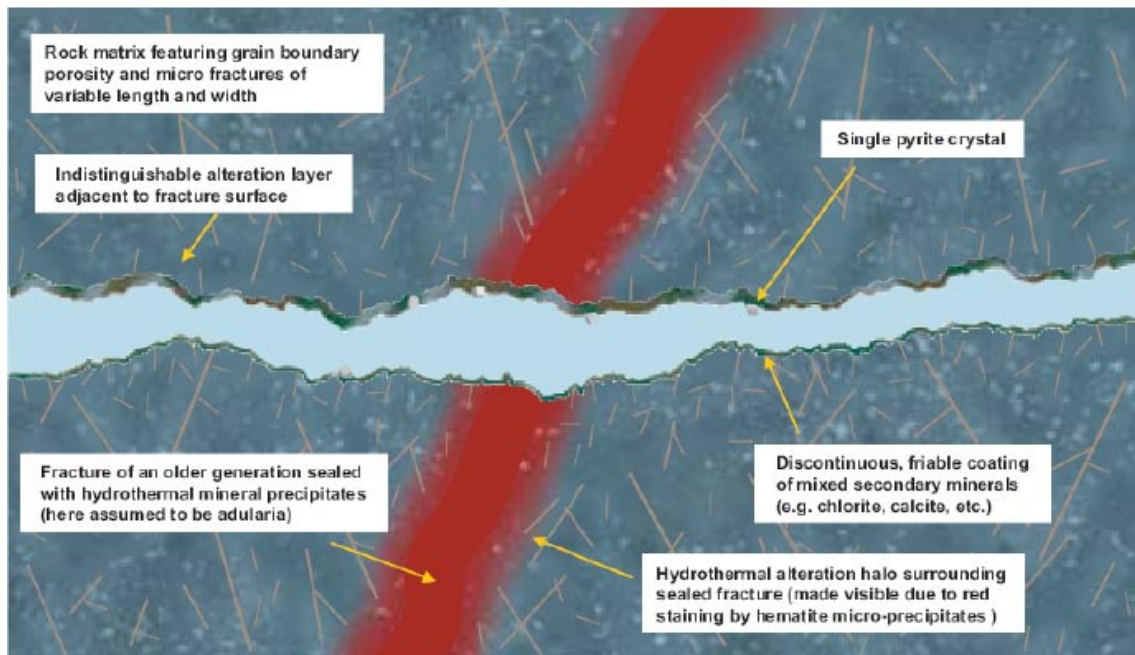
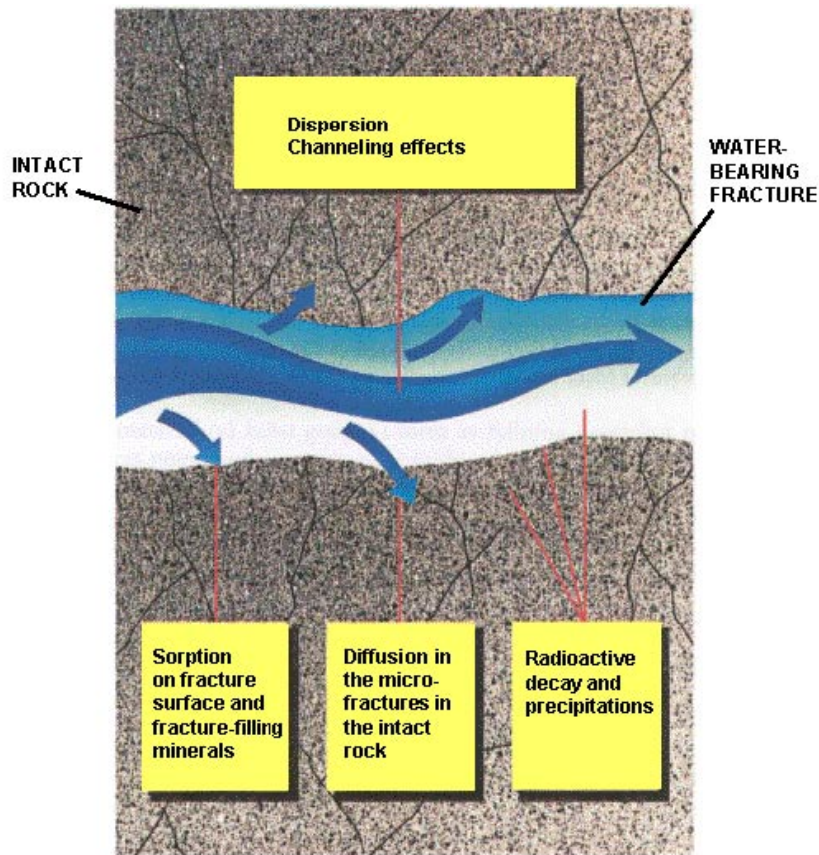


**Figure 1-1.** Conceptualized drawing of transport processes (upper) given in comparison to a schematic illustration of a transport path (lower) based on an example of a transmissive fracture in cross-section at the Forsmark site. The pathway is characteristic of a fracture with a discontinuous coating of secondary minerals. A mix of discontinuous chlorite and calcite coatings are shown in the figure with the occasional pyrite mineral grain. A typical sealed fracture of an older generation is shown transecting the open fracture section.

### **1.2.2 The process of the development of the retardation model**

The development of a retardation model has been a process in which the selection of geological material for laboratory experiments for transport parameters has, for time reasons, been done parallel to the identification and successive refinement of the geological compartments (rock types, fracture types, deformation zone units, etc) of the retardation model. As sorption and through-diffusion experiments are quite time-consuming (month-year only for the laboratory work, additional months for sample preparations), it was necessary to collect rock material during the initial phase of the site investigations, i.e. based on early versions of the geological models. It would, of course, have been advantageous if all sampling for the laboratory programme would have been performed after the final version of the geological models had been established, but this has not been possible.

It has to be acknowledged that it in the early stages of the site investigation in some cases was a difficult task to identify the frequency of different geological features and foresee the impact on the general transport properties based on the few boreholes available. Furthermore, a prerequisite for doing laboratory sorption experiments is that approximately 10 g of material is required, which restricted the possibilities of doing experiments with e.g. very thin fracture coating materials.

### **1.3 Outline of this report**

The present report contains the Forsmark SDM-Site retardation. Thus, the report focuses primarily on the first and second bullet points in the strategy outlined in Section 1.1. The aim of the present report is to give a description of the Forsmark SDM retardation model, and to give the background to the data that are used for the justification of the retardation model. The data and models used are described in Chapter 2, including the inputs from other modelling disciplines. Chapter 2 also presents the identification of the different geological structures (rock types, fracture types, deformation zone unit), which is based on a summary of the geological description of the site and that are used as the backbone of the retardation model. Chapter 3 presents the evaluation of transport data based on the geological structures given in Chapter 2, whereas the resulting retardation model (a summary of the retardation properties for the identified geological structures) is described in Chapter 4.



## 2 Description of input data

### 2.1 Data from geology, hydrogeology and hydrogeochemistry programme

The following section is a brief summary of the geological, hydrogeological and hydrogeochemical models used in the site description of the Forsmark investigation area. These models constitute the base for the evaluation of the results from the laboratory measurements of porosity, sorption and diffusion parameters which are presented in Chapter 3 in this report. The synthesis of these parameters are summarized in a retardation model in Chapter 4, which besides the quantitative number of the retardation parameters is intended to serve as a basis of the understanding of the transport properties of the rock.

The descriptive data for the geology, hydrogeology and hydrogeochemistry presented in this report are a summary of these disciplines aimed to focus on the radionuclide retardation relevant issues. The presentation is subdivided into the following sections:

- Rock types and rock domains
- Rock alteration
- Fractures
- Deformation zones
- Hydrogeology
- Hydrogeochemistry
- Fracture domain model
- Hydraulic rock domain model

The text, tables and figures in this Chapter are mainly extracted from the reports of /Stephens et al. 2007, Olofsson et al. 2007, Follin et al. 2008 and Laaksoharju et al. 2008/ and the models and databases associated with these reports. Supporting descriptive data from the combined geological/hydrogeochemical interpretations of fracture mineralogy and wall rock alteration data are provided by /Sandström et al. 2008/, and detailed studies of deformation zones are provided by /Nordgulen and Saintot 2006/.

#### 2.1.1 Rock types and rock domains

The Forsmark area is dominated by intrusive, igneous rocks with subordinate supracrustal rocks. Outcrop mapping on the mainland and in the archipelago area indicates the presence of four major groups of rock types, Groups A, B, C and D (see Table 2-1), distinguished on the basis of their relative age. Both surface and borehole samples of analysed intrusive rocks (Groups B, C and D) show a distinctive gabbro–diorite–quartz diorite–granitoid igneous compositional trend. The dominating rock type in the target volume, i.e. the north-western part of the candidate area and the rock volume beneath that has been selected as potentially suitable for hosting a repository, is granite to granodiorite metamorphic, medium-grained (rock code 101057) belonging to the Group B intrusive suite. The different rock codes with their corresponding rock type names are presented in Table 2-2; only the Forsmark rock types addressed in this retardation model work have been included in the table.

During single-hole interpretations (SHI) of the cored boreholes different rock units are defined, primarily based on the composition, grain size and inferred relative age of the dominant and subordinate rock types, together with the style and degree of ductile deformation. This information is later used to construct the three-dimensional rock domains for Forsmark (RFM).

**Table 2-1. Major groups of rock types and their relative ages. SKB rock codes are shown in brackets (Table 3-1 in /Stephens et al. 2007/).**

Groups of rock	
<i>All rocks are affected by brittle deformation. The fractures generally cut the boundaries between the different rock types. The boundaries are predominantly not fractured.</i>	
<i>Rocks in Group D are affected only partly by ductile deformation and metamorphism.</i>	
Group D (~1,851 million years)	<ul style="list-style-type: none"> <li>Fine- to medium-grained granite and aplite (111058). Pegmatitic granite and pegmatite (101061).</li> </ul> <p>Variable age relationships with respect to Group C. Occur as dykes and minor bodies that are commonly discordant and, locally, strongly discordant to ductile deformation in older rocks.</p>
<i>Rocks in Group C are affected by penetrative ductile deformation under lower amphibolite-facies metamorphic conditions.</i>	
Group C (~1,864 million years)	<ul style="list-style-type: none"> <li>Fine- to medium-grained granodiorite, tonalite and subordinate granite (101051).</li> </ul> <p>Occur as lenses and dykes in Groups A and B. Intruded after some ductile deformation in the rocks belonging to Groups A and B with weakly discordant contacts to ductile deformation in these older rocks.</p>
<i>Rocks in Groups A and B are affected by penetrative ductile deformation under amphibolite-facies metamorphic conditions.</i>	
Group B (~1,886–1,865 million years)	<ul style="list-style-type: none"> <li>Biotite-bearing granite (to granodiorite) (101057) and aplitic granite (101058), both with amphibolite (102017) as dykes and irregular inclusions. Local albitization (104) of granitic rocks.</li> <li>Tonalite to granodiorite (101054) with amphibolite (102017) enclaves. Granodiorite (101056).</li> <li>Ultramafic rock (101004). Gabbro, diorite and quartz diorite (101033).</li> </ul>
Group A (supracrustal rocks older than 1,885 million years)	<ul style="list-style-type: none"> <li>Sulphide mineralization, possibly epigenetic (109010).</li> <li>Volcanic rock (103076), calc-silicate rock (108019) and iron oxide mineralization (109014). Subordinate sedimentary rocks (106001).</li> </ul>

**Table 2-2. Rock codes with their corresponding rock type names. Only the rock types addressed in the evaluation of the transport data (cf. Chapter 3) are given in the table.**

Code (SKB)	Rock type (relative age group)
101051	Granodiorite, tonalite and granite, metamorphic, fine- to medium-grained (group C)
101054	Tonalite to granodiorite, metamorphic (group B)
101056	Granodiorite, metamorphic (group B)
101057	Granite to granodiorite, metamorphic, medium-grained (group B)
101058	Granite, metamorphic, aplitic (group B)
101061	Pegmatitic granite, pegmatite (group D)
102017	Amphibolite (group C)
103076	Felsic to intermediate volcanic rock, metamorphic (group A)
111058	Granite, fine- to medium-grained (group D)

Of the recognized rock domains, RFM029 dominates the tectonic lens at Forsmark and is the volumetrically most significant domain inside both the local model and target volume (Figure 2-1) and /Stephens et al. 2007/. RFM029 is dominated by granite to granodiorite metamorphic, medium-grained, (rock code 101057). Subordinate rock types are pegmatitic granite, pegmatite, (101061), metamorphic, aplitic granite, (101058), granodiorite, tonalite and granite, metamorphic, fine- to medium-grained (101051), fine- to medium-grained granite, (111058) together with amphibolite (102017) (Figure 2-2).

The second rock domain inside the target volume is the less extensive RFM045. This domain is dominated by Na-K altered (albitized) and metamorphosed granitic rocks of which the most common is granite, metamorphic, aplitic (101058) together with a granitic rock type that is similar to the granite to granodiorite metamorphic, medium-grained, (rock code 101057) which is the dominating rock type in rock domain RFM029. The albitization is not pervasive throughout rock domain RFM045 and fresh rock is also present. The subordinate rock types that are found in rock domain RFM045 are pegmatitic granite, pegmatite (101061), granodiorite, tonalite and granite, metamorphic, fine- to medium-grained (101051) and amphibolite (102017). These rock types occur mainly in the form of isolated minor bodies or lenses and dykes. However, subordinate rock types occur somewhat more frequently in RFM045 relative to what is observed in domain RFM029. The quantitative distribution of rock types within these two rock domains is illustrated in Figure 2-3.

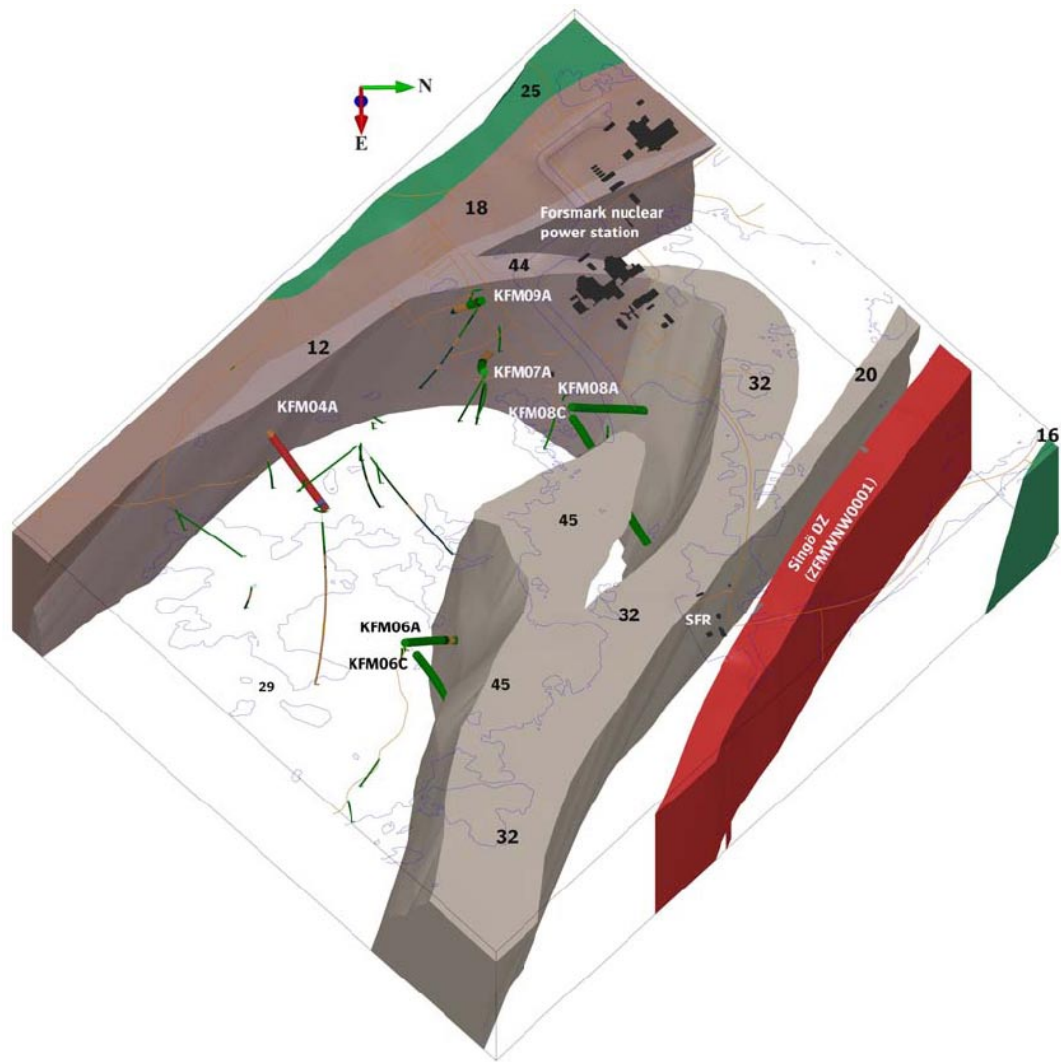


**Figure 2-1.** Three dimensional model for rock domains (numbered) inside the target volume, in the north-western part of the candidate volume. The model is viewed to the west and the regionally significant Singö deformation zone is shown in the foreground. Rock domain RFM029 is illustrated as the non-shaded area to the left in the figure. Boreholes marked with the help of larger cylinders (KFM04A, KFM06A, KFM06C, KFM07A, KFM08A, KFM08C and KFM09A) constrain the boundaries between different domains (Figure 4-6 in /Stephens et al. 2007/).

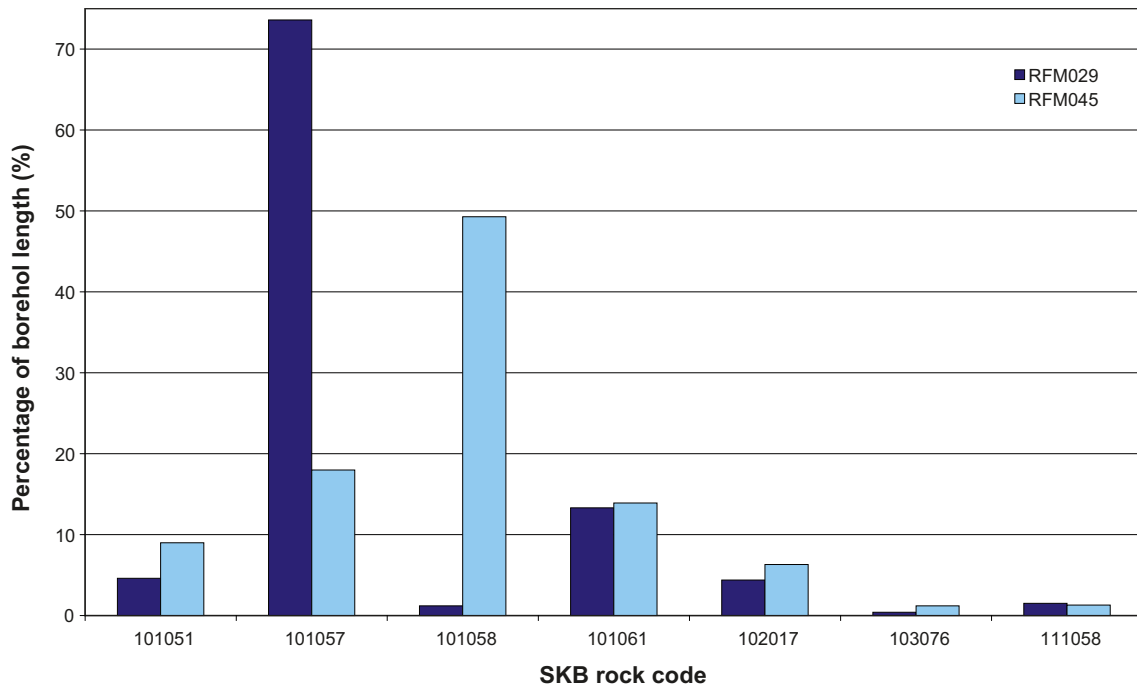
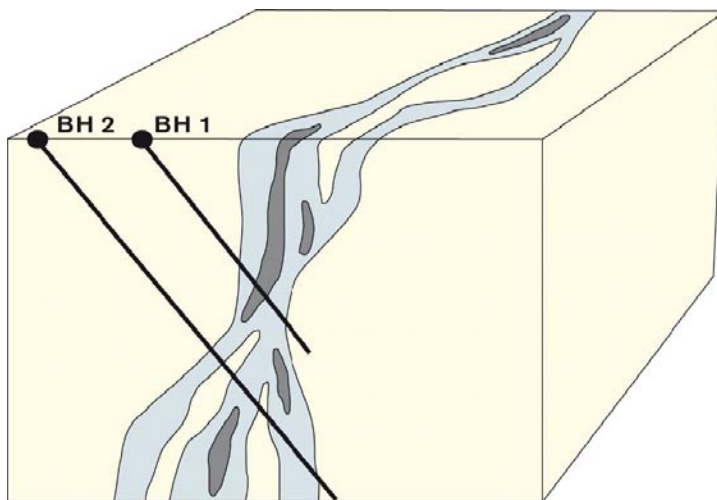


*Figure 2-2. Quantitative estimates in volume% of the proportions of the most important rock types, expressed in rock codes according to Table 2-2, in rock domain RFM029 and RFM045 respectively.*



- Core (e.g. sealed network, fault breccia, cataclasite)
- Transition (damage) zone (fracture frequency anomalous relative to rock outside zone)
- Rock little or unaffected by brittle deformation zone

(redrawn after Caine et al. 1996)

*Figure 2-3. Three-dimensional conceptual model of a deformation zone (Figure 5-1 in /Stephens et al. 2007/).*

RFM012, RFM018, RFM032 and RFM044 are examples of marginal rock domains; i.e. rock domains that are located outside the tectonic lens and form the margins to the target volume. These domains have more inhomogeneous bedrock and are generally affected by strong ductile deformation and also show an increased frequency of fractures or possible deformation zones /Olofsson et al. 2007/.

Opposite to the fracture domain model (later described in Section 2.1.5), the concept of rock domains include the deterministically identified deformation zones as parts of the rock domain. In the important rock domain RFM029, the bedrock between deformation zones is relatively homogeneous with low intensity of alteration and decreasing fracture frequency with depth. As expected, the bedrock within the deformation zones displays a more heterogeneous pattern with increased amount of altered bedrock and increased fracture frequency. However, even within the parts of the rock domain classified as deformation zones, areas of relatively fresh rock also occur. The rock alterations are described in detail in Section 2.1.3.

### 2.1.2 Deformation zones (DZ)

Deformation zone is a general term referring to an essentially two-dimensional structure along which there is a concentration of brittle, ductile or combined brittle and ductile deformation. These structures are referred to as regional (larger than 10 km), local major (1–10 km) and local minor deformation zones (up to 1 km). The term fracture zone is used to denote a brittle deformation zone without any specification whether there has or has not been a shear sense of movement along the zone. Possible brittle deformation zones are identified in the single-hole interpretations, primarily with the help of the data sets on rock fracture frequency, rock alteration and focused resistivity. Sealed fractures, sealed fracture networks, open and partly open fractures, and crush zones are distinguished from each other. Alteration, particularly hematite dissemination (oxidation), is abundant inside deformation zones (Figure 2-3), although the alteration is not always pervasive throughout a deformation zone. Deformation zones are distinguished in both the rock domain model and in the fracture domain concept, described in Sections 2.1.1 and 2.1.5, respectively.

Figure 2-3 illustrates a conceptual model of a brittle deformation zone, with transition zone and core. The transition zone can range in thickness, from a few metres to several tens of metres. This part of the zone has an increased fracture frequency together with a more extensive alteration compared to the surrounding bedrock. However, the transition zone can contain segments that are unaffected with respect to fracture frequency and alteration. The zone core is thinner than the transition zone and varies from a few centimetres to a few metres. The core has even higher fracture frequency and is composed of sealed fractures (mainly in sealed fracture networks), fault breccia or cataclasite (cohesive). Therefore, deformation zone units representing fault breccia/cataclasite and sealed fracture network have been selected for the parameterization of deformation zones (cf. Table 2-4 in Section 2.2.2). The boundaries between the host rock, transition zone and core are commonly diffuse and difficult to define.

Generally, the deformation zones at Forsmark, as evaluated in the geology model, can be divided into the following four sets.

- **Vertical and steeply, SW-dipping deformation zones with sub-sets referred to as WNW and NW.** These zones contain mylonites, cataclastic rocks and cohesive breccias, and are dominated by sealed fractures. They initiated their development in the ductile regime but continued to be active in the brittle regime, i.e. they are composite structures. Generation 1 mineral paragenesis (cf. Section 2.1.4) is conspicuous along the fractures in these zones. Regional zones that are longer than 10 km (e.g. Forsmark, Singö and Eckarfjärden deformation zones) are restricted to this set.
- **Vertical and steeply dipping fracture zones with sub-sets referred to as ENE (NE) and NNE.** These zones formed in the brittle regime and are dominated by sealed fractures. Generation 2 mineral paragenesis (cf. Section 2.1.4) is conspicuous along the fractures in these zones. However, the generation 1 mineral epidote is locally present along fractures with steep ENE to NNE orientation in these zones.
- **Vertical and steeply dipping fracture zones that are referred to as the NNW set.** These zones formed in the brittle regime and are dominated by sealed fractures. Fillings and coatings along the fractures in these zones are similar to those observed in the ENE to NNE set, i.e. similar fracture types. On the basis of their low frequency of occurrence, the NNW set is judged to be of lower significance at the Forsmark site, relative to the other three sets.

- **Gently dipping fracture zones** that formed in the brittle regime and, relative to all the other sets, contain a higher frequency of open fractures and incoherent crush material. It is apparent that these zones include minerals from all four mineral paragenesis (cf. Section 2.1.4) and it is inferred that fluid movement has occurred along these zones at several times during geological history.

Figure 2-4 shows the surface intersections of the deterministically modelled deformation zones in the local model volume. These zones are individually described in /Stephens et al. 2007). Moreover, possible deformation zones recognized during single-hole interpretations (SHI) are described in /Nordgulen and Saintot 2006/ including the subdivision into cores and transition zones as well as the identification of important units such as sealed fractures networks and crushed rock.

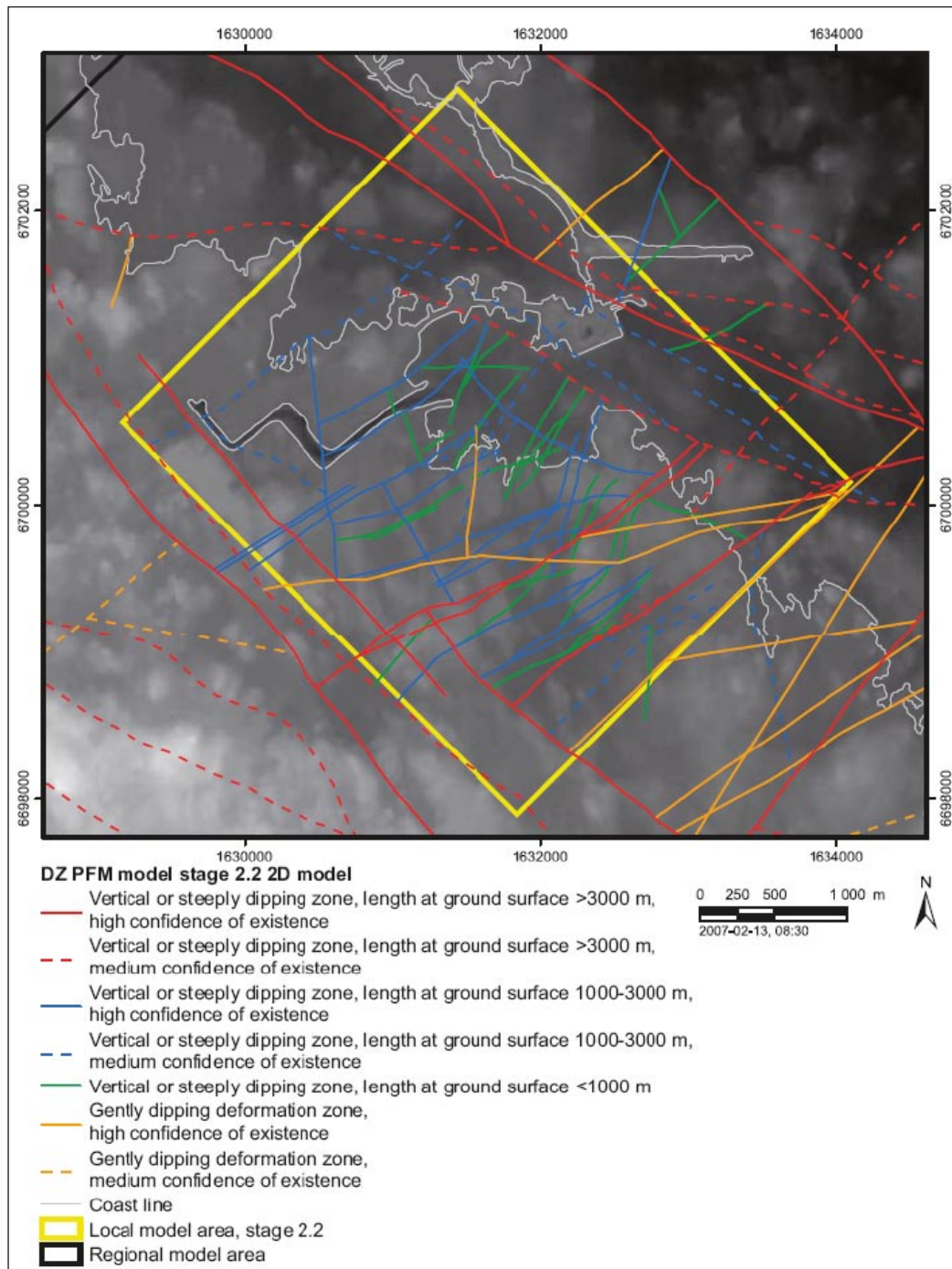


**Figure 2-4.** Surface intersection of deterministic deformation zones in the local model area, stage 2.2. The background corresponds to the digital elevation model for the site. Coordinates are provided using the RT 90 (RAK) system (Figure 5-10 in /Stephens et al. 2007)/.

### 2.1.3 Rock alteration

Rock alteration at the Forsmark site, are displayed in several different ways. The most abundant types of alteration are hematite dissemination, mapped and referred to as oxidation (deformation zone unit #4 cf. Table 2-4 in Section 2.2.2) in SKB site investigation database Sicada, together with albitization (described below). Quartz dissolution and the development of vuggy rock (deformation zone unit #3, cf. Table 2-4 in Section 2.2.2) are also present.

The major mineralogical changes in altered rock are an almost complete saussuritization of plagioclase feldspar, chloritization of biotite and to some extent hematization of magnetite. In oxidized (red-stained) rock a fine dissemination of hematite inside the altered plagioclase grains and along grain boundaries can be observed. According to /Sandström and Tullborg 2006/, an increase in the connected porosity is also associated with this type of alteration, most likely due to the chloritization of biotite and an increased number of micro fractures. Hydrothermal reddening normally extends a few centimetres perpendicular from a fracture although more extensive zones also exist. However, the alteration (especially the chloritization) extends longer into the rock than the reddening suggests and the amount of rock mapped as “oxidized” should therefore be seen as a minimum value of the amount of altered rock. Analyses of oxidation along the cored boreholes demonstrate that it occurs independently of the depth, it is not related to near-surface processes and it is an inherent feature (but non-pervasive distribution) of deformation zones. In albitized rock there is a redistribution of sodium and potassium; producing a fine-grained quartz-plagioclase feldspar-(biotite) rock in especially granitic rocks, with a significant loss of K-feldspar compared with the unaltered rocks. The plagioclase of oligoclase composition has been replaced by a mineral assemblage consisting of albite, adularia, sericite, epidote, hematite and calcite. According to borehole data, albitization is not restricted only to deformation zones.

A quantitative estimate of different types of rock alteration, degree of alteration (faint to weak or medium to strong) together with the distribution inside and outside deformation zones is presented for RFM029 and RFM045 in Figure 2-5. A clear relationship between alteration and deformation zones is indicated. Virtually all the occurrences of vuggy rock occur within or immediately adjacent to possible deformation zones in the single-hole interpretations and along the zones modelled deterministically in model stage 2.2. The occurrences are commonly found close to one side of the zone and it is inferred that the vuggy rock represent channels within deformation zones along which, at some time (or times) during geological history, hydrothermal fluids have moved and affected the quartz content in the bedrock. There is a somewhat higher proportion of the alteration referred to as oxidation outside deformation zones in RFM045.

Fault gouge has not been found, neither during the mapping of drill cores nor during the detailed characterization of deformation zones. However, loss of drill core has been documented along 35 borehole sections of which 23 are located along possible deformation zones. Apparently, the most frequent cause of drill core loss is damage to intact rock induced by the drilling. Yet, at least one section may have contained incohesive material containing fault gouge which was flushed out with the drilling fluid. Since the existence of fault gouge has not been proven it is not included in the retardation model; nevertheless, one must be aware of the possibility of its potential existence.

### 2.1.4 Fractures

Two dominant fracture orientation sets are visible in nearly all boreholes; a NE-striking set and a NW-striking set. Both dominant sets are nearly vertical although the NW-striking set tends to have a larger range of potential dips than the NE-striking set. The NE-striking set is a particularly variable one; the mean pole for this set varies spatially from ENE to NNE. In addition other potential fracture sets of various relative intensities are visible; a clear EW-striking set, a weak NS-striking set and a range of fractures oriented subhorizontally (dips less than 20°). The concentration of open fractures is higher in the subhorizontal sets relative to the subvertical fracture sets. It is noteworthy that the orientations of fracture sets recognized outside deformation zones resemble the orientations of sets and sub-sets of deformation zones that have been modelled deterministically in the local model volume.

The variation in frequency of fractures with depth was analysed in model stage 2.2 and the moving average and cumulative frequency plots for each cored borehole are presented in /Olofsson et al. 2007/. There is an anomalously high frequency of open and partly open fractures in the upper part of the bedrock in the target volume, while, in the lower part of this volume, the bedrock shows a strong dominance of sealed fractures.

During detailed studies of the fracture mineralogy and wall rock alteration at the Forsmark site /Sandström et al. 2008/, four generations of fracture mineralization have been distinguished. These are summarized below.

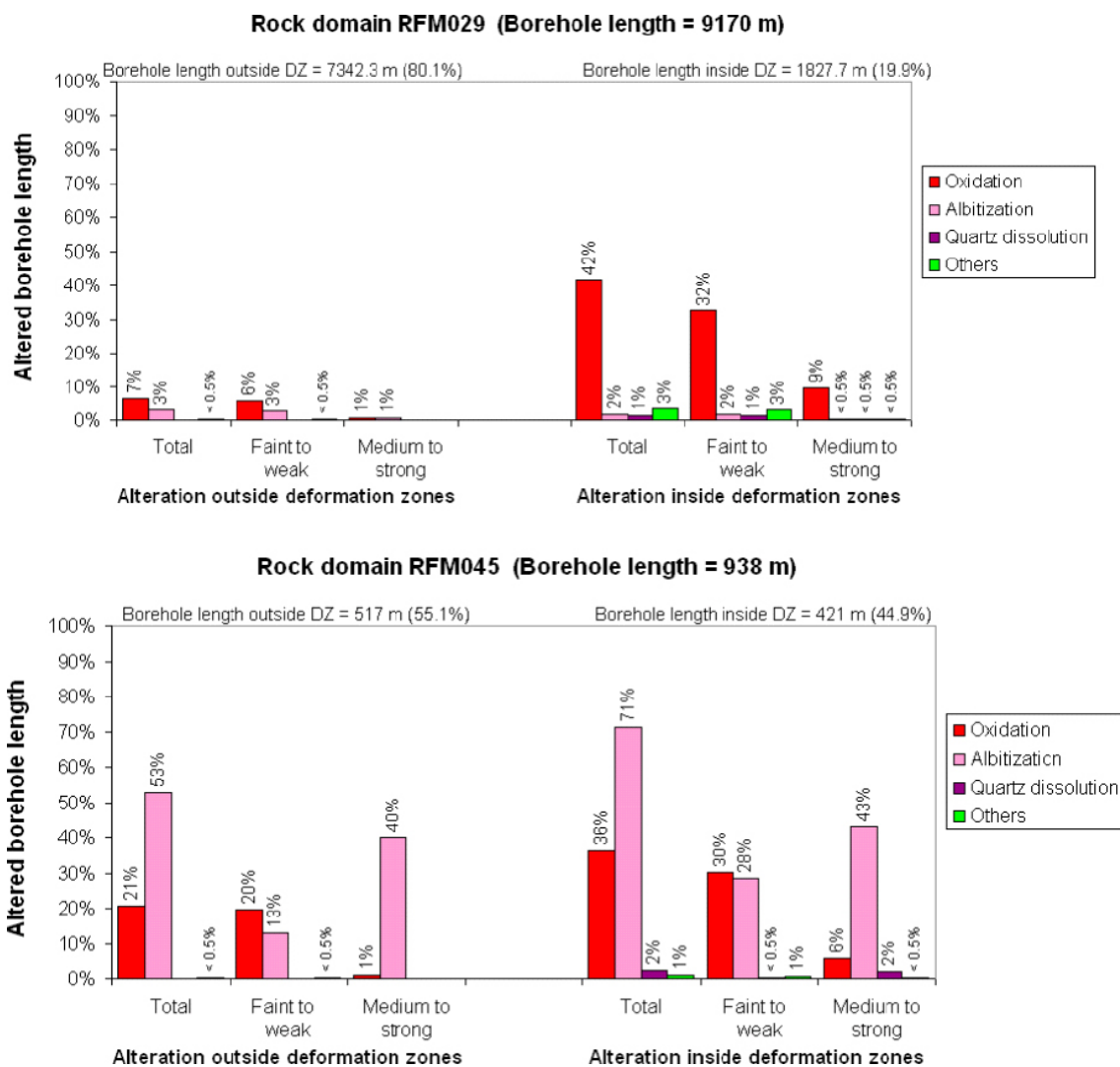


**Figure 2-5.** Quantitative estimates in volume-% of the type and degree of alteration in rock domains RFM029 and RFM045 respectively (Figure 4-13 in /Stephens et al. 2007/).

**Generation 1** consists of epidote, quartz and Fe-rich chlorite (Fracture types C, D, cf. Table 2-3 in Section 2.2.1) in fractures and as sealing in brittle-ductile cataclasites. The minerals precipitated under hydrothermal conditions at temperature in the range of 150–200°C. Generation 1 minerals are conspicuous in sub-horizontal and gently dipping fractures or in steep, WNW-ESE to NW-SE fractures. However, they are also present along fractures in other steeply dipping sets. This generation formed between 1.8 and 1.1 Ga ago.

**Generation 2** consists of a sequence of hydrothermal fracture minerals precipitated at temperatures between 150–280°C and are dominated by adularia, albite, laumontite, prehnite, calcite, chlorite/corrensite and hematite (Fracture types A, B, C, D, and E, cf. Table 2-3 in Section 2.2.1). Generation 2 minerals are particularly common along steep, ENE-WSW to NNE-SSW and NNW-SSE fractures. <sup>40</sup>Ar/<sup>39</sup>Ar ages from adularia indicate a major influence of tectonothermal activity at 1.1 to 1.0 Ga on the development of fracture systems that are coated or filled by generation 2 minerals.

**Generation 3** consists of minerals precipitated under low temperature conditions during the Palaeozoic (542–251 ma). The most abundant minerals are calcite, quartz, pyrite, chlorite/corrensite and asphaltite (Fracture types A, B, D, F and G, cf. Table 2-3 in Section 2.2.1). The formation fluid was influenced by organic material, which may have emanated from an overlying sedimentary cover. The orientation of fractures with generation 3 minerals suggests reactivation of fractures filled with older minerals but new fractures were also formed.



**Generation 4** is dominated by chlorite/clay minerals and thin precipitates of calcite in predominantly hydraulically conductive fractures and fracture zones (Fracture types B, D and G, cf. Table 2-3 in Section 2.2.1). These minerals are prominent along sub-horizontal and gently dipping fractures, but are also present in different sets of steeply dipping fractures. It is inferred that most of the hydraulically conductive fractures are hosted in ancient structures and precipitation of generation 4 minerals has most likely occurred during a long period of time.

### **Fractures within deformation zones**

For each of the possible deformation zones identified in the cored boreholes (SHI and ESHI), an analysis of the fracture mineralogy has been completed. Since fractures with different orientation are present along a zone, it has been considered necessary to establish how the different fracture minerals are distributed according to fracture orientation. Furthermore, the occurrence of hematite staining adjacent to fractures, so-called oxidized walls are included. Data from open and partly open fractures are distinguished from sealed fractures.

Chlorite and calcite are conspicuous along all the zones identified in the single hole interpretation and, with the exception of a few gently dipping zones, the same observation applies to the occurrence of oxidized walls.

Laumontite (and adularia), which show red staining related to a fine-grained hematite dissemination, are conspicuous along the steeply dipping zones with ENE, NE and NNE strike and that transect the target volume. However, epidote is occasionally present in these zones, even along fractures with the steep north-easterly orientation.

The gently dipping zones generally show a simpler fracture mineralogy dominated by chlorite and calcite. Restricted wall-rock alteration and a high frequency of fractures with no mineral filling or coating are present along a few of these zones. However, there is a more complex mineralogy along some gently dipping zones. Clay minerals are common in the possible zones identified close to the surface and considered as gently dipping. However, they are also present, for example, along steeply dipping fractures with NNW strike in DZ4 close to the base of KFM07A. An illustration of the fracture mineralogy in a gently dipping zone and steeply dipping zones of different orientations are presented in Figure 2-6.

### **2.1.5 Fracture domains (FFM)**

Fracture domains, referred to as FFM, are defined on the basis of the geological single-hole interpretation (SHI) work and the results of the initial statistical treatment of fractures /Olofsson et al. 2007/. A fracture domain refers to a rock volume outside deterministically modelled deformation zones in which rock units show similar fracture frequency characteristics. The fractured bedrock has been divided into six fracture domains, FFM01–FFM06. FFM01–03 occurs in rock domain RFM029, with FFM01–02 in the footwall bedrock and FFM03 in the hanging wall bedrock to the deterministically modelled gently dipping deformation zone ZFMA2 and FFM06 coincides with rock domain RFM045. The key fracture domains for the target volume, FFM01 and FFM06, occur below fracture domain FFM02 (Figure 2-7). These domains are briefly described below:

**Fracture domain FFM01:** This domain is situated within rock domain RFM029 inside the target volume. It lies beneath the gently dipping or sub-horizontal zones ZFMA2, ZFMA3 and ZFMF1 and north-west of the steeply dipping zone ZFMNE0065, at a depth that varies from greater than approximately 40 m below sea level (large distance from ZFMA2) to greater than approximately 200 m below sea level (close to ZFMA2). Relative to the overlying fracture domain FFM02, the bedrock in this domain shows a lower frequency of particularly open and partly open fractures. Gently dipping or sub-horizontal deformation zones are uncommon inside this domain. In particular, these zones have not been recognized in the critical depth interval 400–500 m in the north-western part of this domain. It has been suggested that high in situ rock stresses have been able to accumulate inside this volume at one or more times during geological history, in connection with, for example, sedimentary loading processes.

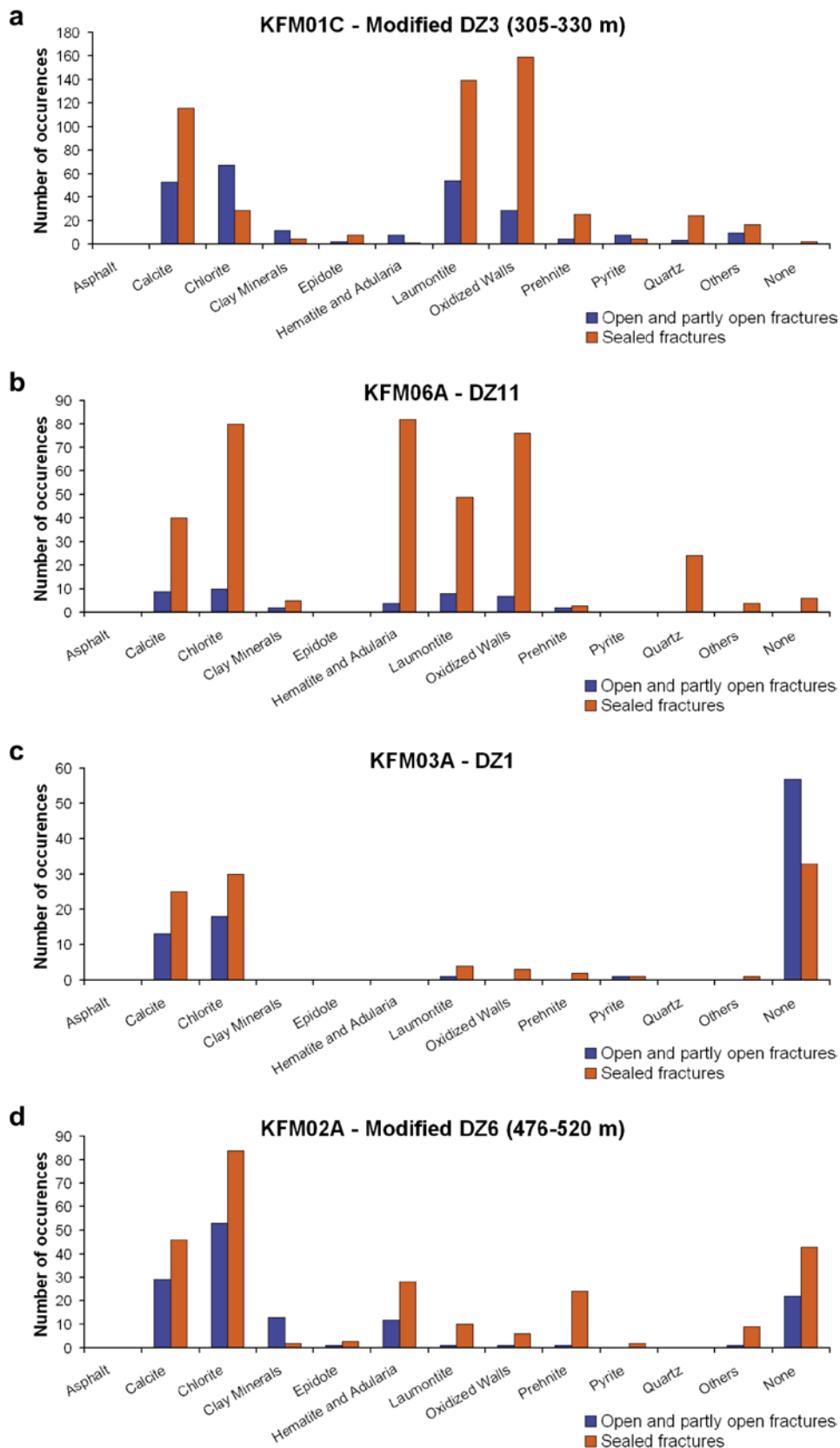


**Figure 2-6.** Occurrence of different minerals as coating and filling along fractures in a) DZ3 (305–330 m borehole length), a steeply dipping zone in the ENE sub-set (ZFMENE0060C). b) DZ11 in KFM06A, a steeply dipping zone NNE sub-set (ZFMNNE2280). c) DZ1 in KFM03A, a gently dipping zone (ZFMA4). d) DZ6 in KFM02A, a gently dipping zone (ZFMF1) (Figure 3-28 in /Stephens et al. 2007/).

**Fracture domain FFM02:** This domain is situated close to the surface inside the target volume, directly above fracture domain FFM01. The domain is characterized by a complex network of gently dipping and sub-horizontal, open and partly open fractures, which are known to merge into at least one deformation zone beneath drill site 7. The transition from more fractured bedrock close to the surface (FFM02) to less fractured bedrock at depth (FFM01) takes place deeper down as the distance from zone ZFMA2 decreases. Thus, the special character of the proposed surface fracture domain FFM02 is not solely determined by elevation. The occurrence of this domain at greater depths beneath ZFMA2 at drill sites 1, 5 and 6, and even above this zone at or close to drill sites 5 and 6, is related to an inferred higher frequency of such older fractures in the vicinity of this zone, to higher rock stresses beneath zone ZFMA2 or to a combination of these two possibilities. The gently dipping and sub-horizontal fractures are oriented at a large angle to the present-day minimum principal stress in the bedrock. This relationship favours their reactivation as extensional joints in the present stress regime, the development of conspicuous apertures along several fractures, and the release of high stress.

**Fracture domain FFM06:** This domain is situated within rock domain RFM045, inside the target volume. It resembles fracture domain FFM01 in the sense that it lies beneath both zone ZFMA2 and fracture domain FFM02. It is distinguished from domain FFM01 by the widespread occurrence of fine-grained, altered (albitized) granitic rock, with slightly higher contents of quartz compared to unaltered granitic rock.

### 2.1.6 Hydrogeology

The following section is a very brief summary of parts of the hydrogeological model of the Forsmark site /Follin et al. 2008/ including the hydraulic properties of; a) the bedrock at repository depth b) the hydraulic properties of the deterministically modelled deformation zones and c) hydraulic properties of fracture domains.

Three fracture sets dominate the flowing fractures above elevation –400 metres above sea level (metres above sea level); horizontal, NS and NE with the horizontal set as very dominant. Below elevation –400 metres above sea level, the few flowing fractures observed occur in the horizontal and NE sets with an average true spacing of approximately 200 m.

There are far fewer flowing fractures in fracture domain FFM01 compared to the conditions in fracture domains FFM02–04. Fracture transmissivity data from several boreholes confirm the impression that the rock in FFM01 at repository depth is very sparsely fractured with flowing fractures. For FFM01 and FFM02, the flow is strongly dominated by horizontal and gently-dipping fractures, with a small handful of features that strike NE or NNE. In both domains, the highest transmissivities are measured in horizontal and gently dipping fractures/Olofsson et al. 2007/.

The moderate decrease in fracture transmissivity with depth in the bedrock between the deformation zones, suggests that it is the significant decrease with depth in the observed intensity of flowing fractures that governs the groundwater flow in a fracture domain and not the decrease in fracture transmissivity. For instance, below elevation –400 metres above sea level there is less than one flowing fracture per hundred metres observed in FFM01. In conclusion, below elevation –400 metres above sea level the flowing fractures in FFM01 are almost exclusively restricted to deformation zones, symptomatic of a very sparse and poorly connected network of fractures that does not reach a threshold for percolation of water into the deep rock.

116 deformation zones intercepts representing 57 different deformation zones have been investigated hydraulically. The gently-dipping deformation zones occurring in the hanging wall bedrock to zone ZFMA2 (Figure 2-7) are the most transmissive. The bordering steeply-dipping deformation zones that strike WNW and NW form structures with a second order of importance as far as transmissivity is concerned. The steeply-dipping deformation zones that strike ENE and NNE occur in the footwall bedrock mainly and are significantly more heterogeneous from a hydraulic viewpoint. In summary, these observations suggest a pronounced hydraulic anisotropy, where the largest transmissivities observed are associated with deformation zones parallel with the orientation of the maximum principal stress, WNW, cf. /Stephens et al. 2007/.

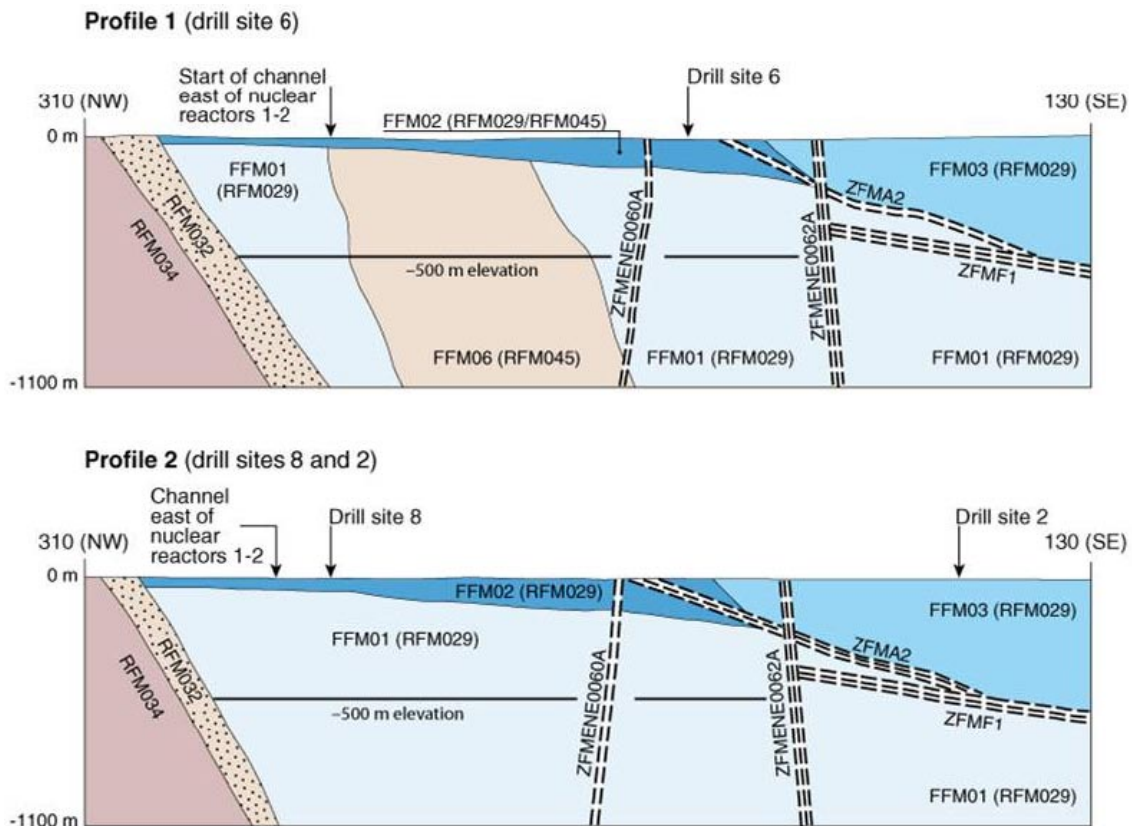


**Figure 2-7.** Simplified profiles in a NW-SE direction (310°–130°) that pass through drill sites 2 and 8 (lower profile) and drill site 6 (upper profile). The labelled fracture domains (FFM01, FFM02, FFM03 and FFM06) occur inside rock domains RFM029 and RFM045. Only the high confidence deformation zones ZFMA2 (gently dipping), ZFMF1 (sub-horizontal), ZFMENE0060A (steeply dipping, longer than 3,000 m) and ZFMENE0062A (steeply dipping, longer than 3,000 m) are included in the profiles. Note the increased depth of fracture domain FFM02 as zone ZFMA2 is approached in the footwall to the zone, and the occurrence of this domain close to the surface directly above ZFMA2 (Figure 5-1 in /Olofsson et al. 2007/).

### 2.1.7 Hydrogeochemistry

The groundwaters at Forsmark are characterized by compositions that range in salinity from fresh (up to 200 mg/L Cl) over to saline water (approximately 15,000 mg/L) and components of meteoric waters from cold and temperate climates as well as marine and deep saline groundwaters have been identified. The following division into different water types has been applied for the description of the hydrogeochemistry at the Forsmark site (cf. /Laaksoharju et al. 2008/);

- **Fresh:** (up to 200 mg/L Cl); Mainly meteoric in origin, i.e. Na(Ca)-HCO<sub>3</sub>(SO<sub>4</sub>)-(Cl).
- **Brackish Marine:** (2,000–6,000 mg/L Cl; Mg > 100 mg/L); Na-Ca-Mg-Cl-SO<sub>4</sub>.
- **Brackish to Saline Non-marine:** (4,000–15,000 mg/L Cl; Mg < 25 mg/L), i.e. Ca-Na-Cl in type.

In the upper part of the bedrock (50–150 m depth), mixing between Fresh and Brackish Marine waters is common. This mixing may be natural as well as anthropogenic and partly due to sampling in relatively long borehole sections, mainly from percussion boreholes.

Another example of natural and/or anthropogenic mixing is the waters sampled in the transition zone between Brackish Marine and Brackish Non-marine groundwaters. These waters range from 4,000–6,500 mg/L Cl and from 25–100 mg/L in Mg.

The conceptual model of the hydrogeochemistry (Figure 2-8) shows the distribution of these groundwater types along a WNW-ESE cross section.

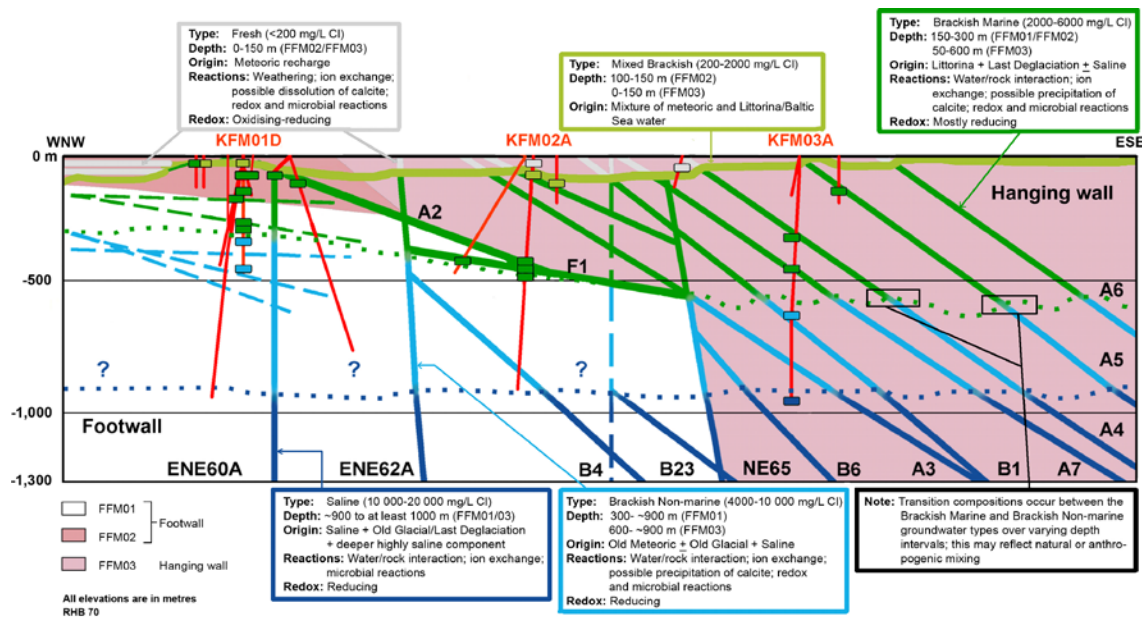


**Figure 2-8.** WNW-ESE cross-section and site descriptive model along the central part of the candidate volume showing the groundwater types and their properties (salinity, origin, major reactions and redox conditions). The footwall (FFM01 and FFM02) and hanging wall (FFM03) are indicated, separated by the major, gently dipping deformation zones ZMFA2 and F1 (Figure 6-1 in /Laaksoharju et al. 2008/).

## 2.2 Data processing for the retardation model

In this section, a synthesis of the transport relevant parts of the geology, hydrogeology and hydro-geochemistry programmes (cf. Section 2.1) are made which gives the basis for the retardation model.

### 2.2.1 Fracture groups

As mentioned in Section 2.1.5, the division into fracture domains is based on fracture frequency, a measure which includes both open and sealed fractures. For obvious reasons, the open fractures (which constitute approximately 25% of the total amount of fractures) are of major interest for retardation model purposes. For this reason, the addressing of fracture statistics is based on results for open fractures only. Although, most of the single fractures at elevations lower than –500 metres above sea level show low transmissivity, open and partly open fractures are nevertheless mapped through out the entire drill cores. The mineralogical composition of the fracture coatings are important e.g. for the sorption interaction of released radionuclides, as well as the presence or absence of an altered zone in the wall rock adjacent to the conductive fractures, as these fractures constitute possible flow paths or, more likely, diffusion path ways. Using the fracture mineralogy (i.e. the fracture generations, cf. Section 2.1.4), together with feasible mapping units (i.e. fracture data from Sicada) and potential transport properties of different materials, eight different fracture types have been identified for the retardation model purposes (Table 2-3). These groups are supposed to represent the current fracture assemblage in open fractures at the Forsmark site. Based on the work of /Sandström et al. 2008/ it is our opinion that the presently recorded fracture mineral distributions will mainly be valid over the life time of a spent nuclear fuel repository.

**Table 2-3. Identified fracture groups selected for the retardation model based on fracture mineralogy.**

Fracture coating	Thickness*	Wall rock alteration		Mainly found in fracture generations, cf. Section 2.1.4
A <b>Chlorite + Calcite</b>	≤0.5 mm	Fresh		2, 3
B <b>Chlorite + Clay</b> ± Epidote ± Prehnite ± Calcite	~1 mm	Altered ~1cm		2, 3, 4
C <b>Chlorite + Hematite</b> ± other	<0.5 mm (0.1 mm)	Altered 0.5 cm		1, 2
D <b>Chlorite</b> ± other	<0.5 mm (0.1 mm)	Fresh		1, 2, 3, 4
E <b>Laumontite</b> ± Calcite ± Chlorite ± Clay	0.1–2 mm	Altered 1–5 cm		2
F <b>Calcite</b> ± Quartz ± Pyrite ± other	0., 1–2 mm	Fresh		3
G <b>Clay</b> ± other	1–5 mm	Altered ≥ 5 cm		3, 4
H <b>No mineral</b>		Fresh		Not known

\* Thickness of the fillings for each fracture type is estimated as an average for the whole fracture surface and is based on conclusions made by geological expertise from general experiences from drill core mapping.

Statistics of the different fracture groups are based on data from Sicada and include the boreholes from which corresponding data are available, i.e. KFM01A–D, KFM02A–B, KFM03A–B, KFM04A, KFM05A, KFM06A–C, KFM07A–C, KFM08A–D, KFM09A–B, KFM10A, KFM11A, and KFM12A. Data are presented as number of open fractures versus elevation and the frequency of each group is illustrated in Figure 2-9 and discussed below.

Chlorite and calcite are the most frequent fracture coating/filling minerals, occurring solely together or together with some other minerals. Fracture type A, chlorite and calcite, are present in approximately 34% of the mapped open fractures. Calcite also occurs together with quartz, pyrite and other minerals (fracture type F) in approximately 15% of the open fractures. There is a slight overweight for fractures with calcite in the upper 300 m.

Clay is present in several of the fracture types. Fracture type G, where the clay exists as illite and/or smectite, is found in at least 3% of the open fractures and is common in the upper 150–200 m (Figure 2-13). This observation is consistent with Sandström et al. 2008/ which state that clay minerals such as illite, smectite and mixed layer clay (smectite/illite) are found at various elevations in different boreholes and fracture domains, but are more abundant in open fractures in FFM02 (i.e. the upper 200 metres). Fracture type B where the clay is present as corrensite (swelling mixed layer clay) and

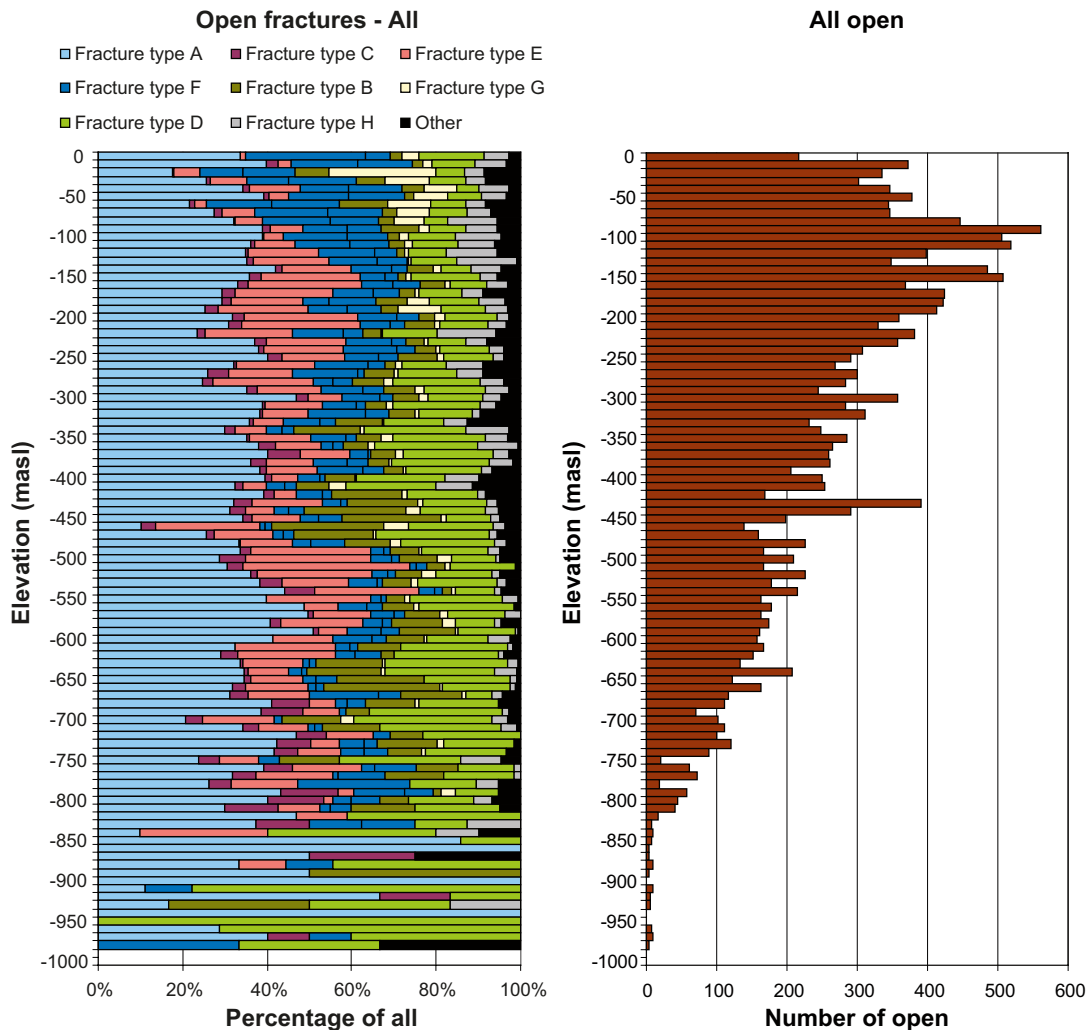


**Figure 2-9.** Relative frequency of different fracture types in all open fractures at various elevations at the Forsmark site, given together with the total number of open fractures. The figures are based on borehole data from Sicada. The apparent variations in the distribution of fracture types observed below elevation –800 metres above sea level is most likely caused by the low numbers of fractures at this depth rather than a real change in the fracture mineralogy.

generally occurs together with chlorite, is not restricted to any particular elevation and constitutes approximately 7% of the total number of open fractures. However, detailed fracture mineralogical studies /Sandström et al. 2008/ show that corrensite might be somewhat underestimated due to difficulties of identification of clay minerals during mapping. Small amounts of clay are also found in e.g. fracture type E, which may explain the relatively low number of fractures classified as fracture type G.

Fracture type E, laumontite ( $\pm$  calcite  $\pm$  chlorite), is common for open fractures, where it constitutes 14%, as well as in sealed fracture networks. It is, however, difficult to determine whether these fractures are originally open or sealed, i.e. if they have broken up as a result of drying processes. This means that the frequency of open, laumontite-coated fractures might be uncertain.

For approximately 6% of all open fractures, no fracture minerals have been found during the mapping. These fractures are to a great extent horizontal to sub-horizontal; i.e. they have a dip less than 25 degrees.

The key fracture domains for the target area are FFM01, FFM02 and FFM06. An illustration of open fractures versus elevation within these fracture domains is shown in Figure 2-10. Noteworthy is the significant differences in FFM01 above and below 350 m.

The fractures in FFM01, FFM02, and FFM06 (Figure 2-11) display the same fracture mineralogy as described for all open fractures above, although the proportion of the different mineral groups varies. This variation is most pronounced for FFM06 and might be due to the relatively low amount of open fractures in this fracture domain. FFM02 has an increased frequency of fractures with calcite as the dominating mineral in the fracture coating (fracture type F). It is difficult to identify any depth dependence of the fracture types in FFM02 and FFM06 respectively. For FFM02 the vertical extension is too limited, for FFM06 because of the lack of open fracture data in this domain. In FFM01, no clear signs of depth dependence have been identified.

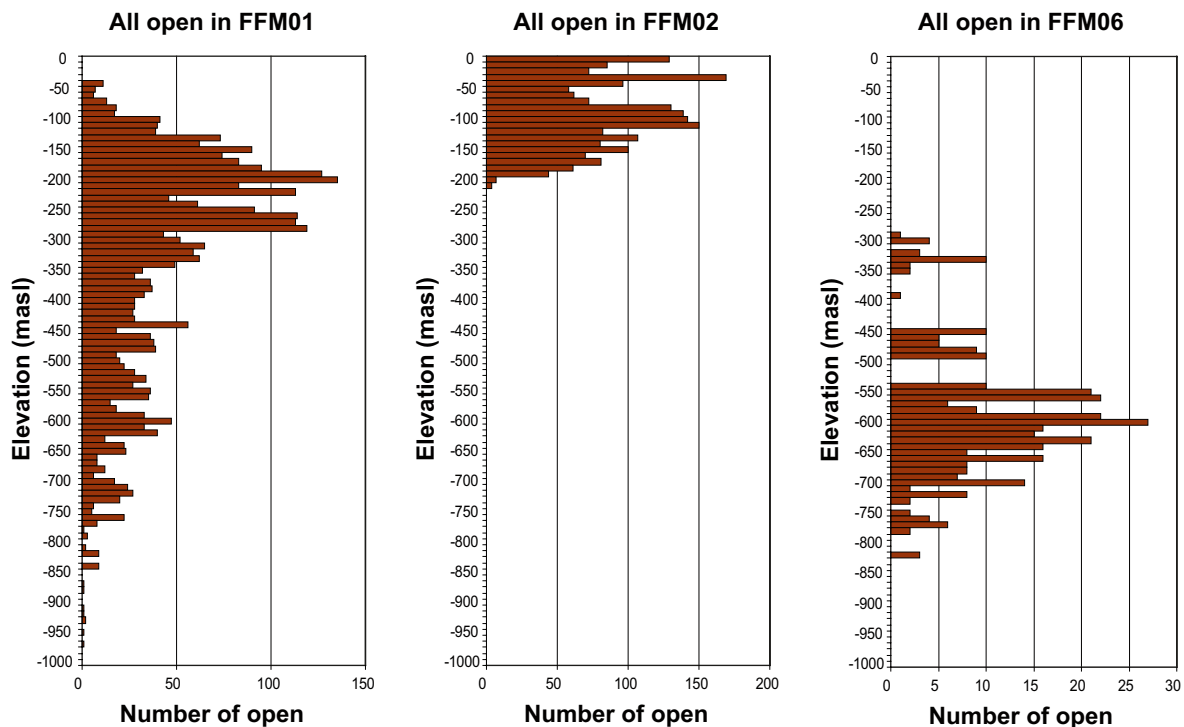


**Figure 2-10.** Number of open fractures within fracture domains FFM01, FFM02 (situated close to the surface) and FFM06 (situated below FFM02). For FFM01 there are relatively great differences in the fracture frequency above and below -350 metres above sea level. Note the different scales in the figure and that the statistical basis in FFM06 is comparatively limited.



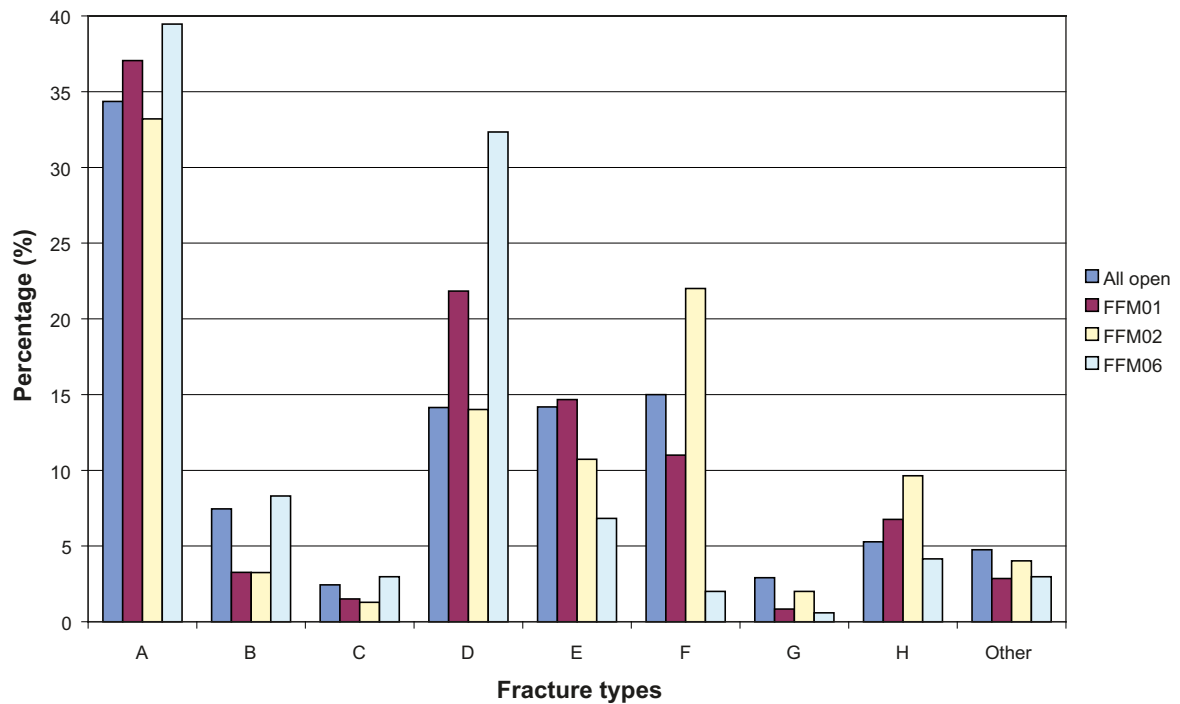


**Figure 2-11.** Distribution of the different fracture types within the fracture domains FFM01, FFM02 and FFM06 respectively, compared to the distribution of fracture types of all open fractures as shown in Figure 2-9 and described in the text.

### 2.2.2 Transmissive fractures

For the retardation model, the hydraulically conductive parts of the rock are of great interest; i.e. single transmissive fractures in the rock matrix between the deformation zones in addition to the transmissive parts of the deformation zones.

The statistics below are based on data available 2007-10-24, involving the cored boreholes KFM01A, KFM01D, KFM02A, KFM02B, KFM03A, KFM04A, KFM05A, KFM06A, KFM07A, KFM07C, KFM08A, KFM08C, KFM08D and KFM10A. A total number of 571 PFL fracture transmissivities (flow anomalies coupled to specific features) measured in open fractures are included. Partly open fractures, crush zones and sections where the increased transmissivity is suspected to be caused by the presence of highly porous rock, are excluded from the dataset.

The distribution of transmissive fractures in each fracture domains shows; 103 PFL fracture transmissivities for FFM01, 81 for FFM02 but no PFL fracture transmissivities at all for FFM06 with its low intensity of open fractures. The distribution of transmissive fractures in deformation zones versus elevation is illustrated in Figure 2-12.

Concerning the mineralogy in transmissive fractures, illustrated in Figure 2-13, the dominating fracture assemblages are chlorite + calcite, chlorite ± others and calcite ± quartz ± pyrite ± other (i.e. fracture types A, D and F), but also fractures with no minerals are relatively common (fracture type H). Only a small number of fractures with laumontite are hydraulically conductive at present. However, the absence of laumontite in transmissive fractures may be due to dissolution of this easily weathered mineral in reactivated older fractures. There is a relatively large span of transmissivity values for all fracture types, generally between  $10^{-10}$ – $10^{-5}$  m<sup>2</sup>/s, except for fracture type H (i.e. no mineral coating) which has a maximum transmissivity value of  $10^{-3}$  m<sup>2</sup>/s due to one single fracture. Nevertheless, the median values for all fracture types within the retardation model (group A–H) are fairly homogenous, approximately  $10^{-8}$  m<sup>2</sup>/s.

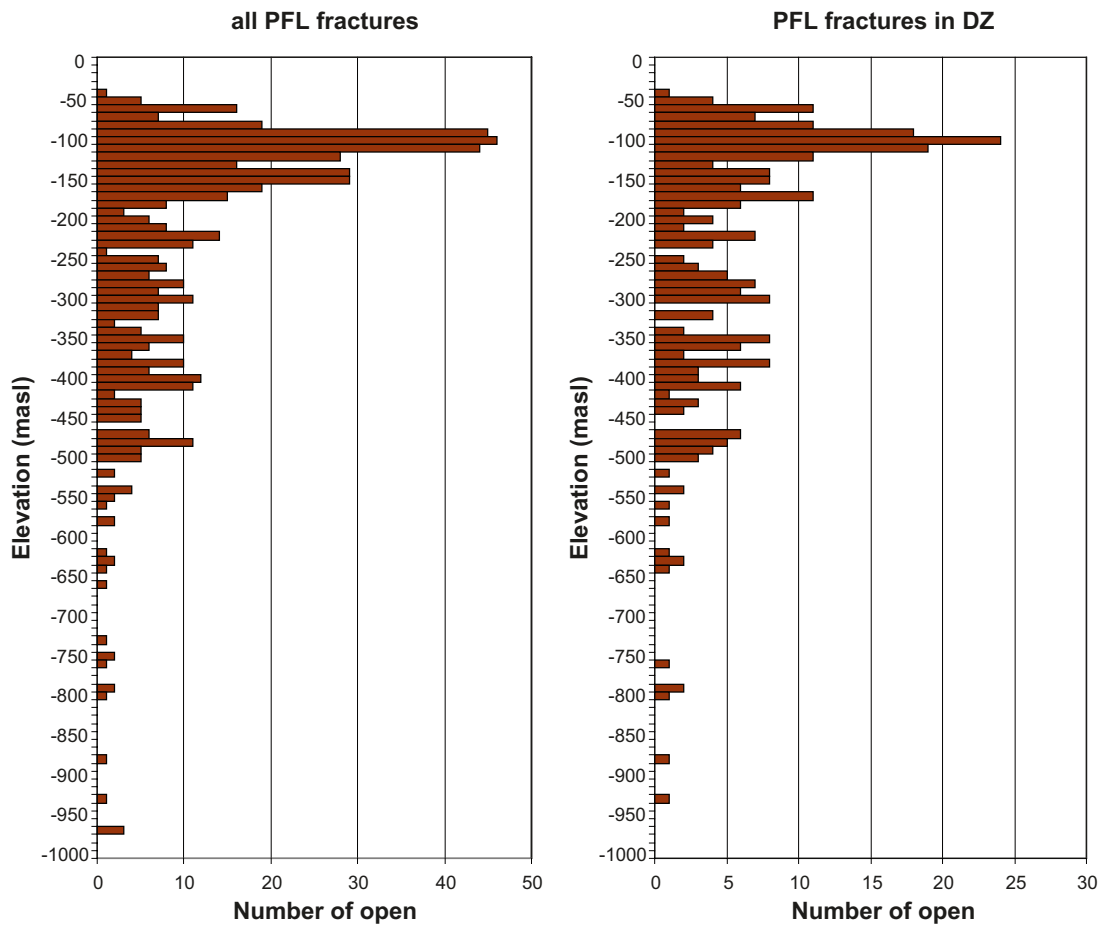


**Figure 2-12.** Distribution of the total number of transmissive fractures at Forsmark (to the left), compared to the transmissive fractures within deformation zones (to the right). The statistic is based on measurements in the cored boreholes KFM01A, KFM01D, KFM02A, KFM02B, KFM03A, KFM04A, KFM05A, KFM06A, KFM07A, KFM07C, KFM08A, KFM08C, KFM08D and KFM10A.

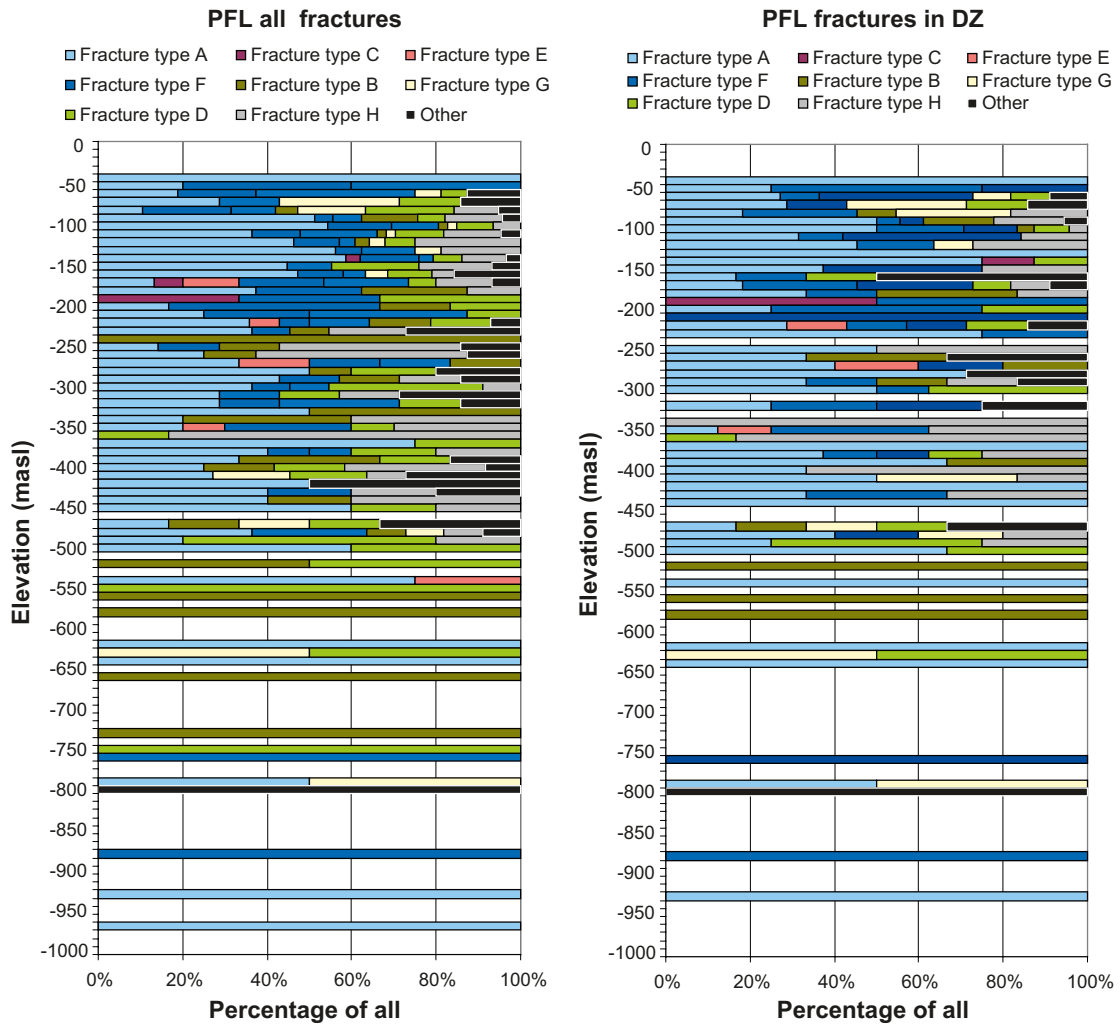


**Figure 2-13.** Mineralogy for the total number of transmissive fractures and transmissive fractures inside deformation zones, respectively, based on data from cored boreholes KFM01A, KFM01D, KFM02A, KFM02B, KFM03A, KFM04A, KFM05A, KFM06A, KFM07A, KFM07C, KFM08A, KFM08C, KFM08D and KFM10A. The apparent variations in the distribution of fracture types observed below elevation –800 metres above sea level is most likely caused by the low numbers of fractures at this depth rather than a real change in the fracture mineralogy.

### 2.2.3 Deformation zones

For the retardation model, four different segments of altered bedrock have been distinguished as recurrent units within (or close to) deformation zones, besides the single fractures (Table 2-4). These units represent both features which are commonly abundant in deformation zones as well as features that are not so common but nevertheless considered to potentially give significant contribution to the total retardation capacity of the deformation zones. The identification of these units was based on macroscopic observations of altered parts of the drilled rock cores during the initial phase of the rock sampling for the laboratory programme. Furthermore, the units can occur individually or together within a deformation zone.

**Table 2-4. Identified segments inside deformation zones sampled for retardation parameters, i.e. deformation zone units.**

<p>1) Strongly altered (tectonized and partly incohesive) wall rock, "fault rock". Altered rock fragments with varied mineralogy dependent on host rock. Chlorite, saussurite and clay are generally present.</p> <p>Potential impact on retardation: Partly very fine-grained material which may have significantly increased surface areas available for adsorption.</p> <p>Estimated occurrence<sup>A</sup>: Sparsely</p>	
<p>2) Sealed fracture networks, mainly with breccia and cataclasite. Different fracture fillings such as laumontite + calcite, epidote, chlorite.</p> <p>Potential impact on retardation: Increased porosity in the sealed fractures may constitute fast diffusion pathways.</p> <p>Estimated occurrence<sup>A</sup>: Relatively common.</p>	
<p>3) Rock exposed to quartz dissolution, Vuggy rock.</p> <p>Potential impact on retardation: Extreme with respect to porosity due to the large voids in the material, may constitute fast diffusion pathways.</p> <p>Estimated occurrence<sup>A</sup>: Sparsely</p>	
<p>4) Oxidized wall rock, mainly medium or strong degree of alteration.</p> <p>Potential impact on retardation: Extreme with oxidized surfaces which may have an impact on adsorption of radionuclides influenced by surface complexation.</p> <p>Estimated occurrence<sup>A</sup>: Relatively common.</p>	

<sup>A</sup> The occurrences are based on judgements by the authors and have not been a subject for elaborate statistical analyses.

Parameterization of deformation zones (DZ) is complicated because of the complexity of the zones. Most of the deformation zones have been reactivated during different geological events and display a wide spectrum of alteration types, brittle and ductile. As described earlier, a deformation zone is divided into transition zones and a core, where the transmissive fractures (if any) often are found in the transition zone, close to the wall rock. A deformation zone might be intersected by several boreholes and yet, it appears in different ways in those intersections (Figure 2-3). The core and transition zone in the deformation zone may contain one or several of the four segments of altered bedrock described in Table 2-4. In addition to this, the fracture frequency and fracture mineralogy varies. Concerning transport properties (sorption, porosity and diffusion), it might be a considerable diversity between these different segments, between the single fractures and finally the combination of all those in the deformation zone. A task during the retardation model work has been to specify how detailed description and parameterization of deformation zones that is required and how detailed it possible can be done. In Figure 2-14, three different ways to deal with these questions are illustrated. In its simplest approach (a) retardation properties could be given to the zone in its entirety as an average of all the geological features involved in the deformation zone. A slightly more sophisticated model (b) could be to divide the deformation zone into high transmissive and low transmissive units and list retardation properties to the different units. The most complicated model (c) would be to also include the different segments/parts of a zone (i.e. core and transition zones).

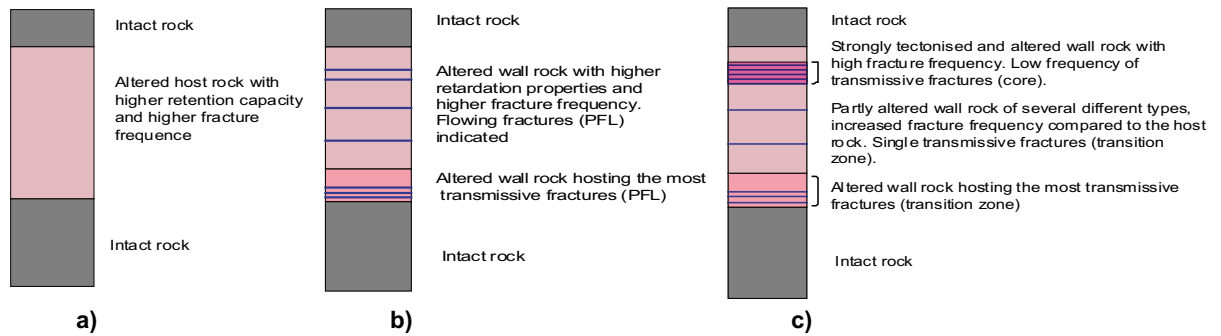


**Figure 2-14.** Schematic illustration of alternative ways to describe a deformation zone with respect to retardation capacity; a) the deformation zone is considered as one unit with higher retardation capacity than the surrounding bedrock; b) the deformation zone is divided into a high transmissive and a low transmissive unit; c) variation including core and transition zone, the latter also divided into a high and a low transmissive unit.

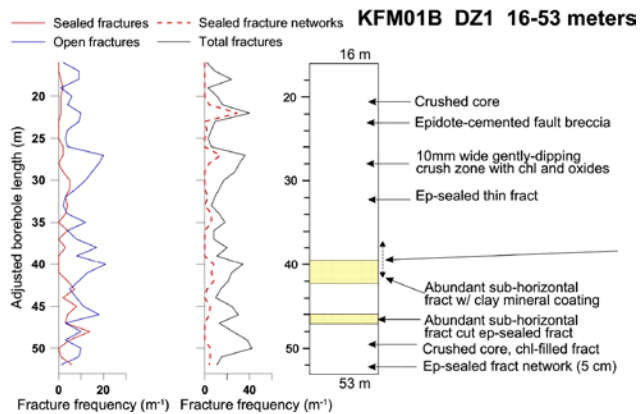
The present report does not specify or give any recommendation of which of the three given alternatives that should be used for transport modelling, but it does outline different ways to include retardation data to the deformation zones in the site description and/or performance assessment. Nevertheless, an example is given below where a parameterization of the ZFMA2 zone is made according to the (c) concept.





Of the mapped deformation zones at the Forsmark site, special attention has been given to the deterministically modelled deformation zones ZFMA2, ZFMENE060A, ZFMENE061A and ZFMNNW0404, which represent different orientations and are located within the target volume. An attempt to describe the retardation properties for these zones has been performed. The methodology for this work is presented below.

1. Summarizing the information about the deformation zones;
  - a) Obtain specific information from single-hole interpretations (SHI) and extended single-hole interpretations (ESHI).
  - b) Recognition of open fracture frequency within the specific deformation zones using mapping data and estimation of the mineralogical distribution of these fractures with the help of single-hole interpretations (SHI) and Sicada.
  - c) Identification of transmissive fractures and/or parts of the deformation zone through PFL data (Posiva flow log, cf. Section 2.2.1) from Sicada.
2. Application of available transport laboratory data (porosity, diffusion and batch sorption experiment) for the core and transition zone within the deformation zones; i.e. data from different fracture types and various types of altered bedrock.

A simplified example from the parameterization of the gently dipping zone ZFMA2, from the intersection in borehole KFM01B (one of six intersections in boreholes), is shown in Figure 2-16. The complexity of the zone and, consequently, the variations in the retardation properties, together with an attempt to quantify the different units are illustrated in this figure. Yet, it should be noticed that there are variations in the observations of the ZFMA2 between the different intersecting boreholes (i.e. KFM01B, KFM01C, KFM02A, KFM04A, KFM05A and KFM10A). According to /Stephens et al. 2007/ and /Nordgulen and Saintot 2006/ the general properties of the ZFMA2 deformation zone can be summarized as consisting of narrower, highly fractured segments (cores) that enclose less fractured rock (transition) in a complex network. The fracture mineralogy are heterogeneous in the zone intersects in different boreholes. In KFM01B, epidote-cemented fault breccia and gently dipping crush fault rock is present. There is a high frequency of sub-horizontal open fractures, at high angles to the borehole axis. The largest transmissivities are found in the upper part of the zone, close to the hanging wall bedrock.

As an example how a deterministic description of a borehole intercept with a deformation zone can be transferred to be used in a retardation model, the zone ZFMA2 intercept in borehole KFM01B is illustrated in Figure 2-15. The zone is described as a unit with an increased frequency of clay-bearing



Fracture type / Deformation zone unit	Percentage of open fracture (n=259) for some of the fracture types in the zone intercept	Percentage of the borehole length in the zone intercept (37 m)
 Fracture type A, Chlorite + Calcite.	10%	
 Fracture type B, Chlorite + Clay ± epidote ± prehnite ± calcite.	12%	
Fracture type D, Chlorite ± other.	15%	
 Fracture type F, Calcite ± quartz ± pyrite ± other.	17%	
Fracture type G, clay ± others.	23%	
Fracture type H and group "others".	12% and 10% respectively	
 Oxidized wall rock, medium to strong degree of alteration (transition zone).		16%
Fault rock (core).		Not estimated* (crush rock 5.5%)
Sealed networks with breccia and cataclasite (core and transition zone).		3%

\* "fault rock" is not a parameter in Sicada, but rock mapped as crushed are supposed to be at least a part of this unit.

**Figure 2-15.** Illustration of the heterogeneity in deformation zone ZFMA2 intersecting borehole KFM01B, 16–53 mbl (named DZ1). To the left; the zone intercept according to /Nordgulen and Saintot 2006/ with fracture frequency  $m^{-1}$  (average for 1 m intervals) and division of the zone into core (marked with yellow, transition zone (white) as well as conspicuous structures. To the right; an estimate to describe the zone with respect to various retardation properties, i.e. percentage of the different fracture types and deformation zone units in the interval. There are no identified flowing features in the intercept as PFL-f logging not has been performed in this borehole.

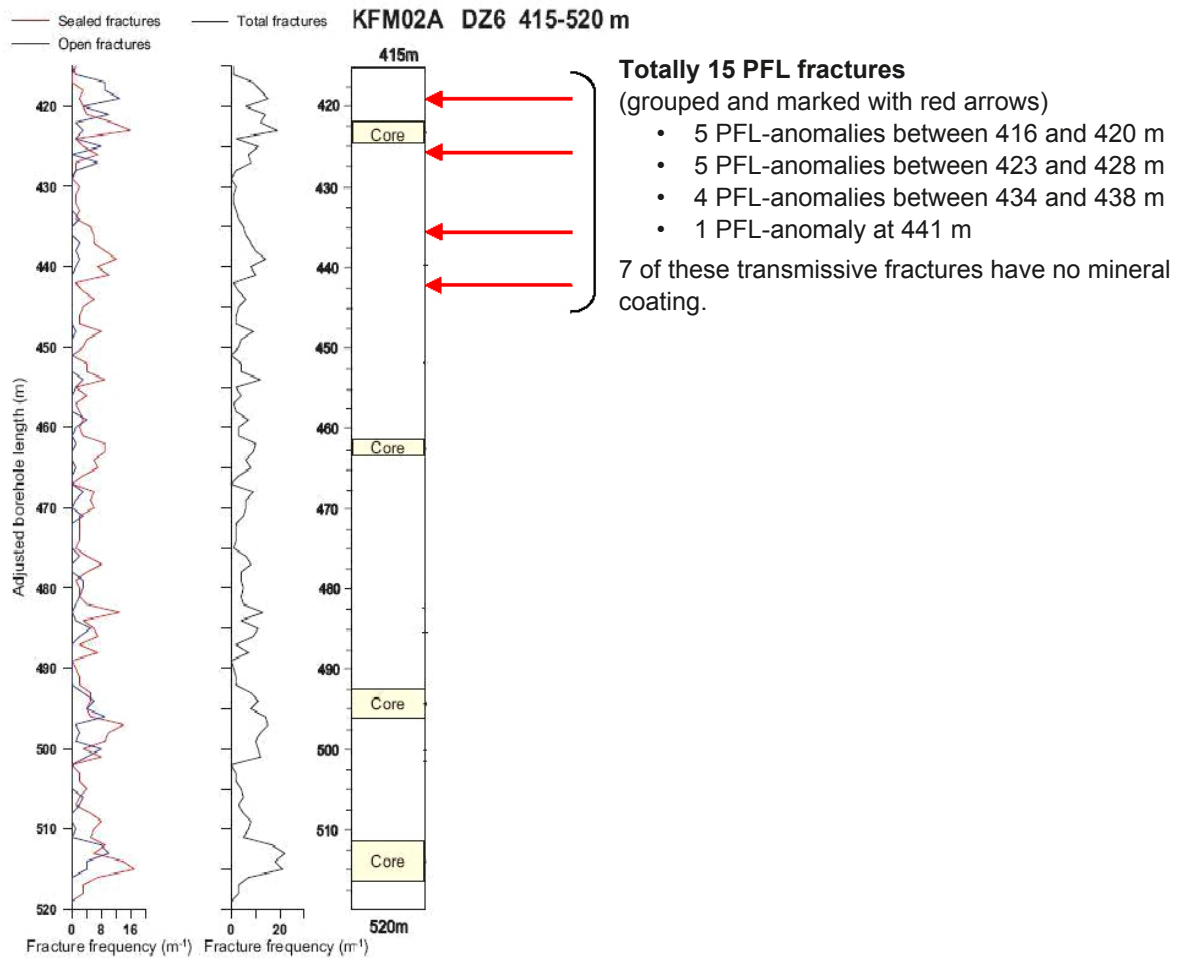


**Figure 2-16.** Simplified illustration of transmissive fractures in zone ZFMA2 where it intersects borehole KFM02A (DZ6 417–442 metres borehole length). The fracture frequency is expressed as an average for 1 m intervals.

fractures (fracture type B and G) in addition to fractures with calcite (fracture type F). The presence of laumontite (fracture type E) and hematite (fracture type C) is very low, less than 1%. Oxidation (red-staining) is common, approximately 70%. However the more intensive degree of this type of alteration, medium to strong, is much lower, approximately 16%. The abundance of the deformation zone unit “fault rock” is difficult to evaluate as the mapping data use several different codes for this rock type. The term *crush* is used in the mapping system for rock core that is incohesive, with rock core pieces not possible to orientate, resembling a network of open fractures. These units are supposed to be comparative to at least parts of the “fault rock” in the retardation model. The frequency of crush rock is approximately 5.5% in zone ZFMA2 where it intersects borehole KFM01B.

There are no available PFL data for zone ZFMA2 in borehole KFM01B, but data from zone ZFMA2 in borehole KFM02A show several transmissive fractures. The distribution of these fractures is illustrated in Figure 2-16 and indicates an overrepresentation of transmissive fractures in the upper part of the zone.

An overview of the data from the zones ZFMENE060A, ZFMENE061A and ZFMNNW0404 /Stephens et al. 2007, Nordgulen and Saintot 2006/ have indicated a similar heterogeneity as for ZFMA2 with respect to both fracture mineralogy and deformation zone units.

## 2.2.4 Hydrogeochemistry

For the laboratory measurements of transport properties it has been important to choose experiment waters that reflects the present water composition at repository depth but also to represent wider ranges of compositions that cover potential variations in groundwater compositions during the future phases of the potential repository. For this reason, four different groundwater compositions were selected for use in the laboratory experiments:

- I. Fresh diluted Ca-HCO<sub>3</sub> water; groundwater currently present in the upper 100 m of the bedrock, but also a water type that can be found at larger depths during late phases of glacial periods.
- II. Groundwater with brackish/marine character, Na-(Ca)-Mg-Cl (5,000 mg/L Cl); This constitutes a large portion of the groundwaters found at 100 to 300 m depth, and it may extend down to 650 m in the more transmissive, gently dipping fracture zones.
- III. Brackish/saline groundwater of Na-Ca-Cl type (5,400 mg/L Cl); this is a water with higher Ca and lower Mg compared to the Type II water.
- IV. Brine type water of very high salinity, Ca-Na-Cl type water with Cl content of 45,000 mg/L; during a glacial period, brine type waters can be forced to more shallow levels than at present.

In all experiments done, synthetically prepared groundwaters were used; naturally sampled groundwater were avoided due to the risk of oxidation and colloid formation because of difficulties to maintain natural reducing conditions during the sampling procedure.

Especially for the batch sorption measurements, the chemical composition of the groundwater is expected to play an important role and attempts were therefore made to mimic the exact chemical composition of these groundwaters. However, for the diffusivity measurements in the laboratory programme, tritiated water (H<sup>3</sup>HO) was the only tracer used and the demand of addressing the groundwater composition in these experiments was not considered necessary. Consequently, a water composition of Type II was chosen for the through-diffusion experiment and only the major components, Ca<sup>2+</sup>, Na<sup>+</sup>, Cl<sup>-</sup> and SO<sub>4</sub><sup>2-</sup>, were included in the synthetic groundwater used in the diffusion experiments.

The compositions of the different groundwaters, type I–IV, are specified in Table 2-5, referring to specific sampling intervals in the boreholes.

**Table 2-5. Groundwater compositions used in the laboratory measurements (methods described in /Widstrand et al. 2003/), Forsmark; concentrations are given in mg/L).**

	Type I (HSH02 0–200m) Fresh water	Type II (KFM02A 509–516m) Groundwater with marine character	Type III (KFM03 639–646m) Saline groundwater	Type IV (KLX02 1,383–1,392m) Brine type water of very high salinity
Li <sup>+</sup>	1.60E–2	5.10E–2	2.80E–2	4.85E+0
Na <sup>+</sup>	1.27E+2	2.12E+3	1.69E+3	7.45E+3
K <sup>+</sup>	2.16E+0	3.33E+1	1.42E+1	3.26E+1
Rb <sup>+</sup>	(2.52E–2) <sup>A</sup>	6.28E–2	3.93E–2	1.78E–1
Cs <sup>+</sup>	(1.17E–3) <sup>A</sup>	1.79E–3	7.09E–4	1.86E–2
NH <sub>4</sub> <sup>+</sup>	(9.47E–2) <sup>A</sup>	4.00E–2	2.04E–1	5.60E–1
Mg <sup>2+</sup>	1.43E+0	2.32E+2	5.27E+1	1.20E+0
Ca <sup>2+</sup>	5.21E+0	9.34E+2	1.47E+3	1.48E+4
Sr <sup>2+</sup>	6.95E–2	7.95E+0	1.69E+1	2.53E+2
Ba <sup>2+</sup>	(1.29E+0) <sup>A</sup>	1.88E–1	9.07E–2	2.40E–2
Fe <sup>2+</sup>	(3.64E–1) <sup>C</sup>	1.20E+0	2.33E–1	3.45E+0
Mn <sup>2+</sup>	2.00E–2	2.12E+0	3.18E–1	1.11E+0
F <sup>-</sup>	3.03E+0	9.00E–1	2.04E–1	(1.60E+0) <sup>D</sup>
Cl <sup>-</sup>	2.15E+1	5.15E+3	5.19E+3	3.68E+4
Br <sup>-</sup>	(2.00E–1) <sup>B</sup>	2.20E+1	3.89E+1	5.09E+2
SO <sub>4</sub> <sup>2-</sup>	8.56E+0	5.10E+2	1.95E+2	1.21E+3
Si(tot)	6.56E+0	5.20E+0	6.28E+0	2.60E+0
HCO <sub>3</sub> <sup>-</sup>	2.52E+2	1.24E+2	2.19E+1	4.20E+1
S <sup>2-</sup>	(1.00E–2) <sup>B</sup>	5.00E–2	2.95E–2	5.00E–2
pH	8.58	7.1	7.55	6.8

<sup>A</sup> No measurements available, data imported from KSH01 #5263.

<sup>B</sup> Based on detection limit.

<sup>C</sup> Based on the Fe-tot measurement.

<sup>D</sup> No measurements available, data imported from KLX02 #2731.



## 2.3 Data from the laboratory programme

Laboratory investigations studying the retardation properties within the Forsmark site investigations /Selnert et al. 2008/ are used to obtain site-specific porosity, sorption and diffusion properties for different rock types and fracture types. Rock core samples for these measurements have been selected, in accordance with /Widstrand et al. 2003/ from several boreholes. Since the laboratory measurements of diffusion and sorption are very time consuming, a majority of the rock samples were collected from the first 6 cored boreholes (KFM01A–KFM06A). In order to describe the heterogeneity of the retardation parameters and the possible effects of stress release, rock samples were also selected from different depths in the boreholes. The selection of samples from open fractures has been controlled by the indications of water flow, as recorded in flow logs, when available. For deformation zones, wall rock alteration in addition to the water flow has been the controlling instruments. A summary of the number of rock samples used in the laboratory programme data (i.e. the quantitative basis for the retardation data in the retardation model) is given in Table 2-6.

**Table 2-6. Number of rock samples used in the laboratory measurements /Selnert et al. 2008/, i.e. the basis for the retardation model presented in this report.**

Method	Total number of rock samples	Number of rock type samples	Number of fracture type samples	Number of samples from deformation zone units
Porosity, by water saturation, cf. Section 3.2.1	211	182*	–	29
Porosity, by polymethylmethacrylate (PMMA) impregnation, cf. Section 3.2.1	13	6	1**	6
Diffusivity, by electrical resistivity, cf. Section 3.3.3	163	142	–	21
Diffusivity, by through-diffusion experiment, cf. Section 3.3.2	72	50	–	22
Specific surface area (BET), on crushed rock, cf. Section 3.4.1	46	29	12	5
Specific surface area (BET), on intact drill core samples, cf. Section 3.4.1	4	4	–	–
Cation exchange capacity (CEC), cf. Section 3.4.2	9	4	2	3
Batch sorption experiment, on crushed rock, cf. Section 3.4.3	17	7	6	4
Batch sorption on intact drill core samples, cf. Section 3.5.1	4	4	–	–

\* Including rock samples with faint to weak oxidation

\*\* Porosity measured across a sealed fracture.

When summarizing the numerical basis and the general outcome of the laboratory programme /Selnert et al. 2008/ it can be concluded that the sample collection is fairly representative with respect to major and minor rock types, different fracture types together with important transmissive deformation zones. Some limitations can, however be identified:

- Because of the time-consuming through-diffusion and batch sorption measurements, it was not possible to include rock core samples from the last stages of the geological and hydrogeological modelling work. This fact gives an overrepresentation in samples from the early boreholes
- It has not been possible to sample material from all fracture types within the retardation model, e.g. batch sorption measurements of the most common fracture coating (Type A, cf. Table 2-3) is missing. The reason for this is the very thin fracture coating which made it difficult to extract enough material for the laboratory measurements.

## 3 Analyses and evaluation of Transport data

This Chapter deals with the task of identifying retardation data (i.e. porosities, diffusivities and sorption coefficients) for the different geological features (i.e. rock types, fracture types, deformation zone units) identified in Chapter 2. The primary source for the data is the report of the Transport laboratory programme /Selnert et al. 2008/ and all data used in this Chapter refers to that report unless stated otherwise.

### 3.1 General model

In this Chapter, the data used (site-specific and/or imported from other works) for establishing the retardation models are described. According to the basic conceptual model for radionuclide retardation, Section 1.2.1, the considered retardation processes can be described as:

- A. Adsorption on surfaces of materials present in or at the fracture walls, which are considered to be directly accessible (no significant diffusion needed) to solutes in flowing groundwater. These fracture surface reactions are considered to be independent of the flow rate and the residence time in the fracture, and can thus be simply described by an equilibrium surface sorption coefficient,  $K_a$  (m). The retardation obtained by this process can be described by a retardation factor,  $R_f$ , defined as:

$$R_f = 1 + \frac{2K_a}{b} \quad (\text{Eq. 3-1})$$

where  $b$  is the aperture of the fracture.

- B. Diffusion into the rock matrix and a potential adsorption on the inner surfaces of the rock material. This process is dependent on the following parameters:
- The amount of inner volume (pores) in the rock matrix that is available for diffusion, i.e. the porosity,  $\theta_m$  (-).
  - The rate at which the radionuclide/solute diffuses in the rock matrix, i.e. the effective diffusivity,  $D_e$  (m<sup>2</sup>/s).
  - The partitioning coefficient describing the distribution of the radionuclide/solute between the inner surfaces of the pores and the water volume of the pores,  $K_d$  (m<sup>3</sup>/kg).

In the time perspective relevant for a final repository, the A process can often be neglected compared to the B process. However, the pure surface retardation process can have an effect on the early arrival in fast flow paths and should therefore also be considered.

#### 3.1.1 Uncertainty in data and statistical representation

Concerning the data for the retardation parameters given to be used in the retardation model, an important issue is the uncertainty and how it should be addressed in this work. One can roughly divide the uncertainty into two parts:

- Uncertainty in the qualitative compartmentalisation of the geological units used in the retardation model, i.e. the judgements made and described in Chapter 2 in this report. These types of uncertainties are often difficult to present in quantitative numbers and must therefore be considered as an underlying conceptual uncertainty which must be generally acknowledged.
- Uncertainty in the numerical values of the experimentally measured retardation parameters.

In this Chapter where the transport data are analysed, the latter uncertainty is addressed. One can easily foresee that with the large number of identified geological units in combination with a realistic experimental programme, the variation and/or uncertainty of the numerical parameters presented will be important.

An important underlying issue in the sampling and investigation of the rock material has been to identify possible extremes, i.e. material with strong deviations from the average values of the different transport properties, e.g. porosity, diffusivity and sorption capacity. This material has almost exclusively been sampled from deformation zones. The rationale behind this sampling strategy is obvious; it is necessary to obtain an identification of specific flow paths in any geologic medium that significantly could contribute to a fast spreading of any dispersed radionuclide. However, from this perspective, one may argue that a general uncertainty has been introduced since it implies an overrepresentation of different deformation zone material compared to its actual occurrence in the rock volume.

Contrary to the earlier version of the retardation model /Byegård et al. 2006/ the uncertainty in the different retardation parameters are given using the approach listed below.

- In the cases where 3 or more measurements have been made of a single parameter, the measurement results are presented as the average value with standard deviation ( $1\sigma$  confidence), the median value and the minimum and maximum values.
- In the cases where only 2 measurement results are available, the average value is given together with the minimum and maximum values.
- In the cases where only a single measurement result is available, uncertainty is (where appropriate) presented using the estimation of the uncertainty in a single measurement. For example, the uncertainty in the sorption coefficients are based on the counting statistics uncertainty in the radioactivity measurements and for the cation exchange capacity (CEC) measurements, the uncertainty is based on the general uncertainty in the ICP-AES measurement of  $Mg^{2+}$ .

The comparatively large variation for some of the parameters causes that the standard deviation in some cases will be larger than the average, which strictly conceptual would involve acceptance of negative values. This is, of course, not the case and the minimum value presented should in these cases be considered as the realistic lower limit of the interval of this parameter value.

One has to acknowledge, however, that a considerable part of the uncertainty involved with a retardation model of this kind is due to the different geological and hydrogeological classifications on which the retardation model relies on. Examples of such classifications are:

- Fracture type classification.
- Groundwater type classifications.

The strict classification of these parameter groups used in this model is certainly a simplification; a large range of intermediates between the different groups do most probably exist. The uncertainty caused by such, most probably, rather subjective decisions are difficult to address in quantitative terms but, nevertheless, has to be acknowledged as an underlying qualitative uncertainty.

Furthermore, the question as to which extent the observations made from a relatively few number of boreholes give a good representation of the whole rock mass is certainly another source of qualitative uncertainty which is difficult to address in quantitative numbers.

## **3.2 Porosity**

### **3.2.1 Methods**

Porosity refers to the volume of the rock that is filled with water and available for diffusion. With the concept used in this work, the porosity is considered in the micro scale to be homogeneously distributed in the rock matrix.

The porosity data used in the site descriptive transport modelling has mainly been obtained from measurements on rock samples aimed for diffusion and sorption studies. The method used for determination (SS-EN 1936) involves drying of the rock samples until constant mass is reached, followed by water saturation in vacuum. The drying of the samples is done at a temperature of  $70^{\circ}C$ , which differs from the temperature ( $105^{\circ}C$ ) used in the method for porosity measurements in the geology programme of the site investigation. The reason for this is that the samples in the transport programme

are designated for other laboratory investigations afterwards. For the interpretation of these laboratory investigations (diffusion and sorption measurements), it is important to avoid the extra chemical and mechanical degradation of the samples that could result from the higher drying temperature.

Estimations of the porosity for the deformation zone units have, due to its general heterogeneity combined with problems with consolidation, been shown to be complicated. For this reason, the mainly used technique for porosity measurement (water saturation) has been complemented using the polymethylmethacrylate (PMMA) impregnation measurement technique /Penttinen et al. 2006/. Using the latter method, a spatial location of the pores as well as spatial porosity distribution information could be estimated.

### **Major rock types**

The results of the porosity measurements are summarized in Table 3-1. The detailed geological characterisation performed using a binocular microscope has shown several samples having small cracks that are 3–15 mm in length and with a width of  $\leq 0.5$  mm, in both fresh and altered rock samples. These cracks are thus larger than intragranular microcracks /Stråhle 2001/, and cut right through mineral grains. Comparison of the porosities determined for samples with and without having observable microcracks (cf. Table 3-1), indicates that these cracks causes an apparently higher porosity.

A dividing of the samples has also been made by respect to their respective location; i.e. whether they originate from deformation zones or not. The results (cf. Table 3-1) indicate that this gives practically no difference in the median values of the porosity. However, there is an indication that there is an overrepresentation of the highest porosity values in the samples from the deformation zones.

For the 101057 rock type, a further division has been performed in which the visible alteration of the samples has been used as a parameter for the porosity interpretation. The results (Table 3-2) show, not very surprisingly, that there is a much higher representation of strong and medium altered rock samples from the deformation zones (9 samples out of 27) compared to samples from outside the deformation zones (4 samples out of 106). It is also shown that the porosities of the altered samples from the deformation zones are higher than the samples without visible traces of strong or medium alteration. However, on the contrary, a similar comparison between samples from the rock outside deformation zones shows no significant increase in porosity for the altered samples. One should, however, consider that especially the latter comparison is based on a quite limited number of samples.

### **Deformation zone units**

Four different deformation zone units have been identified and exposed for diffusivity measurements. The results are presented in Table 3-3 and are summarized below.

- For the Fault rock, (strongly tectonized and partly incohesive material), cf. Figure 3-1, an average porosity of approximately 10% has been estimated using the PMMA technique. The porosity is, however, somewhat heterogeneously distributed, e.g. less altered grains seem to have porosity up to 2%.
- The Sealed fracture network sample (breccia/cataclasite) cf. Figure 3-2, gives an average porosity of 3%, determined by the PMMA technique. A very pronounced heterogeneity of the porosity distribution is found with the large grains having low porosity and the grained matrix in between having regions of very high porosity.
- The strongly altered vuggy rock samples show a very significant increase in porosity compared to all other rock types included in this study. This is of course due to the quartz dissolution that this type of rock has undergone; resulting in “porosity” with mm-scale voids heterogeneously distributed in the rock. In the earlier version of the retardation model, this vuggy rock was named “episyenite” and was considered as one type of alteration of the 101057 rock type. According to the present geological model, this rock type will in this retardation model be considered as a deformation zone unit, since it has been shown to be associated only with deformation zones.
- For the oxidized wall rock (medium and strong alteration), the porosity measurement has been obtained from the results of the 101057 samples which in the stereo microscope investigation was shown to be strong or medium altered, cf. Table 3-3.

**Table 3-1. Porosities (volume-%) of different rock types from the Forsmark area given as the average value with standard deviation, median, min and max values based on the numbers (N) of samples involved in the study.**

Rock type (SKB code)	All rock samples					Rock samples without visible open fractures			
	Zones	Average $\pm \sigma$	Median	Min–Max	N	Average $\pm \sigma$	Median	Min–Max	N
Granite, granodiorite and tonalite, metamorphic, fine- to medium-grained (101051)	Non-def	0.23 $\pm$ 0.09	0.22	0.10–0.54	26	0.23 $\pm$ 0.09	0.22	0.10–0.54	25
	Def	0.55 $\pm$ 0.54	0.38	0.13–1.6	6	0.32 $\pm$ 0.20	0.28	0.13–0.59	4
Granite to granodiorite, metamorphic, medium-grained (101057)	Non-def	0.24 $\pm$ 0.13	0.22	0.03–0.89	108	0.23 $\pm$ 0.11	0.22	0.03–0.89	106
	Def	0.9 $\pm$ 2.2	0.24	0.17–9.19	33	1.0 $\pm$ 2.4	0.22	0.17–9.19	27
Pegmatitic granite, pegmatite (101061)	Non-def	0.40 $\pm$ 0.25	0.27	0.24–0.68	3	0.32	Single sample		1
Amphibolite (102017)	Non-def	0.16 $\pm$ 0.10	0.10	0.08–0.30	5	No samples excluded			
	Def	5.15		0.34–9.95	2	0.30	Single sample		1
Granodiorite, metamorphic (101056)	Def	0.34		0.19–0.48	2	No samples excluded			
Felsic to intermediate volcanic rock, metamorphic (103076)	Non-def	0.36	Single sample		1	No samples excluded			
	Def	0.78	Single sample		1	No samples excluded			
Tonalite to granodiorite, metamorphic (101054)	Non-def	0.16 $\pm$ 0.03	0.16	0.11–0.19	4	No samples excluded			
Granite, metamorphic, aplitic (101058)	Non-def	0.22		0.18–0.26	2	No samples excluded			
Granite, fine to medium-grained (111058)	Non-def	0.32		0.28–0.36	2	No samples excluded			

**Table 3-2. Porosities (volume-%) of the 101057 rock type, based on the alteration of the samples. The alteration analyses were based on the binocular inspection of the individual drill core samples. Samples having observable open fractures have also been excluded.**

Zone type		Average $\pm \sigma$	Median	min	max	N
Non deformation zones	All samples	0.23 $\pm$ 0.11	0.22	0.03	0.89	106
	with observation of medium or strong alteration	0.24 $\pm$ 0.06	0.26	0.15	0.29	4
Deformation zones	without observation of medium or strong alteration	0.23 $\pm$ 0.12	0.22	0.03	0.89	102
	All samples	1.0 $\pm$ 2.4	0.22	0.17	9.19	27
	with observation of medium or strong alteration	2.5 $\pm$ 3.8	0.54	0.18	9.19	9
	without observation of medium or strong alteration	0.25 $\pm$ 0.10	0.22	0.17	0.62	18

**Table 3-3. Porosities (volume-%) of different deformation zone unit from the Forsmark area, given as the average value with standard deviation, median, min and max values based on the numbers (N) of samples involved in the study. The results originate from water saturation measurements, unless stated otherwise.**

Deformation zone unit	Average $\pm \sigma$	Median	Min–Max	N	Comments
Fault rock (strongly tectonized and partly incohesive material)	10	n/a	n/a	1	Determined by PMMA-impregnation /Penttinen et al. 2006/.
Sealed fracture network (breccia/cataclasite)	3	n/a	n/a	1	Determined by PMMA-impregnation, very heterogeneously distributed porosity /Penttinen et al. 2006/.
Vuggy rock	13 $\pm$ 6	16	2.3–19	16	
Oxidized wall rock (medium and strong alteration)	2.5 $\pm$ 3.8	0.54	0.18–9.19	9	Selected from the medium and strongly altered 101057 samples located in deformation zones.

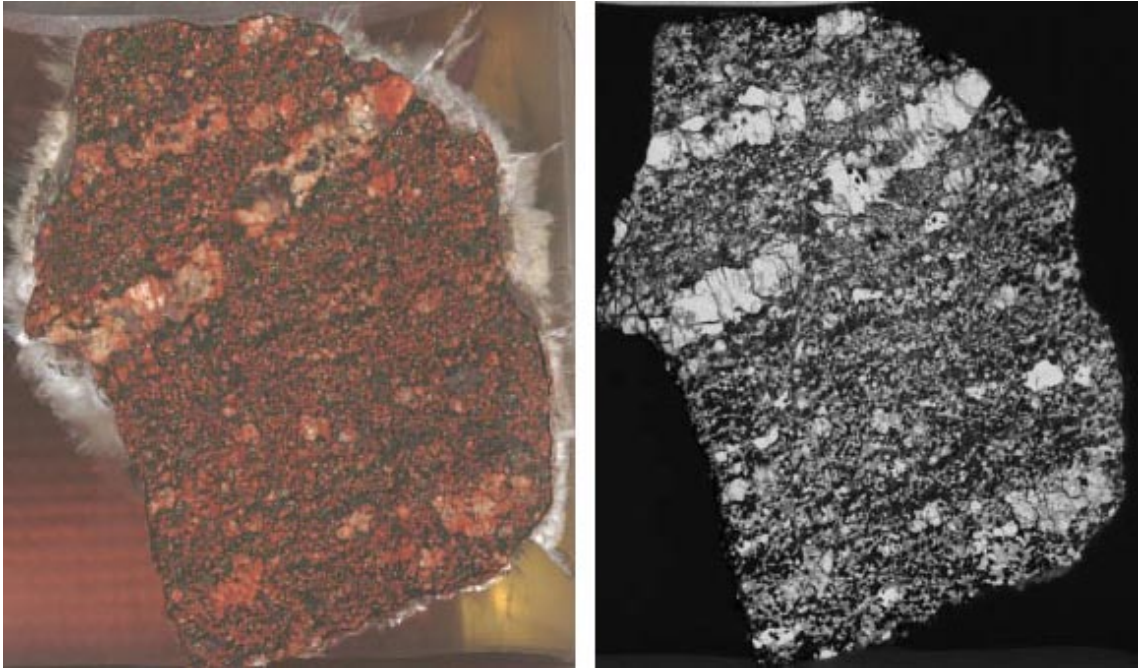


**Figure 3-1.** Photography (left) and corresponding autoradiography for a PMMA impregnated Fault rock sample (strongly tectonized and partly incohesive material).

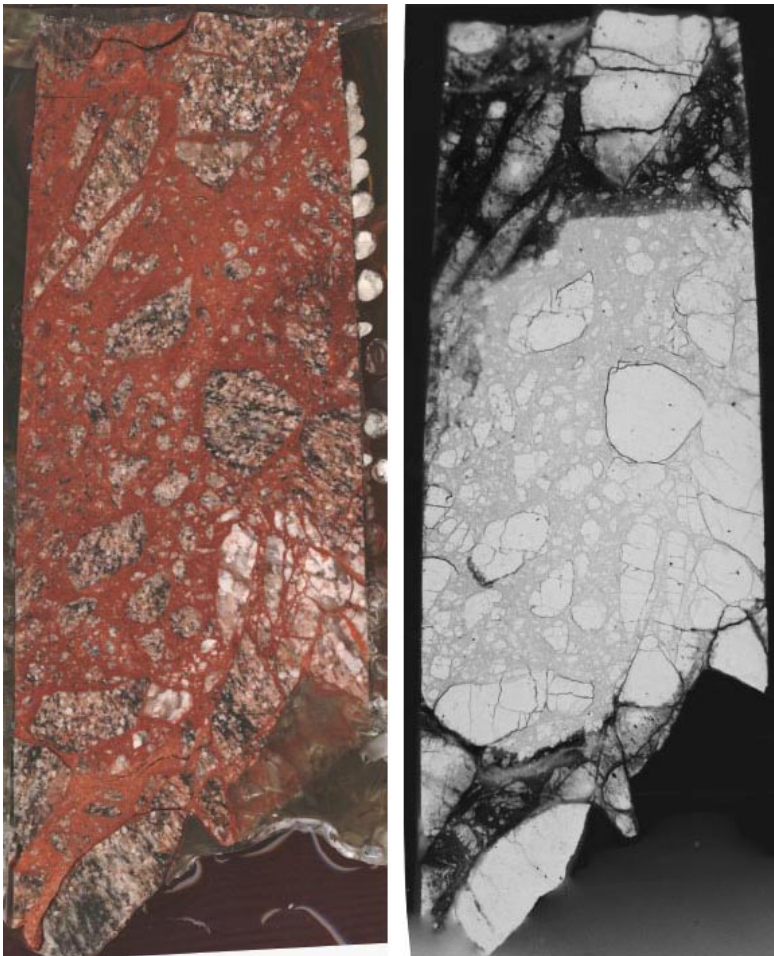


**Figure 3-2.** Photography (left) and corresponding autoradiography for a PMMA impregnated Sealed fracture network (breccia/cataclasite) sample.

### 3.2.2 Statistical representation of the porosity measurements

Since the porosity measurements represent the measurement method with the highest number of samples, an extended attempt to study the statistical representation of the material has been performed with respect to these results. In the study, all the 101057 rock type samples, (however, expelling the deformation zone samples and the samples with open fractures) have been organized using a linear distribution model and a logarithmic distribution model (Figure 3-3). It is indicated that the logarithmic distribution gives a fairly good Gaussian shape which could be regarded as a verification of a log-normal distribution as the best statistical representation of the porosity (and probably therefore also to the closely related parameter, diffusivity). However, it is the opinion of the authors that it is not motivated from these findings alone to consequently in this report use a log-normal distribution neither of the porosity nor of any of the other retardation parameters.

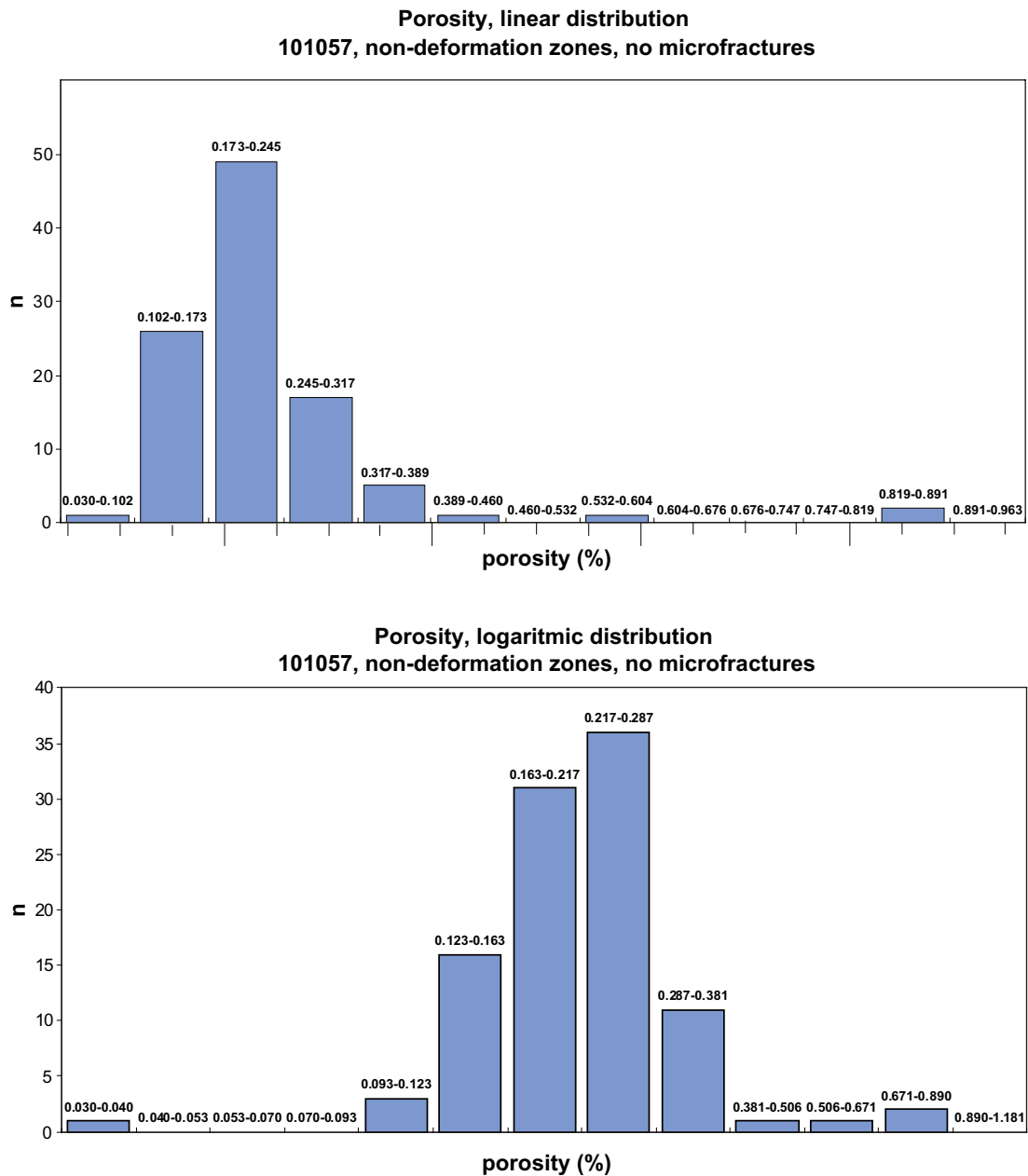


*Figure 3-3. Histograms representing the statistical distribution of the water saturation porosity measurements of the 101057 rock type (numbers, n, of samples with porosity obtained in the given intervals). In the figure above, the intervals have set to obtain a linear representation and, below, in a logarithmic representation.*

### 3.3 Diffusion

#### 3.3.1 Methods and parameters

In this work, the term diffusion refers to the process in which a tracer can diffuse from the fracture water volume into the micro fractures of the rock matrix. Thereby, an interaction can occur in which the inner surfaces of the rock matrix can be available for sorption, and the tracers can be significantly retarded in their transport. This work addresses diffusion processes in the aqueous phase only; potential diffusive mobility in the adsorbed state (so-called surface diffusion /Ohlsson and Neretnieks 1997/) has not been considered.

In this work, primarily two methods are used for the determination of the diffusivity of the rock materials /Widestrand et al. 2003/:

- Through-diffusion measurements; a method where the effective diffusivity,  $D_e$  ( $m^2/s$ ), is determined by studying the diffusion rate of tritiated water ( $H^3HO$ ) through a rock sample ( $H^3HO$  is used in the site investigations; the method can be applied also with other tracer solutions).
- Resistivity measurements; a method where the information on the diffusivity is obtained from the resistivity of electrolyte-saturated rock samples. The concept implies that electrical conduction in the rock can only take place in the electrolyte-saturated pores (no conduction in the crystalline rock) and that the ability of the rock to perform electrical conductance is a similar process to the ability of the tracer to diffuse in the pores.

The diffusion process is quantified in terms of the formation factor,  $F_f$  (-). This parameter quantifies the reduced diffusion rate obtained in the rock material relative to the diffusion rate in aqueous solution. It is thus calculated from the results of the through-diffusion studies, as:

$$F_f = \frac{D_e}{D_w} \quad (\text{Eq. 3-2})$$

where  $D_w$  ( $m^2/s$ ) is the diffusivity of tritiated water in pure water. In this work, a water diffusivity of  $2.1 \cdot 10^{-9} m^2/s$  has been used which is based on /Mills and Lobo 1989/ using a temperature compensation for the somewhat elevated temperatures obtained in the glove box in which the through-diffusion experiments have been performed. It should be noted that solely based on the temperature variation and uncertainty involved therein, one must at least acknowledge an up to 10% additional uncertainty in the values. Nevertheless, this uncertainty is considered to be low compared to the other uncertainties in the concept.

For the resistivity measurements,  $F_f$  is the parameter produced by the method, i.e. the ratio of the resistivity of a given electrolyte to the resistivity of the rock sample with the pores saturated with the same electrolyte.

The resistivity can be measured both in laboratory experiments (where the rock samples are saturated with 1 M NaCl) and in borehole *in situ* experiments. For obvious reasons, no saturation of the rock matrix with a known electrolyte can be done in *in situ* experiments. In this case, the composition of the pore liquid must be estimated based on hydrogeochemical sampling and analysis, commonly assuming the same composition in the matrix as in the groundwater in neighbouring fractures. A further complication is that at a lower salinity than 1 M NaCl, which likely could be present in the pores in rock *in situ* according to /Ohlsson and Neretnieks 1997/ a significant part of the conductivity could be a result of the surface ion mobility, which would overestimate the *in situ* measured formation factors.

#### 3.3.2 Through-diffusion studies

##### **Site-specific data**

Site specific rock materials from the Forsmark site have been sampled and measured using the through-diffusion method according to SKB MD 540.001 (SKB internal document). The determination of diffusivity is performed by studying the diffusion of tritiated water ( $H^3HO$ ) through a slice of rock. A slice of water-saturated rock is mounted in a diffusion cell, where the cell on one side of the rock slice, the start cell, is filled with water spiked with  $H^3HO$  tracer and the cell on the other



side, the target cell, is filled with non-spiked water. The diffusion is determined from the rate of the in-growth of the H<sup>3</sup>HO tracer in the originally non-spiked water volume. The effective diffusivity,  $D_e$  (m<sup>2</sup>/s) and the rock capacity factor,  $\alpha$  (-) is calculated by fitting the model equation:

$$C_r = \frac{C_2 V_2}{C_1 A l} = \frac{D_e t}{l^2} - \frac{\alpha}{6} - \frac{2\alpha}{\pi^2} \sum_{n=1}^{\infty} \frac{(-1)^n}{n^2} \exp \left\{ -\frac{D_e n^2 \pi^2 t}{l^2 \alpha} \right\} \quad (\text{Eq. 3-3})$$

where  $C_2$  (Bq/m<sup>3</sup>) is the accumulated tracer concentration in the target cell at the time  $t$  (s),  $V_2$  (m<sup>3</sup>) is the volume of the target cell,  $C_1$  (Bq/m<sup>3</sup>) is the tracer concentration in the start cell (the low diffusivities gives a concentration decrease that is negligible),  $A$  (m<sup>2</sup>) is the geometric surface area of the rock sample, and  $l$  (m) is the length of the rock sample. The results of the through-diffusion experiments are presented in Table 3-4. For the 101057 rock type, a comparison is made with the corresponding formation factors determined in laboratory resistivity measurements.

From the results (Table 3-4), it can be concluded that formation factors in the range of  $1.0 \cdot 10^{-4}$  to  $1.5 \cdot 10^{-4}$  are observed for the most parts of the non-altered rock types. Exceptions are the amphibolite (102017) which seems to have a somewhat lower diffusivity and felsic to intermediate volcanic rock, metamorphic (103076) which has a somewhat higher porosity than average. A drawback is, however, that except for the more frequent occurring rock types (101057 and 101051) the numbers of measurements are very low and the statistical basis for these observations can be questioned.

An attempt has been made to study the influence of the porosity on the formation factor. The different formation factors determined by through-diffusion experiments are presented in Figure 3-5 as a function of their porosity measured by water saturation technique. As expected, a relationship is indicated and two functions are presented for the interpretation; the Archie law  $F_r = 0.71 \cdot \epsilon^{1.58}$  /Parkhomenko 1967/ and a fit of a similar equation to the actual data in this investigation. However, one must be aware of the fact that the fit is strongly influenced by two groups of materials, on one hand the high number of the low porous rock types (porosity below 1%) and on the other hand the relatively small number of vuggy rock samples with porosities mainly in the range of 10–20%. There are very few samples in between which makes this type of exercise difficult and associated with conceptual uncertainty. Only regarding the area of the low porous rock samples, one can not find any significant trend at all, and the large variation observed is an indication that one has to deal with a sample heterogeneity which probably can not be covered by a simple porosity-diffusivity relation as proposed by e.g. Archie's law or the relationship established by the fit of the experimental values involved in this work.

**Table 3-4. Formation factors ( $F_r$ ) of different rock types from the Forsmark area, determined from the through-diffusion experiment (except for values given within brackets which refer to laboratory resistivity measurements, presented for comparison purposes). The median, min and max values from the numbers (N) of samples involved in the study are presented.**

Rock type (SKB code)	Zones	Average $\pm \sigma$	Median	Min	Max	N
Granite, granodiorite and tonalite, metamorphic, fine- to medium-grained (101051)	Non-def	1.0E-4		4.1E-5	1.6E-4	2
	Def	(2.3 $\pm$ 2.1)E-4	1.5E-4	1.0E-4	7.6E-4	12
Granite to granodiorite, metamorphic, medium-grained. (101057),	Non-def	(1.6 $\pm$ 1.5)E-4	1.2E-4	4.7E-5	6.8E-4	18
		[(3.2 $\pm$ 3.2)E-4]	[2.5E-4]	[6.6E-5]	[2.8E-4]	[83]
	Def	(1.1 $\pm$ 1.0)E-4	5.2E-5	2.5E-5	3.6E-4	14
		[(2.0 $\pm$ 1.2)E-4]	[1.5E-4]	[4.1E-5]	[4.0E-4]	[14]
Deformation zone unit #3, Vuggy rock (101057)	Def	(1.2 $\pm$ 0.8)E-2	1.5E-2	5.2E-4	2.3E-2	12
Amphibolite (102017)	Non-def	2.9E-5	Single sample			1
	Def	2.3E-5	Single sample			1
Felsic to intermediate volcanic rock, metamorphic (103076)	Non-def	5.7E-4	Single sample			1
Tonalite to granodiorite, metamorphic (101054)	Non-def	(7.8 $\pm$ 7.4)E-4	8.1E-5	7.0E-5	8.3E-5	3
Granite, metamorphic, aplitic (101058)	Non-def	1.8E-4		6.2E-5	3.0E-4	2

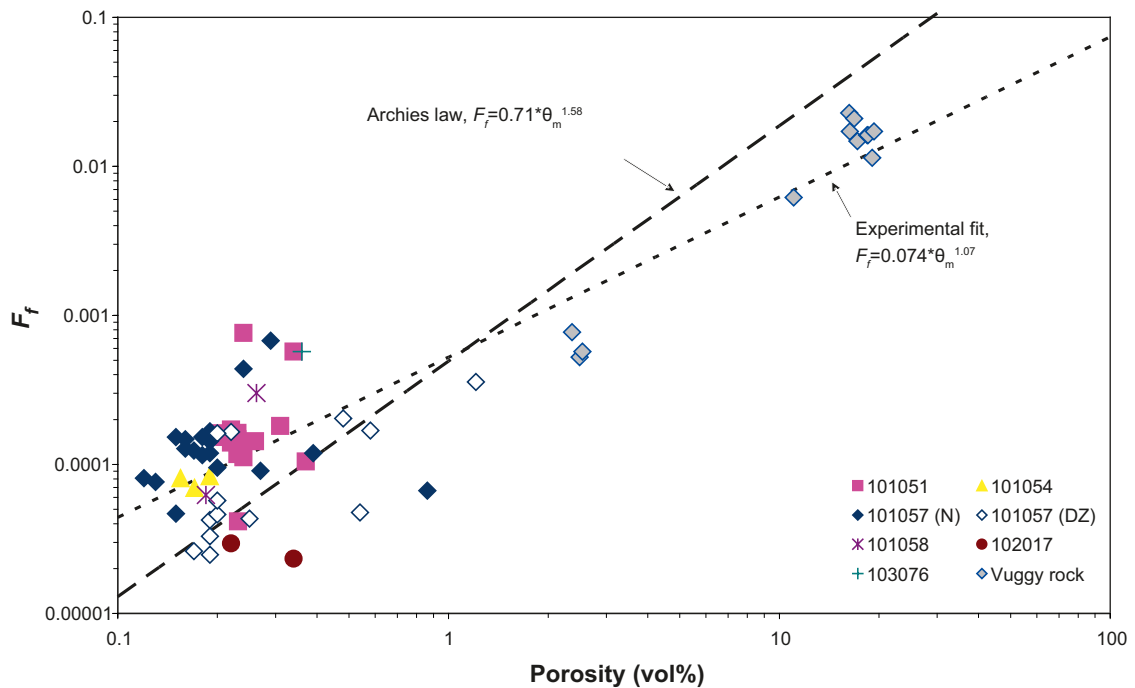


**Figure 3-5.** Formation factor versus the porosity, formation factor determined from through-diffusion experiments. Comparisons are made with a representation of Archies law /Parkhomenko 1967/ and to a fit of a similar equation to the actual results in this investigation. The porosities have been measured using the water saturation method (SS-EN 1936).

### 3.3.3 Electrical resistivity

A comparison of the results of the electrical resistivity measurements reported by /Thunehed 2005ab, 2007ab/ for the 101057 rock type is provided in Table 3-4. Some general observations made from these results are presented in this section.

A thorough investigation has been made where 31 samples, earlier exposed for through-diffusion experiments, were measured for their formation factor by the resistivity measurement method. The results (Figure 3-6) indicate that the resistivity measurements give somewhat higher formation factors compared to the through-diffusion results. There is, however, a large variation in the results; the ratio between the resistivity measurement and the through-diffusion measurement has been found to be  $2.2 \pm 1.2$  based on 33 samples. This could be an indication that surface conduction could be involved in the resistivity measurements. This trend is consistent with the finding of the difference in the formation factors for the rock type 101057 (Table 3-4) where ratios of 2.1 and 2.9 between the median values for the non deformation zone samples and the deformation zone samples, respectively, are found.

Comparisons have also been made between the samples used for through-diffusion experiments and the results of the *in situ* resistivity measurements /Löfgren and Neretnieks 2005ab, Löfgren et al. 2006, Löfgren 2006, 2007/ for the exact location of the sample used in the laboratory investigation. The results (Figure 3-6) show that, opposite to the laboratory resistivity measurements, the *in situ* resistivity measurements give significantly lower formation factors compared to through-diffusion. The ratio between the through-diffusion results and the *in situ* resistivity measurements has been estimated to be  $8.3 \pm 8.9$ , based on 57 samples. Several different explanations for the differences between the results of the different methods are possible, e.g.:

- The drill core samples may have been exposed to stress release which may have caused increased diffusivity for the laboratory methods compared to the *in situ* method. There are earlier works, e.g. /Skagius and Neretnieks 1986/, /Birgersson and Neretnieks 1990/, which have indicated that stress strongly influences the porosity and diffusivity of rock samples.
- Uncertainty concerning the actual pore water composition in the *in situ* electrical resistivity method.
- Possible influence of surface conduction in the electrical resistivity methods.
- Uncertainty concerning the temperature and its influence of the water diffusivity rate, this in combination with the general uncertainty for the tabulated water diffusivity.

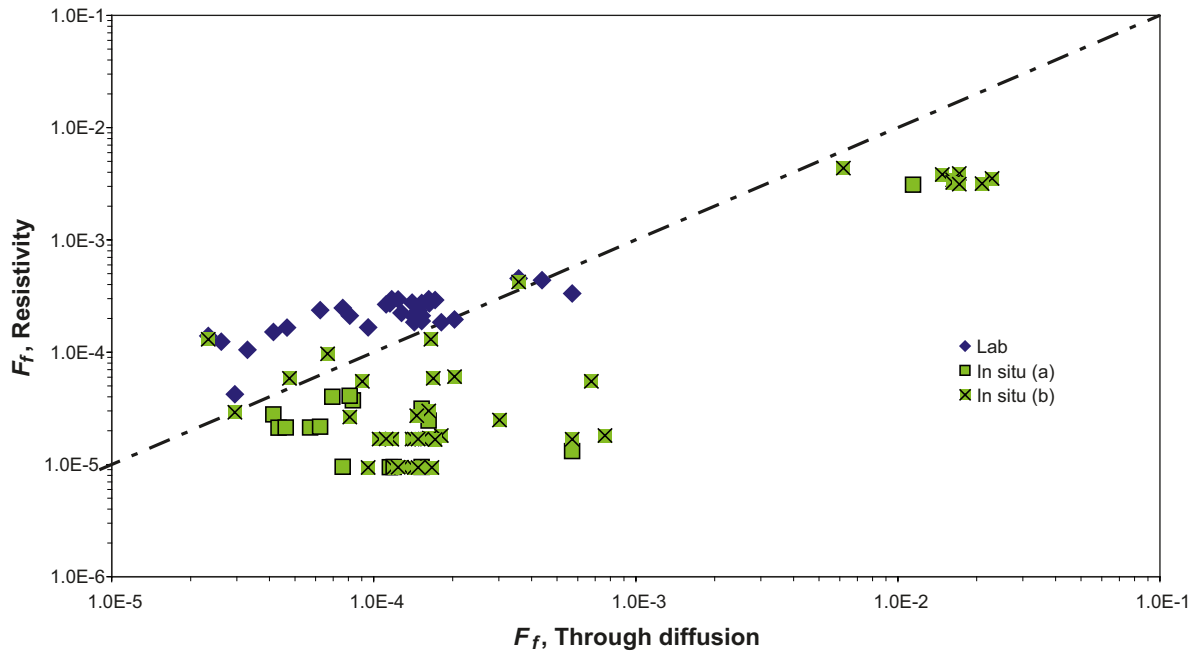


**Figure 3-6.** Comparison of the formation factor determined by the electrical resistivity (Y-axis) and by through-diffusion (X-axis) using the same rock samples. Comparisons between laboratory resistivity measurements and through-diffusion measurements are represented by blue diamonds, while comparisons between in situ resistivity measurements and through-diffusion measurements are represented by green squares. The results from the in situ resistivity measurements have been divided into two groups of measurements namely “In situ (a)” (considered being at an enough distance, more than 0.5 m, from any fracture that could bias the measurement and therefore representative of matrix rock) and “In situ (b)” (considered to be too close to a fracture, less than 0.5 m, and therefore suspected to be influenced by the low resistivity of the fracture itself).

Since the through-diffusion technique is the method that best mimics the actual physical process aimed to be studied, the formation factors which will be presented in the retardation model tables (Chapter 4) in this work are the ones obtained by the through-diffusion measurement. Nevertheless, the possible overestimation of these values due to stress release is acknowledged so an optional decrease of the formation factors in future modelling, e.g. for conservative purposes, could be necessary. It should in this context be mentioned that the retardation tables in Chapter 4 more should be regarded as comparisons of retardation properties between the different geological features and not necessarily as the strictly recommended numerical values of the retardation parameters.

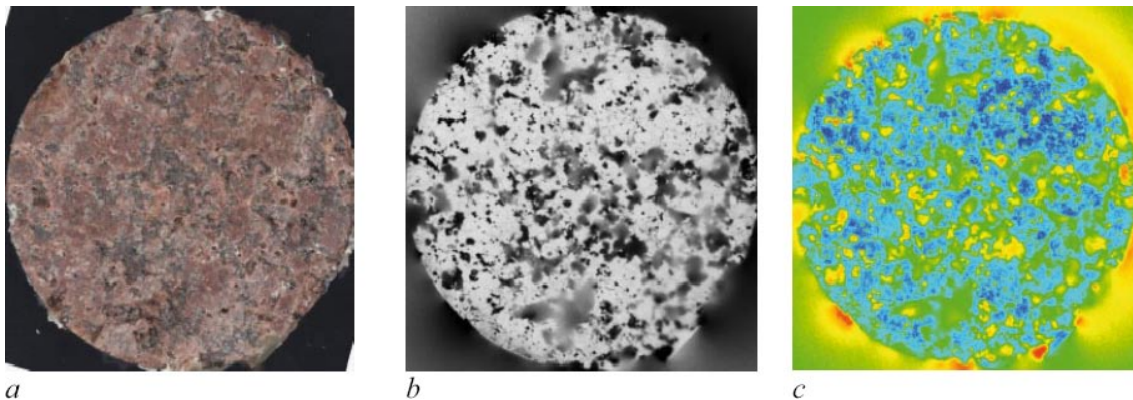


**Figure 3-7.** Photograph (left), autoradiograph of a PMMA impregnated sample (middle) and a porosity distribution illustration (right) of a vuggy rock sample. The average porosity of the sample has been quantified to 10%.

### 3.4 Sorption

The process “sorption” is in this work defined as the adsorptive interaction of radionuclides with the surfaces of the rock material which therefore causes retardation of the transport of the tracer compared to the water velocity. In the somewhat simplified approach taken in this work, sorption is considered to be:

- Linear (i.e. no concentration effect on the sorption).
- Fast and reversible compared to the considered time perspective (no chemical kinetic effects are addressed for the sorption processes).

The concept used for the sorption processes is the same as was outlined in the “laboratory strategy report” /Widestrand et al. 2003/. This means that the source of sorption data will be batch laboratory experiments mainly performed using crushed and sieved rock material. It is outlined that the results from the measured distribution ratio of tracer between the rock and water phase,  $R_d$  ( $m^3/kg$ ), will be interpreted in the terms of:

- Adsorption of the tracers on the outer surfaces of the rock material, determined by the surface sorption parameter,  $K_a$  (m).
- Adsorption of the tracers on the inner surfaces of the rock material, determined by the volumetric sorption parameter,  $K_d$  ( $m^3/kg$ ).

During the progress of this work, it was identified that non-consolidated loose fracture material would play an important role in the retardation process; mainly due to high specific surface area as measured by the BET (Brunauer, Emmet, Teller) method and/or high sorption coefficients. This material was obtained by simple sampling from the fractures in the drill cores (in some cases a careful scraping was used to extract the material) and therefore never underwent any crushing process. It was therefore obvious that a different approach, compared to the crushed material, had to be addressed for the implementation of the sorption results of this material which was used in the sorption experiments in their natural form as it was present in the fractures. Further discussion concerning the strategy for the transfer of laboratory sorption data to the retardation models will be presented in Section 3.4.1.

The sorption properties of the rock material can be regarded as closely related to the active surface and its general ability to interact with solute species. Therefore, measurements of specific surface area (BET surface area, /Brunauer et al. 1938/) and Cation Exchange Capacity (CEC) will give general information on the sorption properties and will therefore also be discussed in the context of sorption.

#### 3.4.1 BET surface area measurements

Since the adsorption of radionuclides is taking place on the surfaces of the rock material, the quantification of available surface areas is a useful proxy for the estimation of the sorption capacity of the rock material. For example, different ferric oxides have significant surface areas and have been shown to be a highly adsorbing mineral for cations that adsorb with surface complexation, see e.g. /Jakobsson 1999/, this of course in combination with the fact that ferric oxides surface groups are strong ligands for surface complexation. Furthermore, the presence of clay minerals (a group identified as a significant potential sink for  $Cs^+$ ) will also cause increased surface areas in the measurements on rock samples.

An establishment of a direct quantitative relationship between the BET-surface and the sorption strength would require detailed knowledge of the exact proportionality of sorptive surface area distributed amongst different minerals. Since literature values of the sorption site densities of a number of surface ligands in various oxides, carbonates and aluminosilicates are available, a detailed knowledge of the mineralogy of the rock sample would together with the results of the BET surface area measurement provide data for determining the total ligand density of the material. However, such an exercise has been considered to be outside the scope of this work and the BET measurements should therefore only be considered as a proxy for sorption capacity of the rock material.

BET measurements have been performed on site-specific materials according to the ISO 9277 standard method. Three types of measurements have been performed for the Forsmark site specific materials.

1. For samples taken from drill core, crushing and sieving has been performed. The size fractions 63–125  $\mu\text{m}$  and 2–4 mm were measured in duplicate samples for each fraction. The results of these measurements are given in Table 3-5. Attempts have also been made to use these results to establish a division of the measured BET surface area,  $A_d$  ( $\text{m}^2/\text{g}$ ), as a sum an inner surface area,  $A_i$  ( $\text{m}^2/\text{g}$ ), of the rock (i.e. the part of the measured surface area which was present in intact rock before it was crushed) and an outer surface,  $A_{\text{out}}$  ( $\text{m}^2/\text{g}$ ), of the rock (i.e. the part of the measured surface area that is associated surfaces obtained during crushing process), i.e.:

$$A_d = A_i + A_{\text{out}} \quad (\text{Eq. 3-4})$$

The concept involves the following assumptions:

- a. Spherical particles of the diameter  $d_p$  (m) are obtained during the crushing process, thus having an outer geometrical surface,  $A_{\text{geo}}$  ( $\text{m}^2/\text{g}$ ), of:

$$A_{\text{geo}} = \frac{4\pi r^2}{m} = \frac{4\pi r^2}{\rho V} = \frac{3}{\rho r} = \frac{6}{d_p \rho} \quad (\text{Eq. 3-5})$$

where  $r$  (m) =  $d_p/2$  is the average radius of the particle,  $m$  (g) =  $\rho V$  is the mass of the particle,  $V$  ( $\text{m}^3$ ) =  $4\pi r^3/3$  is the volume of the particle and  $\rho$  ( $\text{g}/\text{m}^3$ ) is the density of the rock.

- b. The amount of inner surfaces remains the same after the crushing process and is independent of the size fractions.
- c. The amount of outer surface areas created during the crushing process is proportional to the geometrical outer surface of the presumed spherical particles, i.e.:

$$A_{\text{out}} = kA_{\text{geo}} = \frac{6k}{d_p \rho} \quad (\text{Eq. 3-6})$$

Inserting (Eq. 3-6) into (Eq. 3-4) gives:

$$A_d = A_i + \frac{6k}{d_p \rho} \quad (\text{Eq. 3-7})$$

where  $k$  (-) is a proportionality constant between the geometric surface area and the BET surface area (cf. Equation 3.6). A graph of the measured BET surface area as a function of  $1/d_p$  will thus give a line with an intercept corresponding to inner BET surface are ( $A_i$ ) and a slope corresponding to  $6k/\rho$ . Examples of such representations are given in Figure 3-8 and a summary of the evaluated  $A_i$  for 101057 rock type are given in Figure 3-9.

2. For natural fracture samples, scraping of the fracture surfaces was performed and the  $<125 \mu\text{m}$  fraction was isolated through sieving of the scraped material and measured in duplicate samples. The results of these measurements are given in Table 3-6.
3. Attempts have been made for a few number of samples to measure the BET surface area for non-crushed pieces of drill core, i.e. more or less intact rock. The results are presented in Figure 3-9.

### **Comparison of the results for different rock types**

The results of the BET surface area measurement are presented in Tables 3-5 and 3-6. The major finding is the large difference between the non-altered samples and the rock material from fractures. The latter group has in this work a larger representation of samples in the small size fraction which, due to geometrical reason, is presumed to give higher BET surface areas. Nevertheless, comparisons of the results within the smaller size fractions groups (Figure 3-8) show that fracture filling material in several cases gives up to 50 times higher surface areas than e.g. the major rock type 101057. From these results alone, it can be assumed that the rock material in or adjacent to the fractures could constitute a considerable source for adsorption of radionuclides in the performance assessment. However, since the amounts of these fracture filling material in most cases are rather low (indicated by the estimated thicknesses of these layers, cf. Chapter 4), their relative importance in comparison to the rock matrix in the long term scale is more doubtful.

**Table 3-5. Measured BET surface area (m<sup>2</sup>/g) for the fractions 0.063–0.125 mm and 2–4 mm.**

Rock type (SKB code)	2–4 mm size fraction				0.063–0.125 mm size fraction			
	Average ± σ	Median	Min–Max	N	Average ± σ	Median	Min–Max	N
101051	0.023±0.014	0.024	0.002–0.048	14	0.22±0.12	0.24	0.009–0.34	14
101057	0.025±0.015	0.026	0.0003–0.058	27	0.19±0.06	0.19	0.07–0.29	27
101057 medium alteration	0.342		0.335–0.349	2	0.738		0.732–0.745	2
101054	0.042		0.036–0.049	2	0.27		0.25–0.29	2
101061	0.052		0.048–0.055	2	0.307		0.296–0.318	2
101061 def. zone	0.02		0.005–0.030	3	0.233		0.227–0.239	2
102017	0.0002 <sup>A</sup>		0.0001–0.0004 <sup>A</sup>	2 <sup>A</sup>	0.051±0.050	0.052	0.007–0.095	4
102017 def. zone	0.038		0.038–0.039	2	0.316		0.304–0.327	2
101058 def. zone	0.052		0.049–0.055	2	0.183		0.182–0.184	2
103076	0.046		0.042–0.051	2	0.205		0.203–0.207	2

<sup>A</sup>Two measurements below the detection limit (<0.0001 m<sup>2</sup>/g) has not been included.

**Table 3-6. Measured BET surface area (m<sup>2</sup>/g) for the fractions 0.063–0.125 mm and 2–4 mm.**

Description	2–4 mm size fraction				<0.125 mm size fraction				
	Average ± σ	Min	Max	N	Average ± σ	Median	Min	Max	N
Fracture type A					0.49		0.41	0.56	2
Fracture type B					10.3		10.0	10.6	2
Fracture type C					2.3±0.6	2.4	1.7	2.9	3
Fracture type D					5.1±2.2	4.0	3.7	7.7	3
Fracture type E					0.42±0.02	0.43	0.39	0.43	4
Fracture type F	2.98			1	2.2±1.1	2.0	1.2	3.3	3
Fracture type G	1.67	1.66	1.68	2	4.3		3.3	5.3	2
Deformation zone unit, type 1: Fault rock (strongly tectonized and partly incohesive material)	1.98	1.94	2.0 <sup>2</sup>	2	5.6±2.3	5.6	3.6	7.6	4
Deformation zone unit, type 2: Sealed fracture network (breccia/cataclasite)	0.78	0.69	0.88	2	0.64		0.61	0.67	2
Deformation zone unit, type 3; Vuggy rock	0.27	0.26	0.28	2	1.58		1.57	1.59	2
Deformation zone unit, type 4; Oxidized wall rock	0.195	0.189	0.202	2	0.77		0.76	0.78	2

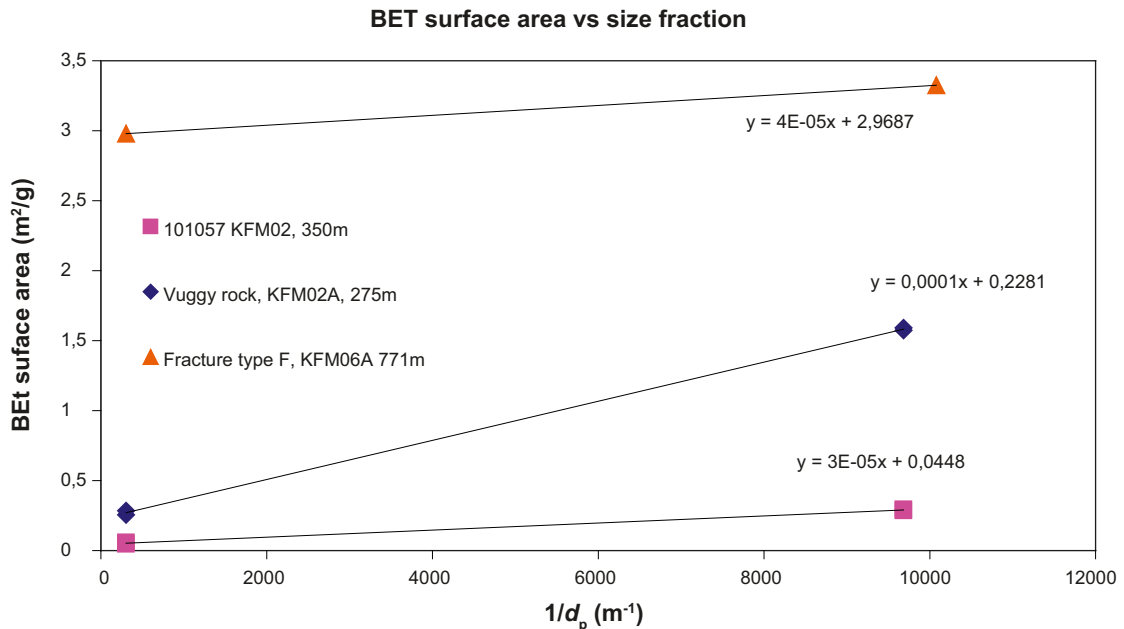


**Figure 3-8.** Examples of results of BET surface area measurements as a function of the inverse of the particle size of the rock material used.

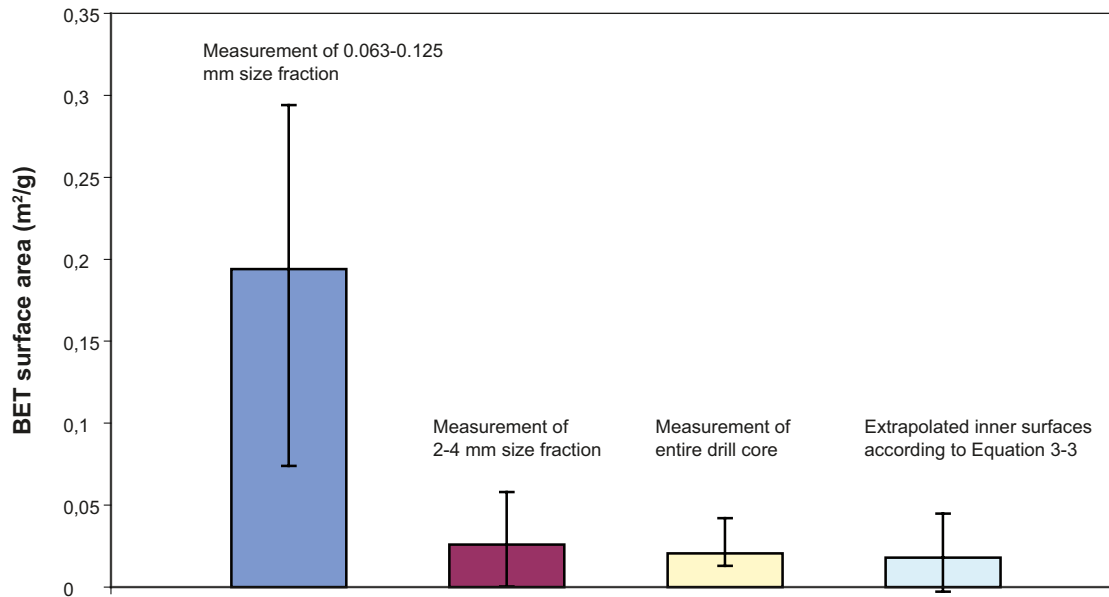


**Figure 3-9.** Comparison between the results of the total number of BET surface area measurement of the 101057 rock type. The values are the median values and the error bars show the uncertainty represented by the minimum and maximum values obtained for all the measurements.

### BET surface area versus particle size

One main purpose of the BET surface area measurements of the crushed rock samples was to estimate the amounts of surfaces created during the crushing process; surfaces that therefore can not be regarded as representative for intact rock. Such surfaces will therefore give increased amounts of surfaces in the batch sorption experiments which are not representative for intact rock and an overestimation of the sorption capacity can therefore be expected.

In the laboratory strategy document /Widstrand et al. 2003/ for the batch sorption experiment, it is stipulated that:

- If it can be established that the largest size fraction (2–4 mm) has a surface area larger than 75% of the surface area of the smallest size fraction (0.063–0.125 mm), it means that only a negligible increase in the total amount of surfaces of the rock material is obtained during crushing and that the major part of the surfaces in the crushed material is representative of the intact rock. The tracer distribution coefficient should then be independent of the size fraction and, in order to avoid diffusion impact, the smallest size fraction is used and the obtained tracer distribution coefficient ( $R_d$ ) could thus directly be input as the  $K_d$  for the rock material.
- In the case where the BET-measurements show that the surface area of the largest size fraction (2–4 mm) has a surface area of less than 75% of the surface area of smallest size fraction (0.063–0.125 mm), it is concluded that a significant part of the surface area in the smaller fraction is caused by the crushing of the rock material and is therefore not representative of the intact rock. For the results of the batch experiments, it is therefore assumed that the sorption obtained is a sum of the:
  - o Interaction with the inner surfaces (representative of the intact rock).
  - o Interaction with the outer surfaces (not representative of the intact rock).

In order to differentiate between these two processes, three different size fractions were proposed to be used for the batch sorption experiment (0.063–0.125 mm, 0.25–0.5 mm, 1–2 mm) and extrapolations of the results were to be performed according to:

$$R_d = K_d + \frac{6K_a}{d_p \rho} \quad (\text{Eq. 3-8})$$

which is analogous to the concept of distinction of inner and outer surfaces in the BET surface area measurements, cf. Equation 3-7. As can be seen in Figures 3-8 and 3-9, it is obvious that a significant increase in the total surface area is obtained with decreased particle size. Except for the

fracture type F material, the increase from the largest size fraction to the smallest size fraction is far much higher than 25%, i.e. the limit for when the extrapolation concept should be used according to the laboratory strategy set up by /Widestrand et al. 2003/. It is indicated that the increase is more pronounced for the crushed fresh rock material than for fracture material and/or altered rock material. The increase is however generally lower than what should be expected for ideally spherical shaped particles since a strict geometrical model would yield an increase of the specific surface area by a factor of 32 from the 2–4 mm size fraction to the 0.63–125  $\mu$ m size fraction. This deviation could be regarded as an indication of presence of a significant part of the surfaces in the larger size fraction being “inner surfaces”. An alternative explanation could be that the surface roughness is not constant as a function of the particle size.

When considering the comparatively high number of samples investigated of the major rock type, 101057, a rather high variation is nevertheless observed. This observation is valid both for the measured values within a size fraction as well as for the ratios between the two measured size fractions. Provided that the BET surface measurement procedure gives reliable values, this could be an indication of a considerable heterogeneity even within what is identified as a single rock type. The large BET-surface area measured for the strongly altered 101057 rock type (5–10 times higher than for corresponding non-altered rock), could indicate that an influence of alteration on the BET surface area occurs even on samples where the alteration is almost impossible to observe by only using ocular methods.

A comparative measurement campaign was performed in which crushed material in the size fractions 0.063–0.125 mm, 2–4 mm and intact drill core samples with a diameter of 50 mm were measured for their BET surface area. The results (Figure 3-9) show that a reasonable agreement (given the uncertainties) is obtained for the large size fraction, the intact drill core and a size fraction extrapolation of inner and outer BET surface area (cf. Equation 3.7). One may from this finding postulate a conceptual model for the interaction of the intact rock in which the matrix diffusion in the intact rock mainly takes part in a network of pores surrounding mineral grains in the size of 2–4 mm with increased surface roughness compared to a spherical shape. If applying such a concept, one would preferably use the batch sorption experiment results from the largest size fraction and use the measured tracer distribution coefficient,  $R_d$ , for that fraction as the  $K_d$ . This means that for the larger size fractions, the  $6K_d/d_p\rho$  term of Equation 3-8 can be neglected and the equation can thus be written as:

$$R_d \approx K_d \quad (\text{Eq. 3-9})$$

### 3.4.2 Cation exchange capacity (CEC)

The method applied for the measurement of CEC of the rock material is the ISO 13536 which consists of:

1. A saturation of the cation exchange sites with  $\text{Ba}^{2+}$  from a 1M  $\text{BaCl}_2$  solution buffered to pH 8.1.
2. An optional step in which the amount of leached cations from the saturation step is specified and measured.
3. A desorption step in which the solid phase is contacted with a 0.02M  $\text{MgSO}_4$  solution, in which the adsorbed  $\text{Ba}^{2+}$  is expected to exchange with  $\text{Mg}^{2+}$  followed by a precipitation of the very insoluble  $\text{BaSO}_4$  (s). The concentration of  $\text{Mg}^{2+}$  is thereafter measured and the decrease in the concentration is thus a measure of the capacity of the solid material to adsorb cations, i.e. the cation exchange capacity (CEC).
4. Optionally, the amount of desorbed cations in step 2 can be compared to the concentration in the naturally abundant groundwater. The ratio of these two measures can be regarded as a sorption distribution coefficient  $K_d$  ( $\text{m}^3/\text{kg}$ ), a quantity which normally is obtained by batch sorption experiments, cf. Section 3.4.3.

However, one should be aware of that for some of the materials studied, the demand of 5–10 g of material could, due to material shortage, not be fulfilled. This resulted in a less sensitive measurement and, consequently, larger uncertainties in the results. Furthermore, the material shortage did not allow triplicate samples; therefore all results reported are based on single samples.



The CEC measurements are in the original laboratory strategy document identified as a rather important parameter for obtaining a general sorption capacity of the rock material and therefore acting as a bridge between the batch sorption methods and a related method obtainable in a standardized form (ISO 13536). However, it was soon realized that the CEC methods were mainly aimed for soil investigations and therefore not likely to be sensitive enough for rock material with much lower CEC than soil. The CEC method was therefore instead decided to be a comparative method only applied on a very limited number of rock materials.

The results of the CEC measurements are given in Table 3-7. There are comparatively high uncertainties associated with the method; mainly due to the fact that only a very small part of the  $Mg^{2+}$  is adsorbed in step #3 which makes it difficult to verify a small concentration decrease from a blank solution (up to 5% uncertainty in  $Mg^{2+}$  concentration determination is reported, (personal communication Analytica 2008)). For this reason, no CEC can be statistically verified for the majority of the fresh rock types.

As expected, a higher CEC can be observed for the fracture material compared to the samples consisting of fresh rock; a difference of a factor larger than 10 is indicated. This is also valid for the fault rock material and the sealed fracture material which also have higher CEC than the fresh unaltered rock. This difference is, however, smaller than the corresponding difference in BET surface area, where corresponding differences of a factor larger than 100 could be observed. A general comparison of the CEC to the BET surface area is presented in Figure 3-10. The relationship between these two parameters is far from linear; however, the obvious conclusion that larger amounts of surface areas increase the capacity of binding cations is supported.

The amounts of desorbed cations from the saturation process in the CEC measurements are also given in Table 3-7. For the majority of the samples, the desorbed amount of the dominating cations (i.e.  $Na^+$ ,  $K^+$ ,  $Mg^{2+}$  and  $Ca^{2+}$ ) was found to be below the detection limit, which could be expected due to the relatively low CEC. However, for the rock materials where the dominating cation  $Ca^{2+}$  could be quantified, a summation of the desorbed cations has been performed and is presented in the table. Under ideal conditions, these measurements should be identical. Generally, the amount of desorbed cations is close to the measured CEC, with the exception for the 101051 rock where the amount of desorbed cations strongly exceeds the CEC, for reasons that are not known. A possible explanation is that traces of calcite could be dissolved during the saturation process, i.e. implying that parts of the  $Ca^{2+}$  in the adsorption solution has not been desorbed by the cation exchange leaching process.

Measurements of e.g. the Cs desorbed during the saturation step of the CEC measurement will provide the total amount of Cs adsorbed in the rock material by cation exchange. From this concentration and the concentration of Cs in the aqueous phase, the sorption coefficient ( $K_d$ ) for the material can be calculated. This coefficient should under ideal conditions be identical to the sorption coefficient determined by the batch sorption experiment technique (dealt with under Section 3.4.3). Comparisons have been made of this type of  $K_d$  relative to the batch sorption  $K_d$  for all materials that were exposed to CEC measurements. In these calculations, it was assumed that all cation exchanged Cs was desorbed during the Ba saturation step and that this rock material was (before sampling) in contact with porewater with the same composition as the saline Forsmark groundwater.

The results of these calculations are presented in Figure 3-11. As can be seen, a general trend is that sorption coefficients for Cs determined using the desorption method gives higher  $R_d$  than the corresponding  $R_d$  measured using the batch sorption method, i.e. more Cs is leached from the rock material than what would be expected from the batch sorption results. The only exception to this trend is two samples of crushed materials from the smallest size fraction, where the amount of desorbed Cs is far much lower than what would be expected from the batch sorption results. This can be regarded as a support for the conclusions made from the results of the BET surface area measurements (Section 3.4.1), i.e. the surfaces created during the crushing process are not equilibrated with Cs adsorbed by cation exchange. However, large variations are observed in the concentrations of desorbed Cs, which indicates that this method could be questionable. A possible source of error could be that small fragments of the intact rock (e.g. colloids) are not fully separated from the water phase.

**Table 3-7 CEC characteristics of different Forsmark rock material.**

Rock material	Size fraction (mm)	Position (borehole, length)	CEC <sup>A</sup> (cmole/kg)	Desorbed amount of cations <sup>B</sup> cmole/kg)	
<i>Rock types</i>					
101057	0.063–0.125	KFM01A, 103.46	0.9±0.7	1.4	
		KFM01A, 487.10	0.7±0.6		
		KFM01A, 908.36	<0.6		
		1-2	KFM01A, 103.46		<1.0
		KFM01A, 487.10	<1.2		
101051	0.063–0.125	KFM01A, 908.36	<0.9		
		1-2	KFM02A, 552.00	2.6±2.0	33
		KFM02A, 552.00	<1.2	6.1	
<i>Fracture materials</i>					
Fracture type B	<0.125	KFM10A, 144.51	15±10	43	
Fracture type E	<0.125	KFM07A, 121.03	18±5	16	
<i>Deformation zone units</i>					
#1 Fault rock	0.063–0.125	KFM01B, 47.72	20±5	12	
		1-2	KFM01B, 47.72		9±1
#2 Sealed fracture network	0.063–0.125	KFM05A, 611.98	5.4±2.4	13	
		1-2	KFM05A, 611.98		4.1±1.8
#3 Vuggy rock	1-2	KFM02A, 275.22	<0.4		

<sup>A</sup> Uncertainties and detection limits are based on the estimation that the Mg<sup>2+</sup> quantification is associated with a 5% uncertainty.

<sup>B</sup> Values are only given for the samples where the desorbed amount of Ca<sup>2+</sup> (the cation that occupies the major cation exchange sites) has been reported to be above the detection limit.

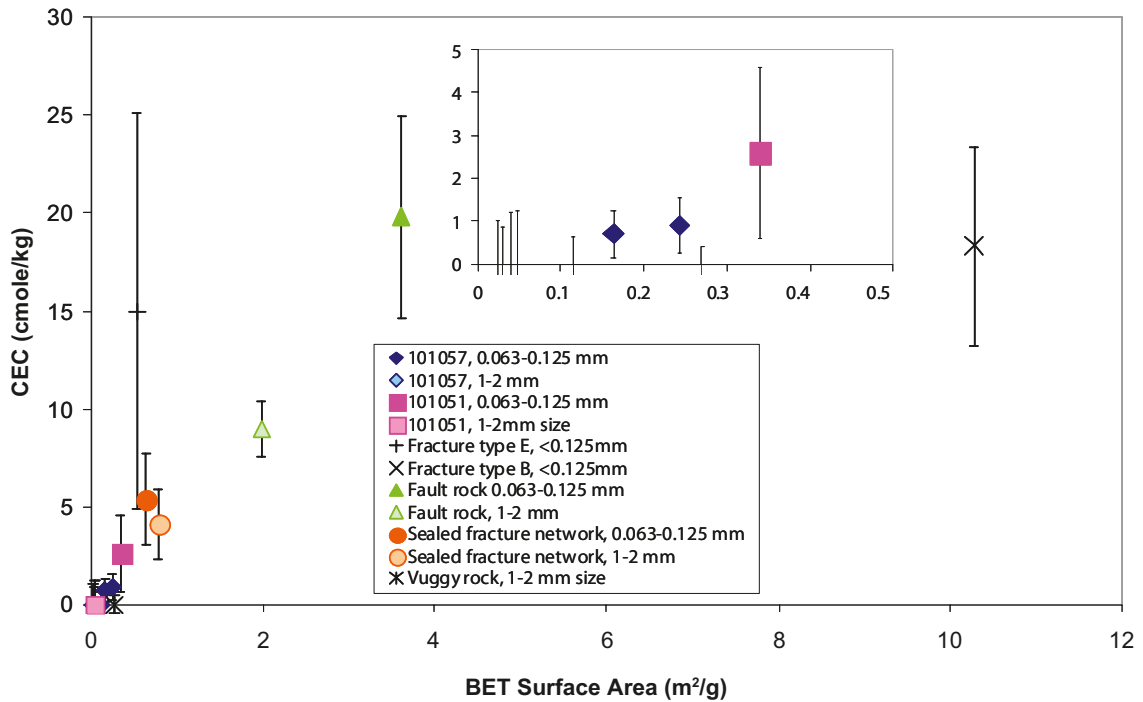


**Figure 3-10.** Results of the CEC measurements as a function of measured BET surface area.

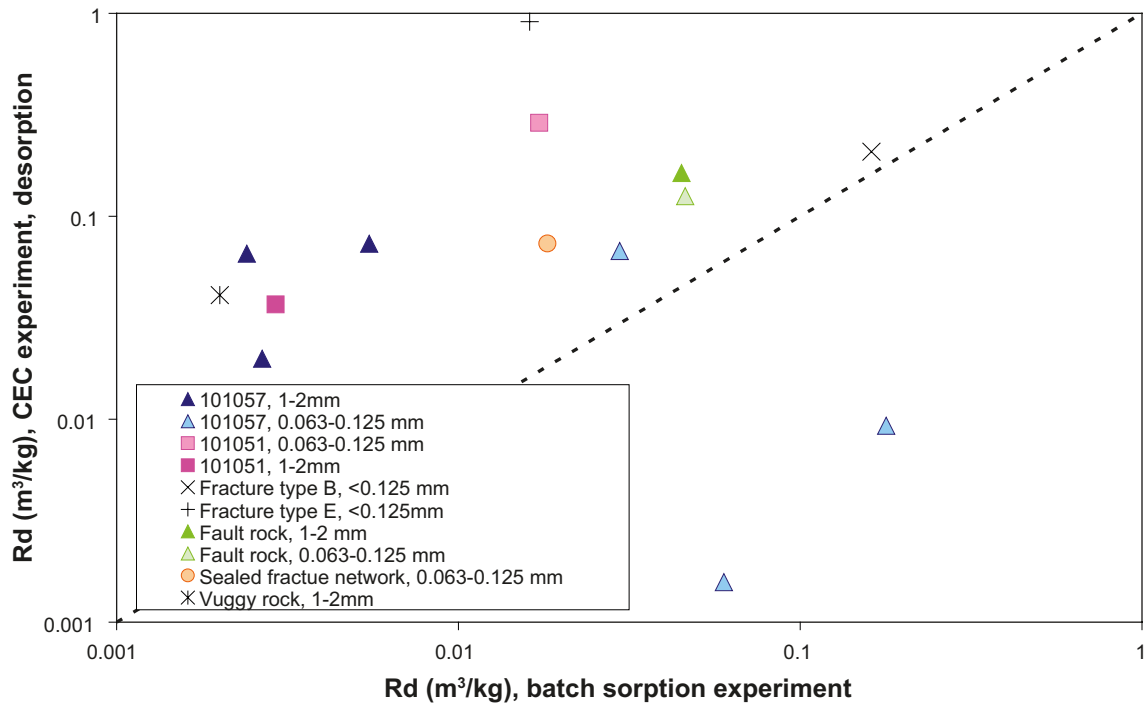


**Figure 3-11.** Comparison of sorption coefficient ( $R_d$ ) for Cs measured using the batch sorption method and estimations made based on the measured amount of cation exchanged Cs and the Cs concentration in the groundwater.

### 3.4.3 Batch sorption data

As been mentioned earlier, the evaluation method that was originally proposed /Widstrand et al. 2003/ for the interpretation of the batch sorption experimental results to sorption parameters consisted of Equation 3-8. A graph of  $R_d$  versus  $1/d_p$  gives an intercept corresponding to the  $K_d$  value, and a slope corresponding to  $6K_d/\rho$ . This concept of evaluation implies the following assumptions:

- Perfect spherical form of the crushed rock particles.
- The size distributions within each particle diameter interval can be represented by the mean of that interval.

Preliminary evaluation according to this concept indicated general difficulties implied with this method. In most cases, the agreement between the results and the model was poor, which gave considerable uncertainties when extrapolating the  $K_d$  value from the intercept. Including the uncertainty in the intercept, estimations resulted in several cases in uncertainty intervals involving negative values; i.e. indicating that no inner surface sorption could be confirmed and validated using this concept.

Parallel to these observations, it was found that the results of the BET measurement of intact drill cores (cf. Section 3.4.1) gave results corresponding to the larger size fractions of the crushed material (i.e. 2–4 mm). The same relation applied to the extrapolations of the different particle sizes (Equation 3.7) where the intercept (corresponding to the inner surface) becomes very similar to the BET surface value obtained for the 2–4 mm size fraction.

Summing up all these facts, a conceptual model for the tracer interaction with crystalline rock is postulated, consisting of:

- An intact rock consisting of the pore volume distributed in a network surrounding grains of rock material of mm size, i.e. the grain boundary porosity.
- Matrix diffusion being a process in which diffusion of the tracer takes place mainly in the grain boundary porosity and to a minor degree into the grains.

- The crushing/sieving process giving:
  - o Larger size fractions, e.g. 2–4 mm and 1–2 mm size fractions, which mainly have undergone cleavage in the naturally occurring grain boundary porosity and, therefore, no formation of extra BET-surface (compared to the intact rock) is obtained.
  - o Crushed rock in the <1mm size fractions which, to a large degree, have undergone cleavage through the natural mineral grains. An increase in the BET surface area compared to intact rock is therefore obtained for these size fractions.

Studying the visualization of the porosity distribution using the PMMA technique for the 101057 rock type (Figure 3-12), one can identify the porosity distributed in a grid system i.e. grain boundary porosity which would correspond to the proposed conceptual model.

Following this conceptual model, the sorption data used in this retardation model are:

- For the matrix rock material which has undergone a heavy crushing procedure before the sieving, the tracer distribution coefficient ( $R_d$ , m<sup>3</sup>/kg) determined for the largest size fraction (1–2 mm) with the longest contact time, 180 days, are directly used as the  $K_d$ , (m<sup>3</sup>/kg).
- For the rock material that is associated with fractures (coatings and/or fracture fillings) sampling has been performed using much milder methods compared to the matrix rock, e.g. by mild scraping or by just collecting loose material. It is therefore not expected that new surfaces will be created to the same extent as in the crushing process for the matrix rock. Therefore, the tracer distribution coefficient ( $R_d$ , m<sup>3</sup>/kg) determined for the largest size fraction (0.063–0.125 mm or the <0.125 mm) with the longest contact time, 180 days, will be directly used as the  $K_d$ , (m<sup>3</sup>/kg)

Since there is no established method available for the validation of the underlying assumptions of this conceptual model, one has to be aware of the conceptual uncertainty in the sorption coefficients given in the retardation model table in this report. This conceptual uncertainty is difficult to give in quantitative numbers but, nevertheless, has to be acknowledged. A reasonable assumption is that the sorption coefficients for strongly sorbing species are underestimated by this method, since it is not likely that a penetrative equilibrium has been obtained within the relatively short time period allowed for the experiments.

### **Sorption results**

Sorption coefficients evaluated using the conceptual model described in the previous sections are presented in Tables 3-8 to 3-11 for the following different groups of geological material:

1. Major rock types.
2. The different fracture types.
3. The different deformation zone units.

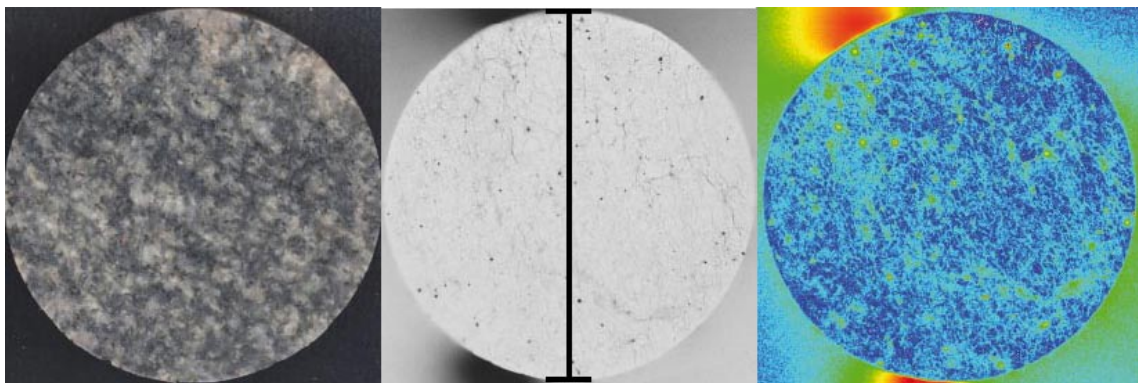


**Figure 3-12.** Photograph (left), autoradiograph of PMMA saturated rock and evaluated digitalized porosity distribution of a 101067 rock sample, KFM01A 486.90 m.

Some general comments can be made from the results:

1. Concerning Sr, the sorption loss from the aqueous phase can only (with a few exceptions) be statistically verified for the fresh groundwater. Based on the variation observed for the blank samples, one can roughly estimate that a 10% concentration decrease in the water phase is generally the lowest sorption that can be detected using this method. Given that a 2 g to 8 ml ratio has been used in the experiments, the detection limit for the  $R_d$  can be calculated to  $5 \cdot 10^{-4} \text{ m}^3/\text{kg}$ . This number has, however, varied during the experimental programme; the stability of the blank signal seems to have varied which has caused both higher and lower detection limits. One should, however, consider  $R_d$  values in the range of  $1 \cdot 10^{-3} \text{ m}^3/\text{kg}$  and lower as potential indicators that no sorption has taken place. For the other groundwater types, the high salinity causes a high competition of the adsorption sites, giving very low adsorption. This can be seen in the minimum values, which range into the negative part, indicative that any possible sorption is lower than the variation of the measurements of the blank solution.
2. Besides Sr, the Ra and Cs tracers are highly influenced by the water compositions. As expected from the presumed high influence of cation exchange mechanism on the sorption mechanism, sorption decreases with increasing salinity.
3. The trivalent actinide/lanthanide is adsorbed to a very high degree; even in the blank sample with groundwater without any geological material present, a severe adsorptive loss of the tracer is observed, i.e. adsorption on test tube walls. Thorough investigations of these samples have, however, shown that in samples with rock material present, the amount of tracer associated with the test tube walls are negligible compared to the adsorption on the rock material.
4. The trivalent actinide/lanthanide, redox sensitive elements U and Np, as well as Ni are not very much influenced by the salinity. This is in agreement with the presumption that the major sorption mechanism for these tracers is surface complexation and not cation exchange. Potentially, the higher concentration of  $\text{HCO}_3^-$  in the fresh groundwater has caused aqueous carbonate complexation of Ln-Ac(III), which could explain an indication of lower sorption of this tracer in the fresh groundwater.
5. The sorption of the redox sensitive elements Np and U is comparatively low, indicating the presence of Np(V) and U(VI) species, respectively (Figure 3-13). In some of the measurements, a pronounced increase of the sorption is found for the smallest size fraction, an increase that is much higher than what would be expected from the BET surface area measurements. A possible explanation for this is that minerals having reducing capacity have been enriched in the smaller size fraction during the crushing/sieving process.
6. The time dependence of the losses of tracer in the aqueous phase could potentially be regarded as a result of the diffusion rate of the solute into the inner surfaces of the crushed particles. An attempt to calculate the losses of the tracer  $\text{Cs}^+$  in the aqueous phase as a function of time by a model consisting of diffusion into spheres /Crank 1975/ is illustrated in Figure 3-14. The result shows that using values of the retardation parameters determined in the laboratory experiment for sorption and diffusivity (the 101057 average values for the  $K_d$  and  $F_i$ , respectively) gives a very reasonable fit to the experimental results of the time dependence of the sorption in the largest size fractions. This can be regarded as an additional indication that the retardation properties (diffusivities and sorption) of the larger size particles are very similar to that of the intact rock and that a reasonable penetrative equilibrium has been reached after 180 days of contact time, at least for the Cs tracer. However, the result that the sorption after 1 day is only approximately 20% of that obtained after equilibrium seems to have been reached is an indication that the major part of the surfaces of the 1–2 mm size fraction is only accessible by diffusion and is therefore not to be considered as “pure surface sites”. This finding is therefore somewhat contradictory to the postulated assumption in Section 3.4.1 that the porosity should mainly consist of grain boundary porosity between larger grains of mm-size. Provided that the sorption surfaces could be related to the porosity, the diffusion characteristics of the batch sorption result indicate that more than 80% of the porosity is to be considered as intra-granular porosity. One also has to consider that alternative processes (e.g. weathering of the geological material, chemical kinetic effects) may influence the time dependence of the sorption process: i.e. diffusion may not be the only process causing the time dependence.

**Table 3-8. Sorption coefficients for 101057 fresh rock types, i.e. the tracer distribution coefficient measured in the 1–2 mm size fraction after 180 days of contact time.**

Rock type (SKB code)	Tracer		$K_d$ (m <sup>3</sup> /kg) Groundwater type			
			Marine	Saline	Fresh	Brine
101057 fresh	Cs	Average ± σ	(3.6±2.5)E-3	(4.0±1.6)E-3	(1.9±0.7)E-2	(1.8±0.6)E-3
		Median	2.5E-3	3.1E-3	1.7E-2	1.7E-3
		Min-Max	(0.98–8.6)E-3	(1.5–7.3)E-3	(1.2–3.1)E-2	(1.1–2.8)E-3
		# samples	12	17	11	11
	Sr	Average ± σ	(3.8±16)E-4	(2.4±8.1)E-4	(4.6±3.2)E-3	(2.1±6.5)E-4
		Median	2.8E-5	9.2E-5	3.8E-3	2.5E-5
		Min-Max	(-1.3–3.4)E-3	(-0.8–2.0)E-3	(0.07–1.1)E-2	(-0.5–2.1)E-3
		# samples	12	17	11	11
	Ln-Ac (III)	Average ± σ	(8.4±9.7)E-1	(5.6±2.3)E-1	(1.3±1.3)E-1	(3.9±2.2)E-1
		Median	4.1E-1	5.2E-1	7.6E-2	3.9E-1
		Min-Max	(0.03–3.2)E+0	(0.13–1.2)E+0	3.8E-1	8.2E-1
		# samples	12	17	11	11
	Ra	Average ± σ	(1.7±0.9)E-2	(6.5±1.2)E-3	(9.3±2.1)E-2	(2.1±0.7)E-4
		Median	1.2E-2	6.8E-3	9.3E-2	2.1E-4
		Min-Max	(1.0–2.7)E-2	(5.1–7.7)E-3	(7.8–11)E-2	(1.6–2.6)E-4
		# samples	3	5	2	2
	Ni	Average ± σ	(2.5±0.4)E-2	(2.2±0.4)E-2	(6.5±0.9)E-2	(3.3±0.3)E-3
		Median	2.7E-2	2.0E-2	6.5E-2	3.3E-3
		Min-Max	(2.1–2.7)E-2	(1.8–2.7)E-2	(5.9–7.1)E-2	(3.1–3.6)E-3
		# samples	3	5	2	2
	Np	Average ± σ	(1.4±1.7)E-3	(3.0±3.9)E-4	(1.3±0.2)E-3	(-1.9±0.1)E-3
		Median	6.0E-4	1.4E-4	1.3E-3	-1.9E-3
		Min-Max	0.3–3.4E-3	(-0.4–8.1)E-4	(1.1–1.4)E-3	(-2.0–1.8)E-3
		# samples	3	5	2	2
U	Average ± σ	(2.9±0.4)E-3	(7.8±3.6)E-4	(1.0±0.2)E-3	(1.9±0.5)E-3	
	Median	2.7E-3	6.0E-4	1.0E-3	1.9E-3	
	Min-Max	(2.6–3.3)E-3	(4.7–12)E-4	(0.9–1.2)E-3	(1.6–2.3)E-3	
	# samples	3	5	2	2	

**Table 3-9. Sorption coefficients for 101051 and 101054 fresh rock types, i.e. the tracer distribution coefficient measured in the 1–2 mm size fraction after 180 days of contact time.**

Rock type (SKB code)	Tracer		$K_d$ (m <sup>3</sup> /kg) Groundwater type			
			Marine	Saline	Fresh	Brine
101051, fresh	Cs	Average ± σ	(2.1±0.1)E-3	(2.9±0.3)E-3	(7.9±1.7)E-3	
		Median	2.1E-3	3.1E-3	7.4E-3	
		Min-Max	(2.0–2.2)E-3	(2.6–3.1)E-3	(6.5–9.8)E-3	
		# samples	3	3	3	
	Sr	Average ± σ	(1.7±0.2)E-4	(2.8±1.3)E-4	(2.9±0.1)E-4	
		median	1.7E-4	3.0E-4	2.9E-3	
		Min-Max	(1.4–1.9)E-4	(1.4–4.0)E-4	(2.7–3.0)E-3	
		# samples	3	3	3	
	Ln-Ac (III)	Average ± σ	(2.9±0.4)E-1	(3.9±0.6)E-1	(1.3±0.2)E-1	
		median	2.9E-2	3.8E-1	1.1E-1	
		Min-Max	(2.5–3.2)E-2	(3.4–4.5)E-1	(1.1–1.5)E-1	
		# samples	3	3	3	
101054, fresh	Cs	Average ± σ	(4.8±0.7)E-3	(8.4±0.2)E-3	(1.8±0.2)E-2	
		median	4.6E-3	8.4E-3	1.9E-2	
		max	(4.3–5.6)E-3	(8.2–8.6)E-3	(1.6–1.9)E-2	
		# samples	3	3	3	
	Sr	Average ± σ	(3.4±0.4)E-4	(0.1±2.2)E-4	(4.1±0.1)E-3	
		median	3.5E-4	-8.4E-5	4.2E-3	
		max	2.9–3.6E-4	-1.4–2.7E-4	(4.1–4.2)E-3	
		# samples	3	3	3	
	Ln-Ac (III)	Average ± σ	(3.5±0.2)E-2	(8.2±1.4)E-1	(2.1±0.3)E-1	
		median	3.7E-2	8.4E-1	2.2E-1	
		max	(3.3–3.7)E-2	(6.7–9.5)E-1	(1.8–2.3)E-1	
		# samples	3	3	3	

**Table 3-10. Sorption coefficients for fracture type material, i.e. the tracer distribution coefficient measured in the <0.125 mm size fraction after 180 days of contact time.**

Location used	Fracture type	Size fraction	Tracer		$K_d$ (m <sup>3</sup> /kg)			
					Groundwater type			
					Marine	Saline	Fresh	Brine
	A			No data				
KFM03A 643.8 m	B	<0.125 mm	Cs	Average <sup>A</sup>		1.6E-1	1.5E+0	4.8E-2
				$\sigma^A$		8.0E-3	1.6E-1	3.9E-3
			Sr	# samples		1	1	1
				Average <sup>A</sup>			2.0E-1	-1.3E-3
				$\sigma^A$			4.3E-2	-1.6E-3
			Ln-Ac (III)	# samples			1	1
Average <sup>A</sup>		7.5E-2		1.0E-1	8.6E-1			
$\sigma^A$		1.7E-2		4.5E-2	9.5E-2			
# samples		1		1	1			
	C			No data				
KFM01B 418.29 m	D	<0.125 mm	Cs	Average <sup>A</sup>	4.1E-3		6.4E-2	1.2E-3
				$\sigma^A$	4.9E-4		1.3E-2	2.6E-4
			# samples	1		1	1	
KFM04A 414.20 m KFM06A 770.69 m	F	<0.125 mm	Cs	Average <sup>A</sup>	3.7E-4		3.7E-1	-3.0E-4
				$\sigma^A$	4.5E-4		1.1E-1	-4.9E-4
				Average	1.3E-2	2.2E-2	1.7E-1	
				$\sigma$	5.9E-3	1.7E-2	5.9E-2	
				median	9.1E-3	1.0E-2	1.4E-1	
				max	2.2E-2	4.3E-2	2.6E-1	
			Sr	min	8.2E-3	9.3E-3	1.3E-1	
				# samples	5	5	5	
				Average	1.3E-3	7.4E-4	1.8E-1	
				$\sigma$	1.2E-3	5.5E-4	1.4E-1	
				median	2.0E-3	9.5E-4	1.1E-1	
				max	2.3E-3	1.3E-3	4.0E-1	
Ln-Ac (III)	min	-3.3E-4	-1.5E-4	6.9E-2				
	# samples	5	5	5				
	Average	8.6E-1	1.4E+0	2.0E-1				
	$\sigma$	6.7E-1	1.2E+0	1.7E-1				
	median	1.1E+0	1.5E+0	1.1E-1				
	max	1.5E+0	2.7E+0	4.5E-1				
KFM02A 118.25 m	G	<0.125 mm	Cs	Average	4.3E-1		5.8E+0 <sup>A</sup>	
				$\sigma$			2.3E+0 <sup>A</sup>	
				max	4.6E-1			
				min	4.0E-1			
				# samples	2		1	
				Average	2.2E-3		9.5E-2	
			Sr	$\sigma$			1.5E-2	
				max	2.3E-3			
				min	2.0E-3			
				# samples	2		1	
				Average	1.6E+0		1.8E+0 <sup>A</sup>	
				$\sigma$			5.0E-1 <sup>A</sup>	
Ln-Ac (III)	max	1.7E+0						
	min	1.5E+0						
	# samples	2		1				
	H				cf. results for 101057 in Table 3-8			

<sup>A)</sup> In the cases when only one sample has been measured, the uncertainty given is based on the counting statistics uncertainty in the activity measurement for that sample.

**Table 3-11. Sorption coefficients for deformation zone material, i.e. the tracer distribution coefficient measured in the 1–2 mm size fraction (unless stated otherwise) after 180 days of contact time.**

Deformation zone unit/sample location/ deformation zone	Size fraction	Tracer		$K_d$ (m <sup>3</sup> /kg)		
				Marine	Groundwater type	
				Saline	Fresh	Brine
Deformation zone unit #1: Fault rock (strongly tectonized and partly incohesive material), KFM01B 47.72 ZFM A2	1–2 mm	Cs	Average		4.5E–2	3.3E–1
			$\sigma$		1.8E–3	5.7E–2
			median		4.6E–2	3.2E–1
		max		4.6E–2	3.9E–1	
		min		4.3E–2	2.8E–1	
		# samples		3	3	
		Sr	Average		7.5E–5	8.1E–2
			$\sigma$		2.4E–4	1.9E–2
			median		–3.0E–7	8.7E–2
			max		3.4E–4	9.6E–2
			min		–1.1E–4	6.0E–2
			# samples		3	3
		Ln-Ac (III)	Average		4.5E+0	1.9E–1
			$\sigma$		1.8E+0	4.9E–2
			median		5.2E+0	2.2E–1
			max		5.9E+0	2.2E–1
			min		2.5E+0	1.4E–1
			# samples		3	3
		Ra	Average		6.1E–2	3.6E–1
			$\sigma$		2.0E–3	2.6E–1
			median		6.1E–2	2.4E–1
			max		6.4E–2	6.6E–1
			min		6.0E–2	1.9E–1
			# samples		3	3
		Ni	Average		2.8E–1	3.0E–1
			$\sigma$		5.5E–2	9.7E–2
			median		2.9E–1	2.5E–1
			max		3.3E–1	4.1E–1
			min		2.2E–1	2.4E–1
			# samples		3	3
Np	Average		2.2E–3	4.4E–3		
	$\sigma$		2.3E–4	4.8E–4		
	median		2.1E–3	4.6E–3		
	max		2.4E–3	4.7E–3		
	min		2.0E–3	3.9E–3		
	# samples		3	3		
U	Average		2.0E–2	1.0E–3		
	$\sigma$		4.3E–3	1.7E–4		
	median		1.9E–2	1.1E–3		
	max		2.5E–2	1.2E–3		
	min		1.7E–2	8.6E–4		
	# samples		3	3		
Deformation zone unit #2: Sealed fracture network (breccia/ cataclasite) KFM05A 611.68 ZFMENE0401B	0.063–0.125 mm	Cs	Average	1.4E–2	1.8E–2	2.1E–1
			$\sigma$		6.6E–4	
			median <sup>A</sup>			
		max <sup>A</sup>	1.4E–2		2.0E–1	
		min <sup>A</sup>	1.4E–2		2.2E–1	
		# samples	2	1	2	
		Sr	Average		2.0E–4	3.6E–2
			$\sigma$		5.7E–4	
			median <sup>A</sup>			
			max <sup>A</sup>			3.7E–2
			min <sup>A</sup>			3.6E–2
			# samples		1	2
		Ln-Ac (III)	Average	7.3E–2	1.1E+0	7.6E–1
			$\sigma$		1.1E–1	
			median <sup>A</sup>			
			max <sup>A</sup>	8.9E–2		7.6E–1
			min <sup>A</sup>	5.6E–2		7.5E–1
			# samples	2	1	2



Deformation zone unit/sample location/ deformation zone	Size fraction	Tracer		$K_d$ (m <sup>3</sup> /kg)			
				Groundwater type			
				Marine	Saline	Fresh	Brine
Deformation zone unit #3: Vuggy rock	1–2 mm	Cs	Average	2.0E–3		9.4E–3	6.4E–04
			$\sigma$	2.1E–4		1.3E–3	5.6E–05
			median <sup>A</sup>	2.1E–3		9.5E–3	6.7E–4
			max <sup>A</sup>	2.1E–3		1.1E–2	6.8E–4
			min <sup>A</sup>	1.8E–3		8.1E–3	5.8E–4
KFM02A 275.22			# samples	3		3	3
			Average	2.8E–4		7.0E–3	–4.4E–04
ZFM 1189		Sr	Average	2.8E–4		6.2E–4	1.8E–04
			$\sigma$	5.4E–4		6.7E–3	–4.2E–4
			median <sup>A</sup>	1.3E–5		7.7E–3	–2.7E–4
			max <sup>A</sup>	9.0E–4		6.5E–3	–6.3E–4
			min <sup>A</sup>	–8.2E–5		3	3
		Ln-Ac (III)	Average	1.4E+0		2.7E–1	9.0E–1
			$\sigma$	8.0E–1		7.1E–2	3.7E–1
			median <sup>A</sup>	1.4E+0		2.8E–1	9.6E–1
			max <sup>A</sup>	2.2E+0		3.3E–1	1.2E+0
			min <sup>A</sup>	6.4E–1		1.9E–1	5.1E–1
			# samples	3		3	3

<sup>A</sup> In the cases when only one sample has been measured, the max-value is replaced by uncertainty estimation, based on counting statistics of the activity measurement.

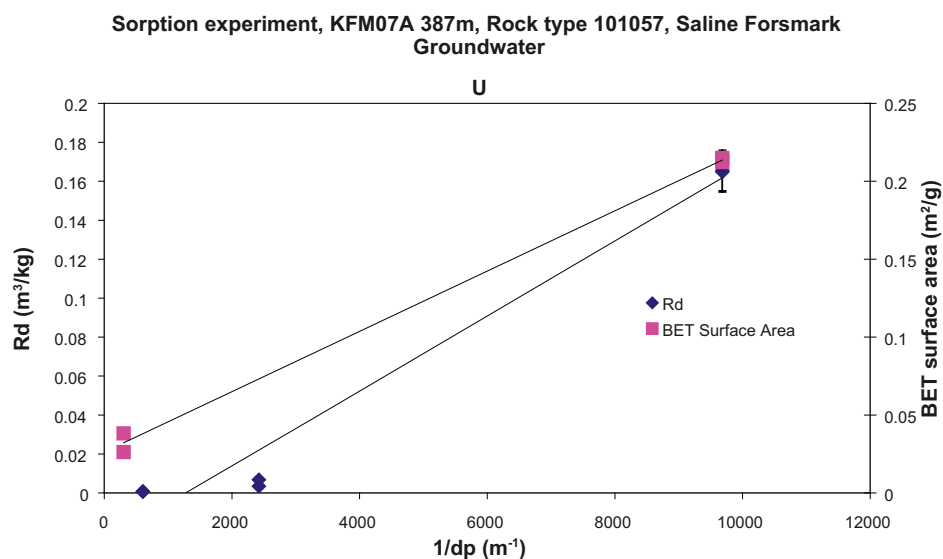
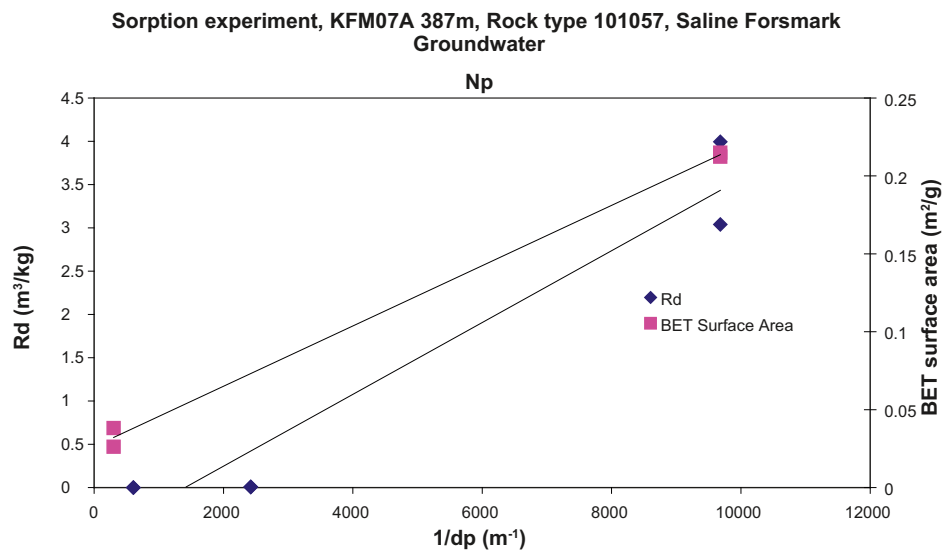


**Figure 3-13.** Sorption of Np (upper) and U (lower) as a function of the inverse of the particle size of the crushed rock material. The results of the corresponding BET surface area measurements are also shown.

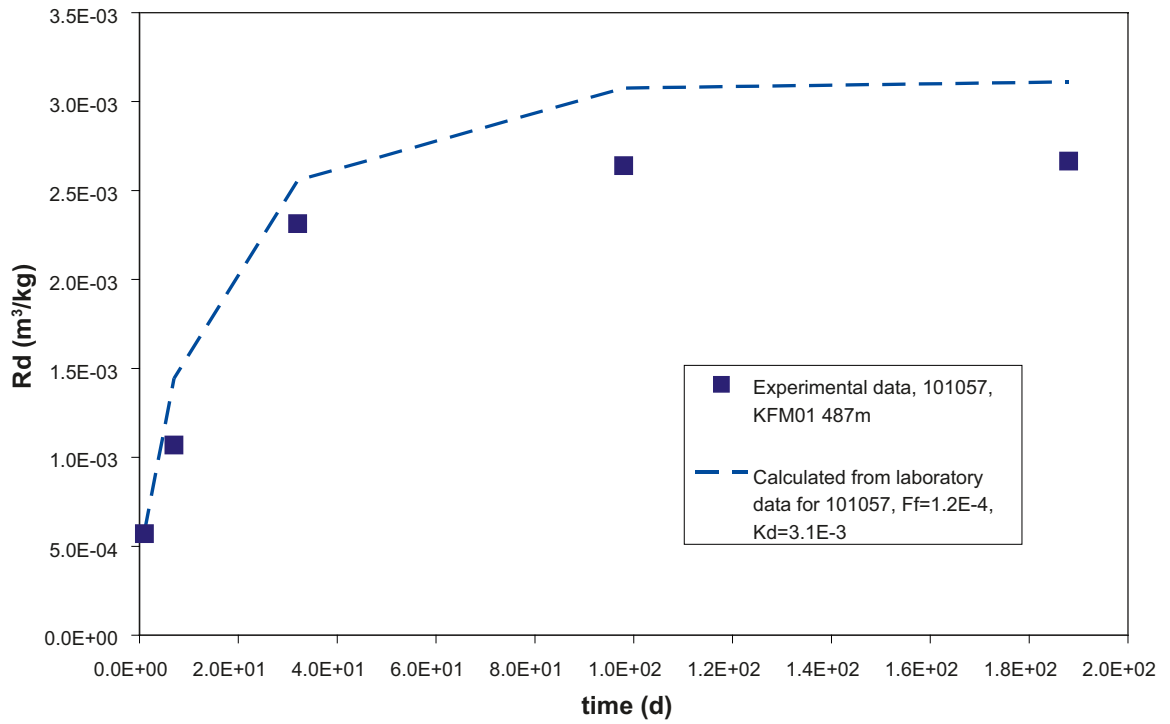


**Figure 3-14.** Sorption of Cs as a function of contact time. Experimental results are given in comparison to predictions using a model consisting of diffusion in a sphere.

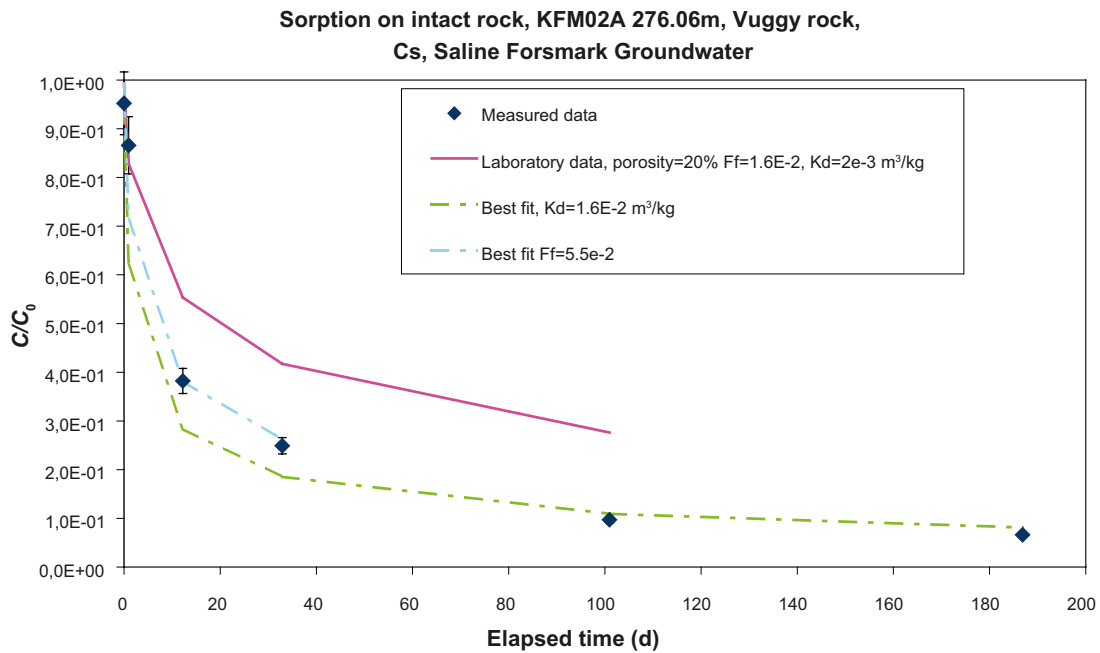
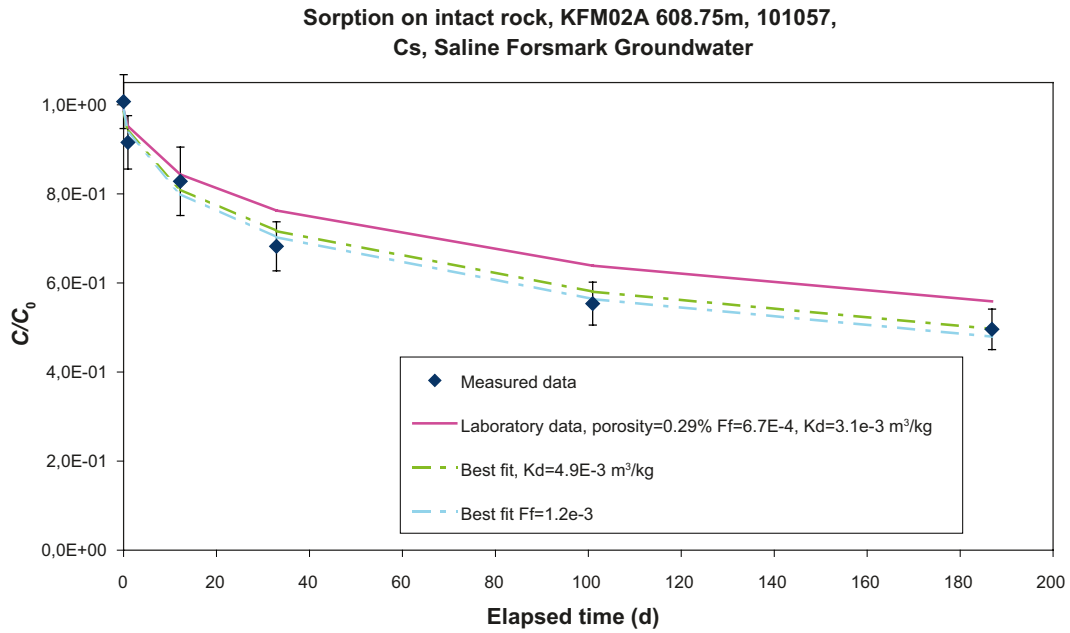


**Figure 3-15.** Results of the adsorption experiments using intact drill core samples, see text for details. Comparative results are also given for calculation using the laboratory data (solid lines), as well as for the cases in which the  $K_d$  and the  $F_f$ , respectively, has been varied in order to obtain the best fit to the experimental results (dashed lines).

### 3.5 Confirmation studies

The retardation data used in this model can be criticized due to the fact that the major mechanisms for radionuclide retardation (i.e. diffusion into the rock matrix and adsorption) are not studied interactively and are mainly addressed using disturbed rock material. At least for confirmation purposes, it would be advantageous to be able to see if the retardation parameters determined on a very small scale can be used to correctly predict radionuclide retardation in larger scale.

Two sets of experiments are therefore described in which retardation in intact drill cores is addressed:

- Radionuclide adsorption on intact drill cores /Byegård et al. in prep./.
- Adsorption of Cs using electromigration to speed up the reaching of the diffusion sorption equilibrium, data and evaluation procedures according to /André et al. 2008ab/.

#### 3.5.1 Adsorption studies using intact drill cores

##### *Diffusion and sorption on intact drill core samples*

In these experiments, the diffusion cells used for the through-diffusion experiment were spiked with a radionuclide cocktail on one side of the cell. The loss of tracer in the injection cell of the diffusion cell was thereafter studied as a function of time. According to the sorption concept used, the rate of losses should thus be dependent on the diffusion rate as well as the sorption coefficient. A prediction of the expected rate of loss of tracer in the injection cell was made (based on the analytical solution for diffusion in a sheet /Crank 1975/), based on the:

- Diffusivity calculated using the formation factor determined for that particular diffusion cell using H<sup>3</sup>HO as a tracer and the tabulated water diffusivity of the tracer.
- $K_d$  values determined for that particular rock type.

Two sets of comparisons are presented in this report, one is for the Cs adsorption on 101057 rock type and the other is for Cs adsorption on highly (approximately 20%) porous vuggy rock. Both examples refer to the use of saline Forsmark groundwater as the aqueous phase. The results displayed in Figure 3-15 show a fairly good fit of the predicted rate for tracer losses which could be regarded as a support for both the conceptual sorption model and the proposed retardation model.

However, in both cases, the calculated sorption rate using the laboratory retardation data (i.e.  $K_d$  and  $F_f$ ) seem to slightly underestimate the actual measured sorption rate. For that reason, an attempt was made to perform calculations in which either the  $K_d$  or the  $F_f$  has been varied in order to obtain the best fit to the experimental results. The results show that:

- For the fresh 101057 rock type, the best fit is obtained either by:
  - o Increasing the laboratory determined  $K_d$  of  $3.1 \cdot 10^{-3}$  m<sup>3</sup>/kg to  $4.9 \cdot 10^{-3}$  m<sup>3</sup>/kg, i.e. an increase by a factor 1.6.
  - o Increasing the laboratory determined  $F_f$  of  $6.7 \cdot 10^{-4}$  to  $1.2 \cdot 10^{-3}$ , i.e. an increase by a factor 1.8.
- For the vuggy rock, the best fit is obtained either by:
  - o Increasing the laboratory determined  $K_d$  of  $2 \cdot 10^{-3}$  m<sup>3</sup>/kg to  $1.6 \cdot 10^{-2}$  m<sup>3</sup>/kg, i.e. an increase by a factor 8.
  - o Increasing the laboratory determined  $F_f$  of  $1.6 \cdot 10^{-2}$  to  $5.5 \cdot 10^{-2}$  i.e. an increase by a factor 3.4.

Altogether, based on the uncertainties addressed in the sections describing the diffusivity and sorption data, no severe deviation of the data and/or conceptual sorption model is indicated from this slight upscaling of the laboratory data.

#### 3.5.2 Electromigration sorption studies

Comparative studies on adsorption on crushed rock material in different size fractions in combination with adsorption studies on intact drill cores have been performed by /André et al. 2008ab/. In these experiments, the adsorption on intact drill cores was done by applying an electrical field which speeded up the migration rate of the sorbing tracer, Cs, in the experiment, i.e. diffusive equilibrium was expected to be reached in a much shorter time.

Parallel to this, BET surface area measurements were performed using both the crushed material in different size fractions as well as intact drill cores.

The results (Figure 3-16) show that for the BET surface area measurements the conceptual model for interpretation of sorption data proposed in this report seem to be valid. The specific surface area for the intact rock is, as also found in the results described in Section 3.4.1, not significantly lower than for the largest size fraction (in this case 1–2 mm) of the crushed rock, indicating that for the larger particles very few extra surfaces have been created during the crushing process. This supports the assumption that the sorption results obtained from the larger size fractions are the most representative for the intact rock.

However, the sorption results of  $C_s$  indicate that even the results obtained from the larger size fraction seem to overestimate the adsorption of intact rock by a factor of 7. This is a little unexpected considering the BET surface area results. The reason for this deviation is not fully understood and must probably be further investigated. However, the general assumption that crushed rock gives extra surfaces that are non-representative for intact rock is not contradicted by the results.

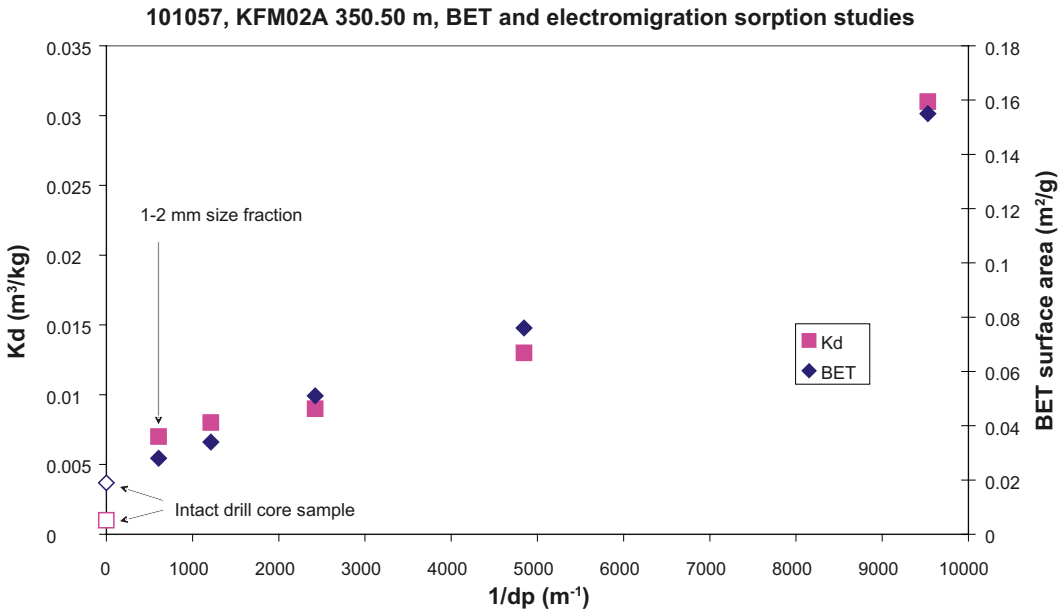


**Figure 3-16.** Results from the batch experiments with  $C_s$  sorption on crushed material and from the electromigration-induced sorption studies using intact drill core. The results of the corresponding BET surface area measurement are given in the same figure. All results for the crushed rocks are given with filled markers (diamonds for  $K_d$ , squares for BET) while non-filled markers are used for the intact drill core samples.

## 4 Development of retardation model

In accordance with the general concept for a site descriptive retardation model proposed by /Widestrand et al. 2003/, the model should consist of tables in which the geological description is combined with the selected transport parameters for each unit (rock types, fracture types or deformation zone unit, i.e. the different geological units where retardation of radionuclides can take place) are given.

It should be noted that the exemplified proposed conceptual model set up by /Widestrand et al. 2003/ implies a description of retardation occurring in a fracture where discrete layers of altered material are surrounding the fracture; layers of several mm thicknesses which should make them possible to sample for laboratory determination of the different retardation parameters, i.e. diffusivity and sorption. The actual case for the Forsmark area is, however, that the fractures mainly are characterized by a relatively thin fracture coating and the altered rock is found in deformation zones and not necessarily in the vicinity of the individual fractures. For this reason, the description and parameterization of the Forsmark retardation model will vary considerably from the originally proposed retardation model concept; e.g. the retardation parameters for the fracture coatings have to be more thoroughly addressed.

### 4.1 Methodology

The developed retardation model description consists of three sections, one for the major rock types, and one for the fractures and deformation zones, respectively. In the first section, the retardation characteristics of the major rock types, i.e. rock matrix interaction parameters, are described. The second section provides a description of the retardation in the water-conducting fractures and a retardation parameter description for the deformation zones are provided (stochastically and, to some extent, also deterministically) in the third section.

The numerical values presented in the retardation model concept are based on the data presentation part of this report (Chapter 3) where the representation and discussions concerning uncertainties are given.

#### 4.1.1 Selection and presentation of retardation data

According to the retardation concept applied in the present work (cf. Section 1.2 and Chapter 3), the retardation of radionuclides in the rock matrix can be described using the parameters listed below.

- **Rock matrix porosity,  $\theta_m$  (-):** The results from the water saturation porosity measurements on site-specific rock materials have been selected in this work (cf. Table 3-1).
- **Rock matrix formation factor,  $F_r$  (-):** This parameter is used to multiply literature values of the radionuclide-specific free diffusivities in water ( $D_w$ ,  $m^2/s$ ; a tabulation of applicable numerical values is given by, e.g. /Ohlsson and Neretnieks 1997/) to obtain the effective diffusivities,  $D_e$  ( $m^2/s$ ), for the different radionuclides. Values given in the retardation model tables refer to the values obtained by the laboratory through-diffusion method using tritiated water, which is motivated by the use of the identical physical process in these studies. However, for a potential conservative purpose it is necessary to acknowledge that the *in situ* formation factors have been found to be a factor of approximately 8 lower than the through-diffusion measurement, possibly explained by the stress release obtained in the laboratory samples.
- **Rock matrix sorption coefficient,  $K_d$  ( $m^3/kg$ ):** Values presented in the retardation model tables are based on the following assumptions (more thoroughly motivated in Chapter 3):
  - o For the samples representing matrix rock which has undergone sawing, crushing and sieving, the results from the 1–2 mm size fraction with the 180 days contact time has been selected, i.e. choosing the tracer distribution ratio directly as the  $K_d$ .
  - o For the samples representing fracture coating and/or fracture filling, the samples have been sampled in its natural form (no crushing process) and the results from smallest size fraction (<0.125 mm or 0.063–0.125 mm) with 180 days contact time has been selected. Also for this case, the tracer distribution ratio has directly been adopted as the  $K_d$ .

The same selection concept has been applied in the presentation of the other parameters closely related to the sorption, i.e. the *specific surface area* measurements (*BET*) and the *Cation Exchange Capacity* (*CEC*).

For simplicity and to provide an overview of the parameter values, the presentation of sorption coefficients from a tracer point of view has in the tables been restricted to Cs<sup>+</sup> (ion exchange sorbing tracer) and a trivalent lanthanide actinide (more specifically, Am(III) or Eu(III), expected to be influenced by surface complexation). Furthermore, only results for the saline groundwater composition are included in the tables, except for two cases where sorption coefficients were unavailable and, therefore, were replaced by sorption coefficients for the comparatively similar marine groundwater. For sorption coefficients for other tracers and/or other groundwater compositions, it is referred to Tables 3-8 to 3-11.

#### 4.1.2 Rock types

For the rock types, the following retardation parameters are included in the tables:

- Porosity
- Formation factor (to be used in calculations of the diffusivities of the different radionuclides, as described in Chapter 3)
- Specific surface area (BET)
- Cation exchange capacity (CEC)
- Sorption distribution coefficients,  $K_d$  (m<sup>3</sup>/kg)

#### 4.1.3 Fracture types and deformation zones units

Retardation capacity in the vicinity of fractures and in deformations zones are of particular interest since the water transport occurs here. Even though diffusion of any potentially escaped radionuclide into the microfractures in the rock followed by adsorption on the microfracture walls often is considered as the major retardation mechanism, one must be aware of that the fractures are the starting place for the retardation processes. Furthermore, diffusion of very strongly sorbing tracers should according to the matrix concept be so low that they will be present in the fracture vicinity for a long time. The finding of strongly increased specific surface area for the fracture material may also have a substantial impact on the importance of the fracture material to the total retardation of radionuclides.

The geological materials in the fractures in the Forsmark area can roughly be generalized as thin fracture coatings, sometimes located in altered rock, sometimes without alteration of the wall rock. In the retardation modelling, attempts are made to quantify the following parameters of obvious importance for the retardation process:

- Thickness of the fracture coatings.
- Porosity.
- Formation factor (to be used in calculations of the diffusivities of the different radionuclides).
- Sorption distribution coefficients,  $K_d$  (m<sup>3</sup>/kg).
- Mineral contents.

In addition, the following data for each particular fracture type are given:

- Abundance (percentage) of the fracture type, i.e. a quantification of the portion of the entire fracture class for which the given description is valid.
- Preferential direction of the particular fracture type (if any).

## 4.2 Retardation model

### 4.2.1 Rock types

The geological model is based on rock domains, whereas the sampling for the transport programme was based on rock types and mainly focused on the major rock type; granite (to granodiorite), metamorphic, medium-grained together with some minor rock types (listed below). The sample collection represents both fresh and slightly altered (mainly oxidized and faint to weak degree of alteration) samples of these rock types. The proportion of rock types within rock domains RFM029 (dominating rock domain within the target area) and RFM045 (subordinate rock domain within the target area) are presented in Table 4-1. A few of the minor rock types investigated in the laboratory programme have been excluded from the retardation model (Table 4-2) since they constitute less than 2% of the rock mass within RFM029 and RFM045, or are located in rock domains that are not part of the target volume.

**Table 4-1. Proportions of different rock types in the two rock domains that constitute the target volume, RFM029 and RFM045. /Stephens et al. 2007/.**

Code (SKB)	Rock type	RFM029	RFM045
103076	Felsic to intermediate volcanic rock, metamorphic	0.4%	1.2%
102017	Amphibolite	4.4%	6.3%
101057	Granite to granodiorite, metamorphic, medium-grained	73.6%	18.0%
101058	Granite, metamorphic, aplitic	1.2%	49.3%
101051	Granodiorite, tonalite and granite, metamorphic, fine- to medium-grained	4.6%	9.0%
101061	Pegmatitic granite, pegmatite	13.3%	13.9%
111058	Granite, fine- to medium-grained	1.5%	1.3%

**Table 4-2. Suggested transport parameters for the rock types (more than 2% occurrence), expressed with rock codes within the dominant rock domains RFM029 and RFM045.**

	101051	101057	101057 rock within deforma- tion zones	101058	101061	102017
<b>Porosity (vol-%)</b>	0.23±0.09	0.23±0.11	1.0±2.4	0.22	0.32	0.16±0.10
<b>Formation factor</b>	1.0E-4	(1.6±1.5)E-4	(1.1±1.0)E-4	1.8E-4	2.8E-4 <sup>A</sup>	2.9E-5
<b>BET (m<sup>2</sup>/g)</b>	0.023±0.014	0.025±0.015	0.342 <sup>B</sup>	0.052	n/a	0.0002
<b>CEC (cmoles/kg)</b>	<1.2	<1	n/a	n/a	n/a	n/a
<b>K<sub>d</sub> (m<sup>3</sup>/kg) (here only exemplified by the K<sub>d</sub> for Cs in saline Forsmark groundwater, full coverage of sorption data cf. Tables 3-8 to 3-11)</b>	(2.9±0.3)E-3	(4.0±1.6)E-3	n/a	n/a	n/a	n/a

<sup>A</sup> Based on laboratory resistivity measurement, cf. Chapter 3.

<sup>B</sup> Based on BET measurements on two samples which were identified as medium altered and therefore can be suspected to give an overestimate of the general conditions for intact rock within deformation zones.

### **Summary of retardation properties of rock types**

The limited data available for the different rock types indicate that there are generally no significant differences in the retardation properties between the rock types present in the dominant rock domain within the target area, RFM029. Furthermore, when also considering the variation reported for the parameter values (cf. data tables in Chapter 3) there are very few indications of significant differences between the different rock types:

- The amphibolite (102017) is indicated to have a lower porosity and, probably therefore also, a lower formation factor than the other rock types. One can also identify a very low BET surface area (below the detection limit).



- Comparing the 101057 samples from deformation zones with samples from rock outside the deformation zones gives no significant differences in the retardation parameters, except for the BET surface area. However, as pointed out in the table, the value provided for rock in deformation zones is based on two measurements on samples which are medium altered and therefore probably gives an overestimation of the average values of BET surface areas within the deformation zones. Nevertheless, the altered rock is more predominant within deformation zones and the result can be regarded as a qualitative conclusion that increased alteration in deformation zones gives increased surface areas and therefore also higher sorption capacities. Due to the low numbers of measurements available, this finding is difficult to quantify accurately.

The subordinate rock domain within the target volume, RFM045, consists to the major part of the 101058 rock type. This rock domain and its potential importance were not identified until very late in the site investigation and data from laboratory investigations are therefore very few. However, based on the data available, one can not identify any significant difference of this rock type to the others.

#### 4.2.2 Fracture types

Retardation parameters for the identified fracture types are given in Tables 4-3 to 4-10. Transmissivity intervals are not specified according to the discussion in Chapter 2.1.7.

**Table 4-3. Retardation model for Fracture type A.**

	Fracture coating <i>Chlorite + Calcite</i>
Thickness	≤0.5 mm
Porosity	n/a
Formation factor	n/a
BET surface area (m <sup>2</sup> /g)	0.49
CEC (cmoles/kg)	n/a
Sorption properties	n/a
Percentage of all open fractures	34%
Percentage of transmissive fractures	38%
Preferred orientation	No
Altered rock surrounding the fracture?	No

**Table 4-4. Retardation model for Fracture type B.**

	Fracture coating <i>Chlorite + Clay ± epidote ± prehnite ± calcite</i>
Thickness	≤1 mm
Porosity	n/a
Formation factor	n/a
BET surface area (m <sup>2</sup> /g)	10.3
CEC (cmoles/kg)	15±10
Sorption properties	Cs: 0.16±0.01 Ln-Ac(III): 0.075±0.017
Kd (m <sup>3</sup> /kg), saline Forsmark groundwater	
Percentage of all open fractures	7%
Percentage of transmissive fractures	7%
Preferred orientation	Horizontal to gently dipping
Altered rock surrounding the fracture?	Yes, ~1 cm

**Table 4-5. Retardation model for Fracture type C.**

	Fracture coating <i>Chlorite + hematite ± other</i>
Thickness	<0.5 mm (0.1 mm)
Porosity	n/a
Formation factor	n/a
BET surface area (m <sup>2</sup> /g)	2.3±0.6
CEC (cmoles/kg)	n/a
Sorption properties	n/a
Percentage of all open fractures	2%
Percentage of transmissive fractures	1%
Preferred orientation	ENE-NW, steeply dipping
Altered rock surrounding the fracture?	Yes, ~0.5 mm

**Table 4-6. Retardation model for Fracture type D.**

	Fracture coating <i>Chlorite</i> ± other
Thickness	<0.5 mm (0.1 mm)
Porosity	n/a
Formation factor	n/a
BET surface area (m <sup>2</sup> /g)	5.1±2.2
CEC (cmoles/kg)	n/a
Sorption properties	Cs: 0.0041±0.0005
K <sub>d</sub> (m <sup>3</sup> /kg), marine Forsmark groundwater	Ln-Ac(III): 2.4±0.5
Percentage of all open fractures	14%
Percentage of transmissive fractures	12%
Preferred orientation	No
Altered rock surrounding the fracture?	No

**Table 4-7. Retardation model for Fracture type E.**

	Fracture coating <i>Laumontite</i> ± calcite ± chlorite
Thickness	0.1–2 mm
Porosity	n/a
Formation factor	n/a
BET surface area (m <sup>2</sup> /g)	0.42±0.02
CEC (cmoles/kg)	18±5
Sorption properties*	Cs: 0.016
K <sub>d</sub> (m <sup>3</sup> /kg), marine Forsmark groundwater	Ln-Ac(III): 1.2
Percentage of all open fractures	14%
Percentage of transmissive fractures	1%
Preferred orientation	ENE-NW, steeply dipping
Altered rock surrounding the fracture?	Yes, 1–5 cm

**Table 4-8. Retardation model for Fracture type F.**

	Fracture coating <i>Calcite</i> ± quartz ± pyrite ± other
Thickness	0.1–2 mm
Porosity	n/a
Formation factor	n/a
BET surface area (m <sup>2</sup> /g)	2.2±1.1
CEC (cmoles/kg)	n/a
Sorption properties*	Cs: 0.022±0.017
K <sub>d</sub> (m <sup>3</sup> /kg), marine Forsmark groundwater	Ln-Ac(III): 1.4±1.2
Percentage of all open fractures	15%
Percentage of transmissive fractures	19%
Preferred orientation	Steeply dipping NE and NW + subhorizontal to gently dipping
Altered rock surrounding the fracture?	No

**Table 4-9. Retardation model for Fracture type G.**

	Fracture coating <i>Clay</i> ± other
Thickness	1–5 mm
Porosity	n/a
Formation factor	n/a
BET surface area (m <sup>2</sup> /g)	4.3
CEC (cmoles/kg)	n/a
Sorption properties	Cs: 0.43
K <sub>d</sub> (m <sup>3</sup> /kg), marine Forsmark groundwater	Ln-Ac(III): 1.6
Percentage of all open fractures	3%
Percentage of transmissive fractures	3%
Preferred orientation	Horizontal to gently dipping
Altered rock surrounding the fracture?	Yes, ≥5 cm

**Table 4-10. Retardation model for Fracture type H.**

	Fracture coating <i>No mineral</i>
Thickness	n/a
Porosity	For all retardation properties, it is referred to the properties of the non-altered 10157 rock
Formation factor	
BET surface area (m <sup>2</sup> /g)	
CEC (cmoles/kg)	
Sorption properties*	
Percentage of all open fractures	5%
Percentage of transmissive fractures	13%
Preferred orientation	Horizontal to gently dipping
Altered rock surrounding the fracture?	No

### Summary of retardation properties of fractures

For all of the different fracture types included in the retardation models except for the H type (“no mineral”), a thin layer of fracture coating (0.1–5 mm) has been identified. Due to their limited thickness and to the fact that they sometimes were not consolidated, it was not possible to carry out porosity and/or diffusivity determinations. It seems, however, likely that these layers have a higher porosity and therefore a higher diffusivity (i.e. formation factor) compared to fresh rock. In the time perspective relevant for a safety assessment, it therefore seems motivated to consider the entire fracture coatings/fillings to be in immediate contact with flowing water and that the retardation caused by the interaction with these materials could be treated as a surface effect.

A possible limitation in the applicability of the presented fracture data is the lack of sorption data for the most frequent fracture type, i.e. type A. The major reason for this is the very thin coating with chlorite and calcite that never gave the amount of material required for a sorption experiments. Despite the large frequency of fractures of this type, the total impact may thus be reduced by the totally relative low amount of this fracture filling.

The measured BET surface areas of the fracture material are significantly higher than the corresponding BET surface areas of samples from the rock types. They vary from 0.42 m<sup>2</sup>/g to 10.3 m<sup>2</sup>/g, which is in the order of 20–500 times higher than the corresponding value for the unaltered 101057 rock type. This finding is an indication that fractures with their content of material with high specific surfaces constitute a considerable source for adsorption of any released radionuclides.

However, the large differences found for the BET values between fracture material and intact rock is not accompanied by a similar trend in the  $K_d$  values. For this case the differences are much more moderate, e.g. sorption of Cs for the clay containing fracture type G gives a  $K_d$  of  $4.3 \cdot 10^{-2}$  m<sup>3</sup>/kg which is approximately a factor 14 higher than the corresponding value for adsorption of Cs on intact 101057, i.e.  $3.1 \cdot 10^{-3}$  m<sup>3</sup>/kg. Comparison of their measured BET surface area (4.3 m<sup>2</sup>/g and 0.026 m<sup>2</sup>/g, respectively) yields a ratio of approximately 170 which is an indication that a high measured BET surface area for a fracture material does not necessarily imply a corresponding increase in sorption capacity of the fracture material.

### 4.2.3 Deformation zones units

Summaries of the retardation properties of the different deformation zone units are presented in Tables 4-11 to 4-14.

**Table 4-11. Retardation model for Fault rock (strongly tectonized and partly incohesive material), deformation zone unit #1.**

Mineral content	Altered rock fragment, mineralogy dependant on host rock. Generally, chlorite, saussurite and clay.
Porosity (vol%)	10
Formation factor	n/a
BET (m <sup>2</sup> /g)	5.6±2.3
CEC (cmoles/kg)	9±1
Sorption coefficient, $K_d$ (m <sup>3</sup> /kg)	Cs: 0.045±0.02
Saline Forsmark groundwater	Ln-Ac(III): 4.5±1.8

**Table 4-12. Retardation model for Sealed fracture networks, (usually brecciated) ), deformation zone unit #2.**

Mineral content	Due to mineral paragenesis: a) laumontite +calcite ±others b) epidote ±chlorite ±prehnite ±others c) chlorite ±others
Porosity (vol%)	3
Formation factor	n/a
BET (m <sup>2</sup> /g)	0.64
CEC (cmoles/kg)	5.4±2.4
Sorption coefficient, $K_d$ (m <sup>3</sup> /kg)	Cs: 0.018±0.001
Saline Forsmark groundwater	Ln-Ac(III): 1.1±0.1

**Table 4-13. Retardation model for Vuggy rock, ), deformation zone unit #3.**

<b>Mineral content</b>	K-feldspar +albite +Fe-oxides +chlorite ±quartz ±sericite± calcite±others
<b>Porosity (vol%)</b>	13±6
<b>Formation factor</b>	(1.2±0.8)E-2
<b>BET (m<sup>2</sup>/g)</b>	1.58
<b>CEC (cmoles/kg)</b>	<0.4
<b>Sorption coefficient, K<sub>d</sub> (m<sup>3</sup>/kg)</b>	Cs: 0.0020±0.0002
<b>Marine Forsmark groundwater</b>	Ln-Ac(III): 1.4±0.8

**Table 4-14. Retardation model for oxidized (medium to strong alteration) wall rock, ), deformation zone unit #4.**

<b>Mineral content</b>	Hydrothermally altered host rock. Red staining from small hematite grains, K-feldspar, saussurite, plagioclase, quartz, chlorite
<b>Porosity (vol%)</b>	2.5±3.8
<b>Formation factor</b>	n/a
<b>BET (m<sup>2</sup>/g)</b>	0.77
<b>CEC (cmoles/kg)</b>	n/a
<b>Sorption coefficient, K<sub>d</sub> (m<sup>3</sup>/kg)</b>	n/a

### **Summary of retardation properties of deformation zone units**

The deformation zone units for which retardation properties have been tabulated are all comparatively heterogeneous in their structure. The porosities are considerably higher than for intact rock (3–16%) except for the oxidized wall rock which is only slightly more porous than the intact rock type 101057.

A higher porosity should consequently be accompanied by an increased diffusivity (formation factor). However, this has only been proven for the vuggy rock samples where a formation factor of  $1.5 \cdot 10^{-2}$  has been measured. Altogether, these parts of highly porous rock could be suspected to act as conductors in the rock mass.

The measured sorption parameters (BET-surface areas and sorption coefficients) indicate that these deformation zone units have sorption properties that are slightly higher than those of intact rock. This implies that these deformation zone units potentially are strong adsorption features for any radionuclides released from a repository.

## **4.3 Application of the retardation model**

Tables 4-1 and 4-2 provide a basis for parameterization of the rock domains RFM029, and RFM045. The parameterization of each rock domain could range from a simple selection of a single parameter value for the dominant rock type in that domain to, for instance, volume averaging using data for fresh or altered rock, or both.

The quantitative descriptions of the identified fracture types, including the available retardation parameters, are given in Tables 4-3 to 4-10 and the corresponding descriptions of the deformation zones are presented in Table 4-11 to 4-14. The fracture types and deformation zones can be used as a basis for modelling radionuclide transport along flow paths in the fractured medium.

Combined with the variation/uncertainty of the different numerical values (presented in Chapter 3 as the maximum, minimum, median values of the measurements) an interval is given that can be used as a basis for stochastic parameterization of transport models.

As a general conclusion, it is considered that the retardation tables presented overall gives a fairly good description of the retardation properties of the site specific geologic features. The most abundant rock type (SKB code 101057) is well described; the major drawback is the low amount of experimental data available for the most abundant fracture type, (i.e. type A, thin fracture coating of chlorite and calcite).

This report should be regarded as a proposal how to formulate a descriptive and qualitative retardation model based on the available database. Recommendations on the selection of data are given, however with an acknowledgement to the qualitative uncertainty as well as to the numerical uncertainty for the retardation parameters. This implies that the model does not provide exact and detailed guidelines on how to “dress” the geological model with transport parameters using the retardation model tables, but, nevertheless, it provides the authors opinion on what is the best representation that can be done with the data available. The retardation model should be viewed as a presentation of the interpreted site-specific information on retardation parameters, intended to provide a basis for the formulation of alternative parameterizations and/or necessary simplifications within the Safety Assessment modelling.

## 5 References

- André M, Neretnieks I, Malmström, M E, 2008a.** Measuring sorption coefficients and BET surface areas on intact drillcore and crushed granite samples, *Radiochim. Acta* 96, 1–5 (2008).
- André M, Malmström, M E, Neretnieks I, 2008b.** Determination of sorption properties of intact rock samples: New methods based on electromigration, *J. Contam. Hydrology* (2008), doi: 10.1016/j.jconhyd.2008.09.006.
- Birgersson L, Neretnieks I, 1990.** Diffusion in the matrix of granitic rock. Field test in the Stripa mine. *Water Resources Research* 26 p 2833–2841.
- Berglund S, Selroos J-O, 2004.** Transport properties site descriptive model – Guidelines for evaluation and modelling. SKB R-03-09, Svensk Kärnbränslehantering AB.
- Brunauer S, Emmett PH, Teller E, 1938.** Adsorption of gases in multimolecular layers. *J Amer Chem Soc* 60: 309–319.
- Byegård J, Gustavsson E, Tullborg E-L, Selroos J-O, 2006.** Bedrock transport properties. Preliminary site description Forsmark area – version 1.2. SKB R-05-86, Svensk Kärnbränslehantering AB.
- Byegård J, Selnert E, Andersson P, in prep.** Diffusion and sorption experiments using drill core samples – a test of the general applicability of the site specific laboratory retardation data, SKB R-report.
- Caine J S, Evans J P, Forster C B, 1996.** Fault zone architecture and permeability structure. *Geology*, 24, 11, 1025–1028.
- Crank J, 1975.** The mathematics of diffusion, 2<sup>nd</sup> ed. Oxford University Press, New York.
- Follin S, Hartley L, Jackson P, Roberts D, Marsic N, 2008.** Hydrogeological conceptual model development and numerical modelling using CONNECTFLOW, Forsmark modelling stage 2.3. SKB R-08-23, Svensk Kärnbränslehantering AB.
- Jakobsson A-M, 1999.** Measurement and modelling using surface complexation of cation (II to IV) sorption onto mineral oxides, Thesis, Chalmers University of Technology, Department of Nuclear Chemistry, Göteborg, Sweden.
- Laaksoharju M, Smellie J, Tullborg, E L, Gimeno M, Hallbeck L, Molinero J, Waber N, 2008.** Bedrock hydrogeochemistry Forsmark, Site descriptive modelling, SDM-Site Forsmark. SKB R-08-47, Svensk Kärnbränslehantering AB.
- Löfgren M, Neretnieks I, 2005a.** Formation factor logging in situ by electrical methods in KFM01A and KFM02A. Measurements and evaluation of methodology. SKB P-05-29, Svensk Kärnbränslehantering AB.
- Löfgren M, Neretnieks I, 2005b.** Formation factor logging in-situ by electrical methods in KFM03A and KFM04A. Forsmark site investigation. SKB P-05-108, Svensk Kärnbränslehantering AB.
- Löfgren M, 2006.** Formation factor logging in situ by electrical methods in KFM07A and KFM08A. Forsmark site investigation. SKB P-06-187. Svensk Kärnbränslehantering AB.
- Löfgren M, Pettersson M, Widén H, Crawford J, 2006.** Formation factor logging in situ by electrical methods in KFM05A and KFM06A. Forsmark site investigation. SKB P-06-91, Svensk Kärnbränslehantering AB.
- Löfgren M, 2007.** Formation factor logging in situ by electrical methods in KFM01D and KFM08C. Forsmark site investigation. SKB P-07-138. Svensk Kärnbränslehantering AB.
- Mills R, Lobo V M M, 1989.** Self-Diffusion in electrolyte solutions, *Physical Sciences Data* 36, Elsevier.
- Nordgulen O, Saintot A, 2006.** The character and kinematics of deformation zones (ductile shear zones, fault zones and fracture zones) at Forsmark – report from phase 1. SKB P-06-212, Svensk Kärnbränslehantering AB.

- Ohlsson Y, Neretnieks I, 1997.** Diffusion data in granite – Recommended values. SKB TR-97-20, Svensk Kärnbränslehantering AB.
- Olofsson I, Simeonov A, Stephens M, Follin S, Nilsson A-C, Röshoff K, Lindberg U, Lanaro F, Fredriksson A, Persson L, 2007.** Site descriptive modelling Forsmark, stage 2.2. A fracture domain concept as a basis for the statistical modelling of fractures and minor deformation zones, and interdisciplinary coordination, SKB R-07-15, Svensk Kärnbränslehantering AB.
- Parkhomenko E I, 1967.** Electrical properties of rocks. Moscow, Institute of Physics of the Earth, Academy of the Sciences of the USSR, 277 p.
- Penttinen L, Siitari-Kauppi M, Ikonen J, 2006.** Determination of porosity and micro fracturing using the <sup>14</sup>C-PMMA technique in samples taken from Forsmark area. Forsmark site investigation. SKB P-06-60, Svensk Kärnbränslehantering AB.
- Sandström B, Tullborg E-L, 2006.** Fracture mineralogy. Results from KFM06B, KFM06C, KFM07A, KFM08A, KFM08B. Forsmark site investigation. SKB P-06-226, Svensk Kärnbränslehantering AB.
- Sandström B, Tullborg E-L, Smellie J, MacKenzie A B, Suksi J, 2008.** Fracture mineralogy of the Forsmark site. SKB R-08-102, Svensk Kärnbränslehantering AB.
- Selnert E, Byegård J, Widestrand H, 2008.** Laboratory measurements within the site investigation programme for the Transport properties of the rock. Final report. SKB P-07-139. Svensk Kärnbränslehantering AB.
- Skagius K, Neretnieks I, 1986.** Diffusivity measurements and electrical resistivity measurements in rock samples under mechanical stress. Water Resources Research 22 (4), p 570–580.
- Stephens M B, Fox A, La Pointe P, Simeonov A, Isaksson H, Hermansson J, Öhman J, 2007.** Geology Forsmark. Site descriptive modelling Forsmark stage 2.2. SKB R-07-45, Svensk Kärnbränslehantering AB.
- Stråhle A, 2001.** Definition och beskrivning av parametrar för geologisk, geofysisk och bergmekanisk kartering av berget. SKB R-01-19, Svensk Kärnbränslehantering AB.
- Thunehed H, 2005a.** Resistivity measurements on samples from KFM01A and KFM02A. Forsmark site investigation. SKB P-05-26, Svensk Kärnbränslehantering AB.
- Thunehed H, 2005b.** Resistivity measurements on samples from KFM03A, KFM04A and KFM05A. Forsmark site investigation. SKB P-05-76, Svensk Kärnbränslehantering AB.
- Thunehed H, 2007a.** Resistivity measurements on samples from KFM01A, KFM01B, KFM02A, KFM05A and KFM06A. Forsmark site investigation. SKB P-07-51, Svensk Kärnbränslehantering AB.
- Thunehed H, 2007b.** Resistivity measurements on samples from KFM01A, KFM02A, KFM06A, KFM08A, KFM08C and KFM09A. Forsmark site investigation. SKB P-07-137, Svensk Kärnbränslehantering AB.
- Widestrand H, Byegård J, Ohlsson Y, Tullborg E-L, 2003.** Strategy for the use of laboratory methods in the site investigations programme for the transport properties of the rock. SKB R-03-20, Svensk Kärnbränslehantering AB.